



---

**Forschungszentrum Karlsruhe**  
in der Helmholtz-Gemeinschaft

---

**Wissenschaftliche Berichte**  
FZKA 7257

# **Prototypical Experiments on Air Oxidation of Zircaloy-4 at High Temperatures**

**M. Steinbrück, U. Stegmaier, T. Ziegler**  
Institut für Materialforschung

Januar 2007



**Forschungszentrum Karlsruhe**

in der Helmholtz-Gemeinschaft

Wissenschaftliche Berichte

FZKA 7257

Prototypical Experiments on Air Oxidation  
of Zircaloy-4 at High Temperatures

M. Steinbrück, U. Stegmaier, T. Ziegler

Institut für Materialforschung

Forschungszentrum Karlsruhe GmbH, Karlsruhe

2007

Für diesen Bericht behalten wir uns alle Rechte vor

Forschungszentrum Karlsruhe GmbH  
Postfach 3640, 76021 Karlsruhe

Mitglied der Hermann von Helmholtz-Gemeinschaft  
Deutscher Forschungszentren (HGF)

ISSN 0947-8620

urn:nbn:de:0005-072572

## **Abstract**

The report presents the results of extensive experimental work on the oxidation of Zircaloy-4 in air at high temperatures. The experimental program was aimed at mechanistic phenomenology of the reaction between Zircaloy and air and investigation of air attack under prototypical conditions for air ingress under the conditions of an hypothetical severe nuclear reactor accident, i.e. at temperatures 800-1500 °C and consideration of mixed air(nitrogen)-steam atmospheres and pre-oxidation.

The oxidation in air as well as in air and nitrogen-containing atmospheres leads to strong degradation of the cladding material. The main mechanism for this process is the formation of zirconium nitride and its re-oxidation. From safety point of view, the barrier effect of the fuel cladding is lost much earlier than during accident transients with only a steam atmosphere.

Pre-oxidation in steam prevents air attack as long as the oxide scale is intact, i.e. at temperatures above 1050 °C (beyond breakaway regime) and as long as oxidising gases are available (no steam starvation conditions). Under steam/oxygen starvation conditions the oxide scale is reduced and significant external nitride formation takes place.

Stronger degradation of cladding tubes was also observed in air-steam and nitrogen-steam mixtures over a wide range of compositions.

Regarding modelling of air ingress in severe accident computer codes one conclusion is that parabolic correlations for oxidation in air may be applied only for high temperatures (>1400 °C) and for pre-oxidized cladding ( $\geq 1100$  °C). For all other conditions faster, more linear reaction kinetics should be applied.

The results presented in this report are mainly of phenomenological nature. Therefore, the program will be extended by selected experiments oriented on the determination of kinetic correlations.

# Prototypische Experimente zur Luftoxidation von Zircaloy-4 bei hohen Temperaturen

## Zusammenfassung

In diesem Bericht sind die Ergebnisse umfangreicher Studien zur Reaktion von Zircaloy-4 Hüllrohren mit Luft im Temperaturbereich 800-1500 °C zusammengefasst. Es wurden für einen Reaktorstörfall mit Lufteinbruch prototypische Bedingungen gewählt, d.h. die Reaktion von Hüllrohrsegmenten in gemischten Luft-Dampf-Atmosphären sowie die sequentielle Reaktion zuerst in Dampf und nachfolgend in Luft. Außerdem wurden Sauerstoffmangelbedingungen betrachtet, bei denen das Hüllmaterial Stickstoff bzw. Stickstoff-Dampf-Mischungen ausgesetzt ist.

Generell hat Luft einen großen Einfluss auf die verstärkte Degradation von Hüllrohren. Deren Barrierewirkung gegen die Freisetzung von Spaltprodukten geht während einer Unfallsequenz mit Lufteinbruch früher und bei niedrigeren Temperaturen verloren als in reiner Dampf-Atmosphäre. Die Bildung von Zirkoniumnitrid an der Phasengrenze Metall-Oxid sowie dessen Oxidation führt zu sehr porösen Oxidschichten, die keine Schutzwirkung aufweisen. Andererseits ist die Reaktion von metallischen Zirkoniumlegierungen in reinem Stickstoff um Größenordnungen langsamer als in Sauerstoff enthaltenden Atmosphären.

Die Voroxidation von Zircaloy in Sauerstoff oder Dampf verhindert die Nitridbildung und damit die beschleunigte Zerstörung des Hüllrohres, solange die Oxidschicht dicht ist und den Zutritt von Stickstoff zum Metall unterbindet. Reine Stickstoffatmosphäre, wie sie bei Sauerstoffmangelbedingungen auftritt, führt dagegen zur Bildung beträchtlicher Mengen von Zirkoniumnitrid.

Experimente zur Aufklärung des Mechanismus des Stickstoffangriffs haben gezeigt, dass Stickstoff bevorzugt mit  $\alpha$ -Zr(O) und unterstoichiometrischem Oxid reagiert, während die Reaktionsgeschwindigkeiten mit der  $\beta$ -Zr Phase um Größenordnungen geringer sind.

Gemischte Luft-Dampf und Stickstoff-Dampf Atmosphären, wie sie bei Störfällen zu erwarten sind, führen in weiten Zusammensetzungsbereichen auch zur verstärkten Degradation der Hüllrohre.

Die hier vorgestellten Untersuchungen waren hauptsächlich phänomenologischer Natur; deshalb sind weitere Experimente zur Bestimmung kinetischer Parameter für ausgewählte Versuchsbedingungen geplant.

# CONTENTS

- 1 Introduction..... 1
- 2 Experimental Details ..... 2
  - 2.1 Test set-ups ..... 2
  - 2.2 Specimens ..... 4
  - 2.3 Test conduct ..... 5
  - 2.4 Post-test examinations (PTE) ..... 7
- 3 Experimental Results ..... 8
  - 3.1 Simple tests in oxygen, nitrogen and air ..... 8
  - 3.2 Tests in mixed air-steam atmospheres ..... 12
  - 3.3 Tests in mixed nitrogen-steam atmospheres ..... 20
  - 3.4 Influence of pre-oxidation on subsequent oxidation in air and nitrogen ..... 24
  - 3.5 Tests on the mechanisms of nitrogen attack ..... 30
- 4 Discussion ..... 34
- 5 Summary and Conclusions ..... 37
- Acknowledgements ..... 38
- References ..... 38
- Appendix A Test parameters and main results of the tests in the BOX rig ..... 40
- Appendix B Test parameters and main results of the tests in the thermal balance ..... 46
- Appendix C Post-test results for the specimens oxidised in mixed air-steam atmosphere ..... 50
- Appendix D Post-test results for the specimens oxidised in nitrogen-steam mixtures ..... 69
- Appendix E Metallographic post-test examinations of pre-oxidised specimens ..... 73
- Appendix F Influence of pre-oxidation in steam on subsequent reaction in air and nitrogen at 1200 °C ..... 79
- Appendix G Phase diagrams ..... 84

## LIST OF TABLES

<b>Table 1:</b> Influence of temperature and composition of the atmosphere on the degradation of the oxide scale.	20
<b>Table 2:</b> Reaction kinetics of Zircaloy-4 in oxygen, air, and nitrogen with and without pre-oxidation in steam or oxygen (simplified).	36
<b>Table A 1:</b> Test matrix of 1 h isothermal experiments in mixed air-steam atmospheres at 800, 900, 1000, 1100, and 1200 °C.	41
<b>Table A 2:</b> Test matrix of 10 min isothermal experiments in mixed air-steam atmospheres at 1200, 1300, 1400, and 1500 °C.	43
<b>Table A 3:</b> Test matrix of experiments in mixed nitrogen-steam atmospheres at 1000 and 1200 °C.	44
<b>Table A 4:</b> Tests on influence of pre-oxidation in steam on subsequent reaction in air and nitrogen.	45
<b>Table A 5:</b> Test matrix of first TG experiments at 1000 and 1100 °C.	46
<b>Table A 6:</b> Test parameters and results of TG experiments on influence of pre-oxidation on subsequent reaction in air and nitrogen.	47

## LIST OF FIGURES

<b>Figure 1:</b> Schematic view of the BOX Rig for the investigation of the oxidation kinetics of Zircaloy in steam containing atmosphere.	3
<b>Figure 2:</b> Photo of the BOX Rig.	3
<b>Figure 3:</b> Schematic view of the thermal balance coupled with MS and TG measuring head with specimen.	4
<b>Figure 4:</b> BOX Rig: Sample holder with Zry-4 cladding segment.	5
<b>Figure 5:</b> Specimen with closed bottom and top to prevent internal oxidation; left: macro photo after test 51216b, right: sketch with dimensions (in mm).	5
<b>Figure 6:</b> Test conduct of a series at 1000 °C under different air-steam mixtures in the BOX Rig, showing temperature and gas flow rates.	6
<b>Figure 7:</b> Example for test conduct in the thermal balance: Pre-oxidation in oxygen and subsequent oxidation in air at 1200 °C.	7
<b>Figure 8:</b> Thermo-gravimetric results for the reaction of Zircaloy-4 in oxygen, nitrogen, and air at 800, 1000, 1200, and 1400 °C. Left: mass gain versus time; right: squared mass gain versus time.	9
<b>Figure 9:</b> Reaction rates of Zircaloy-4 in air, oxygen and nitrogen at various temperatures.	10
<b>Figure 10:</b> Appearance of the specimens after tests in pure atmospheres.	11
<b>Figure 11:</b> Metallographic images of the Zircaloy-4 specimens after reaction in pure atmospheres. The numbers above the pictures indicate test name and approx. time of reaction.	12
<b>Figure 12:</b> Test conduct showing gas and steam injection rates and temperature (top) and MS results with flow rates of steam, oxygen, nitrogen, and hydrogen in the off-gas (bottom) for the test series at 1000 °C.	13
<b>Figure 13:</b> Test conduct showing gas and steam injection rates and temperature (top) and MS results with flow rates of steam, oxygen, nitrogen, and hydrogen in the off-gas (bottom) for the test series at 1500 °C.	14
<b>Figure 14:</b> Detailed MS results of tests in pure steam (left) and in air-steam mixture with low air content at 800, 1000, and 1200 °C.	15
<b>Figure 15:</b> Mass gain of specimens after isothermal tests 1 h at 800-1200 °C (left) and 10 min at 1200-1500 °C (right) in dependence on the composition of the air-steam mixture.	15
<b>Figure 16:</b> 1 h, 800 °C: Optical microscopy images of selected specimens.	16
<b>Figure 17:</b> 1 h, 900 °C: Optical microscopy images of selected specimens.	17
<b>Figure 18:</b> 1 h, 1000 °C: Optical microscopy images of selected specimens.	17
<b>Figure 19:</b> Bright-field (left) and dark-field (right) image of the same position of the specimen oxidised one hour at 1000 °C in air.	18
<b>Figure 20:</b> 10 min, 1300 °C: Three images at different positions of the specimen after oxidation in 30% air and 70% steam.	18
<b>Figure 21:</b> Comparison of specimens oxidised 10 min in pure air at various temperatures.	19
<b>Figure 22:</b> Off-gas analyses by MS during tests in mixed nitrogen steam atmospheres.	21
<b>Figure 23:</b> Integral hydrogen release during isothermal reaction of Zircaloy-4 in nitrogen-steam mixtures.	21

<b>Figure 24:</b> Mass gain of Zircaloy-4 samples after reaction in mixed nitrogen-steam atmosphere.	22
<b>Figure 25:</b> Microscopic details of oxidised Zircaloy-4 specimens after reactions in 5/95 and 50/50 nitrogen-steam mixtures.	23
<b>Figure 26:</b> Test conduct and results of an isothermal test at 1100 °C with pre-oxidation in oxygen and succeeding reaction in air.	25
<b>Figure 27:</b> Mass gain of Zircaloy-4 specimens during oxidation in oxygen, nitrogen and air, with and without pre-oxidation in oxygen.	25
<b>Figure 28:</b> Metallographic images of Zry-4 specimens after 80 min reaction in oxygen, air, and nitrogen, with and without pre-oxidation (PO).	26
<b>Figure 29:</b> Influence of pre-oxidation on subsequent oxidation in air. The vertical lines indicate the transition from pre-oxidation to reaction in air.	28
<b>Figure 30:</b> Influence of pre-oxidation on subsequent oxidation in nitrogen.	28
<b>Figure 31:</b> Off-gas analysis by MS for the tests with 5, 1, and 0 min PO in steam and following oxidation in air at 1200 °C.	29
<b>Figure 32:</b> Mass gain of Zircaloy-4 specimens after 0, 1, and 5 min pre-oxidation in steam and subsequent reaction in air and nitrogen. For comparison, results of reference tests in only steam are also shown.	30
<b>Figure 33:</b> Phase diagram Zr-ZrO <sub>2</sub> . The arrows indicate compositions of specimens prepared and investigated.	31
<b>Figure 34:</b> Example for conduct and results of the test series on the mechanism of nitrogen attack. Here: pre-oxidation in oxygen till 5.7% mass gain at 1200 °C, homogenisation at 1400 °C and reaction in nitrogen at 1200 °C.	31
<b>Figure 35:</b> Mass gain of pre-oxidised and homogenised Zircaloy-4 specimens during annealing in nitrogen at 1200 °C.	32
<b>Figure 36:</b> Micro images of specimens pre-oxidised in oxygen (PO), homogenised, and partly (right column) annealed in nitrogen at 1200 °C.	33
<b>Figure 37:</b> Magnified images of the specimen with 5.7% PO and subsequent annealing in nitrogen shown in Fig. 36.	34
<b>Figure 38:</b> Microscopic images of a Zry-4 cladding after pre-oxidation in oxygen and oxidation in air at 1000 °C under two different illuminations. The dark-field image clearly shows the formation of micro-cracks in the external part of the oxide where the nitride already has been re-oxidised.	35

# 1 Introduction

Most investigations of core degradation during severe nuclear reactor accidents have considered oxidation of metal core components by steam only. However, there are various scenarios where air may have access to the core. So, air ingress is possible under shutdown conditions when the reactor coolant system is open to the containment atmosphere. Air oxidation of the remaining outer core regions after reactor pressure vessel failure in the late phase of core degradation during severe accidents was identified to be another possible scenario [1]. Furthermore, the failure of a storage or transportation cask may result in air intrusion and consequent interaction with the spent fuel rods.

The special impact of air ingress on reactor safety is due to:

- The vigorous oxidation and degradation of the remaining cladding. Zr oxidation by air releases about 85% more heat than oxidation by steam. The oxidation kinetics in air are much faster due to the formation of non-protective oxide (nitride) scales,
- the oxidation of the  $\text{UO}_2$  fuel to  $\text{U}_3\text{O}_8$ , leading to lower melting temperature and impairment of the mechanical stability of the fuel, and
- its influence on the volatility of the fission products. So, e.g. in highly oxidizing atmosphere, the formation of volatile ruthenium oxides is preferred.

Experimental and analytical work on air ingress was performed within the EC 4<sup>th</sup> Framework projects OPSA [2] and COBE [3]. Recently, this topic is again under examination in the USA with emphasis on storage and transportation cask accidents [4] and in Europe focusing on shutdown scenarios and the late phase of severe accidents [5]. Recently, IRSN launched the MOZART program focused on investigation of various zirconium alloys in air-steam atmospheres at intermediate temperatures (600-1000 °C) for spent fuel storage pool accidents [6].

The experimental data available up to now on air oxidation at higher temperatures are limited to the reaction in pure air. The more prototypical scenarios of air oxidation of zirconium alloys pre-oxidized in steam and their reaction in mixed air-steam atmospheres have not been investigated at all. This report presents results of investigations on air oxidation under such conditions obtained in parametric small-scale separate-effects tests in the temperature range 800-1500 °C. A part of these results has been already published in open literature [7] and at conferences [8]. Most of the experiments on the influence of pre-oxidation on subsequent reaction in air or nitrogen have been performed in the frame of a diploma thesis at FZK-IMF I [9]. Further information can be obtained from results of the large-scale bundle test QUENCH-10 on air ingress performed at Forschungszentrum Karlsruhe in 2004 [10].

## 2 Experimental Details

### 2.1 Test set-ups

Two experimental set-ups have been mainly used for the experiments presented in this report: the BOX rig and a commercial thermal balance which are briefly described in the following.

#### ***BOX Rig***

All tests with steam in the atmosphere were performed in the so-called BOX rig. This facility (see Figs. 1 and 2) consists of

- A gas supply system for Ar, H<sub>2</sub> and steam (0-4 mol/h each), consisting of two gas flow controllers, one liquid flow controller and a so-called controlled evaporator mixer unit (CEM), where the liquid water was evaporated and mixed with the non-condensable gas. The whole system is delivered by Bronkhorst High-Tech B.V.
- A tube furnace with maximum temperatures of 1700 °C, with an alumina reaction tube (inner diameter: 32 mm, length: 600 mm) and molybdenum heaters, delivered by HTM Reetz GmbH Berlin.
- A quadrupole mass spectrometer (MS) Balzers GAM 300.
- An air lock, allowing change of specimens at reaction temperature and under defined atmosphere.

The off-gas tube from the furnace to the MS (SS, inner diameter: 6 mm, length: 2.7 m) is heated to about 150 °C to prevent steam condensation. The mass spectrometer allows the quantitative analysis of all gaseous reaction products including steam. If possible, the hydrogen release rate was used as a continuous measure for the reaction kinetics. The mass spectrometer is calibrated for H<sub>2</sub>, N<sub>2</sub>, and O<sub>2</sub> with certificated Ar-gas mixtures. The Bronkhorst supply system for steam and gas was used for steam calibration. All parts of the system are computer controlled by a LabView program especially written for the BOX Rig.

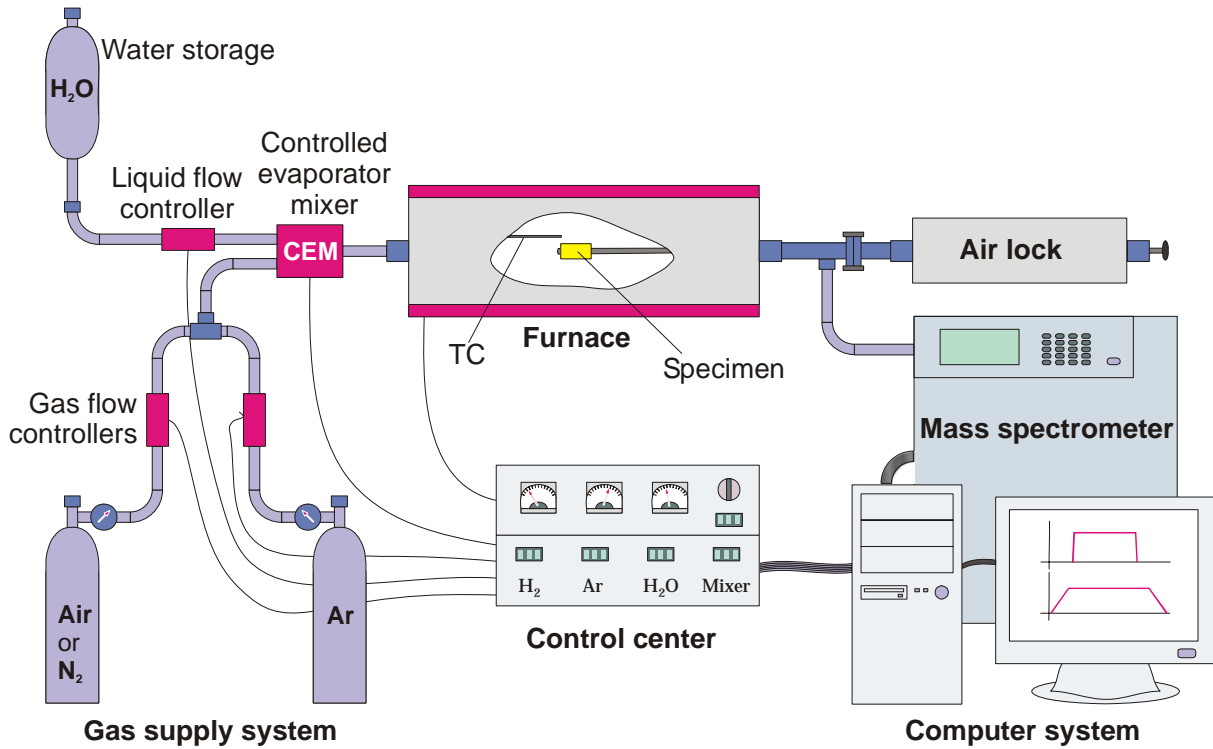


**Figure 1:** Schematic view of the BOX Rig for the investigation of the oxidation kinetics of Zircaloy in steam containing atmosphere.

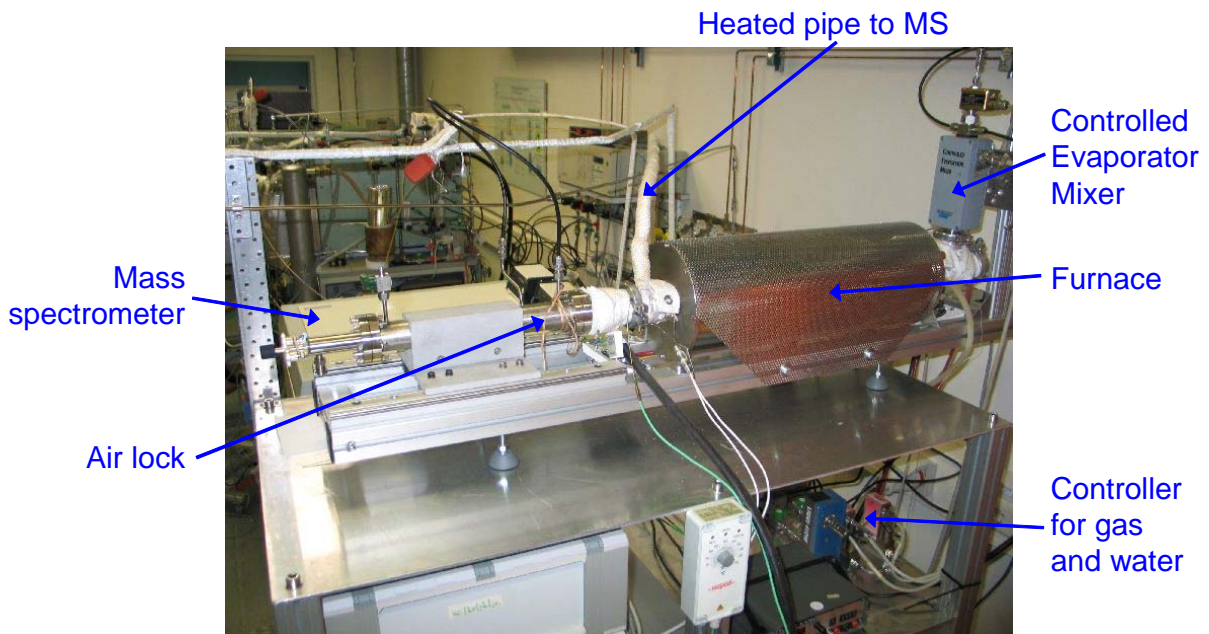


**Figure 2:** Photo of the BOX Rig.

***Thermal balance***

Kinetic experiments were performed in a commercial thermal balance (NETZSCH STA-409) coupled via a capillary with a 6 mm quadrupole mass spectrometer (NETZSCH Aeolos). Figure 3 gives a schematic of the set-up. The gases (Ar, O<sub>2</sub>, N<sub>2</sub>, air) are again supplied via

Bronkhorst flow controllers at the lower part of the vertical tube furnace. Argon flows through the balance containment into the furnace; the reaction gases are directly injected into the reaction tube to prevent contamination of the balance and to ensure a well-defined gas mixture in the furnace. All gases used were highly pure gases with less than 1 or 10 ppm impurities, respectively.

The thermal balance is not designed for working under steam-containing atmospheres. Thus, here oxygen had to be used to simulate (pre-)oxidation in steam. Oxide scales obtained by oxidation of Zircaloy in oxygen are known to be very similar to those formed in steam. The main difference between the two reaction gases is the absence of hydrogen absorbed by the metal and in the off-gas during oxidation in oxygen. A limited test series in the BOX rig with pre-oxidation in steam confirmed the comparable behaviour of specimens pre-oxidised in oxygen and steam (see chapter 3.4).

The specimens were supported by a yttria plate to prevent interactions between the Zircaloy and the alumina sample plate. The temperature of the furnace was controlled by the thermocouple located directly below the sample plate (STC = sample temperature control).

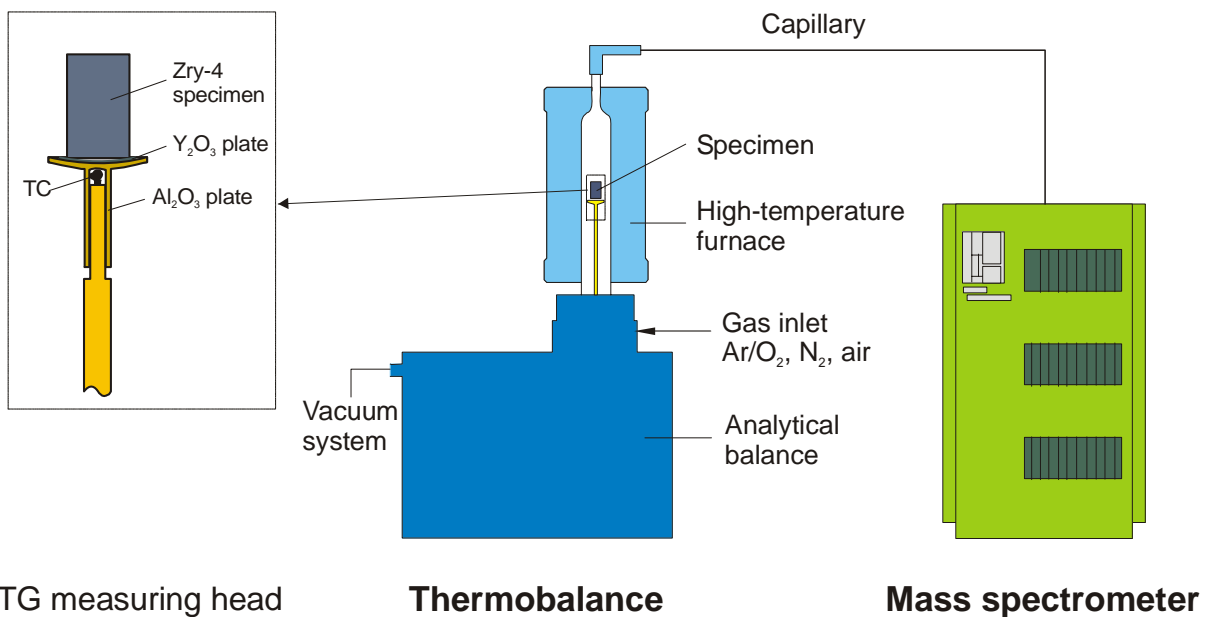


**Figure 3:** Schematic view of the thermal balance coupled with MS and TG measuring head with specimen.

## 2.2 Specimens

Zircaloy-4 tube segments (10.75 mm outer diameter, 0.725 mm wall thickness) were investigated in all tests. Segments 1 cm long were used in the TG tests; they were positioned vertically as can be seen in the inset of Fig. 3. In the BOX Rig 2-cm tube segments were horizontally suspended on a zirconia rod (Fig. 4).

Both types of specimens were open, i.e. allowing external and internal oxidation. Some tests needed to be performed without internal oxidation (see chapter 3.4). Thus, ten closed

specimens were produced with electron-beam welded bottom and top. A thin (thin enough to exclude internal oxidation) hole at the centre of the bottom prevented pressure build-up in the specimens. Figure 5 gives a photo and a sketch of that kind of specimens.

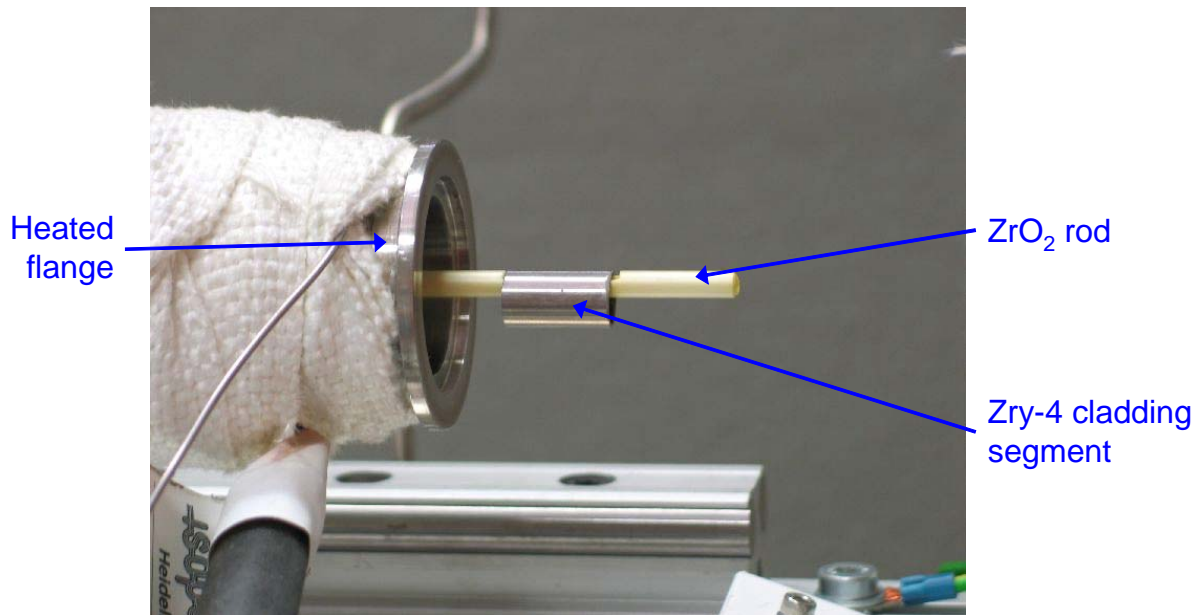


**Figure 4:** BOX Rig: Sample holder with Zry-4 cladding segment.

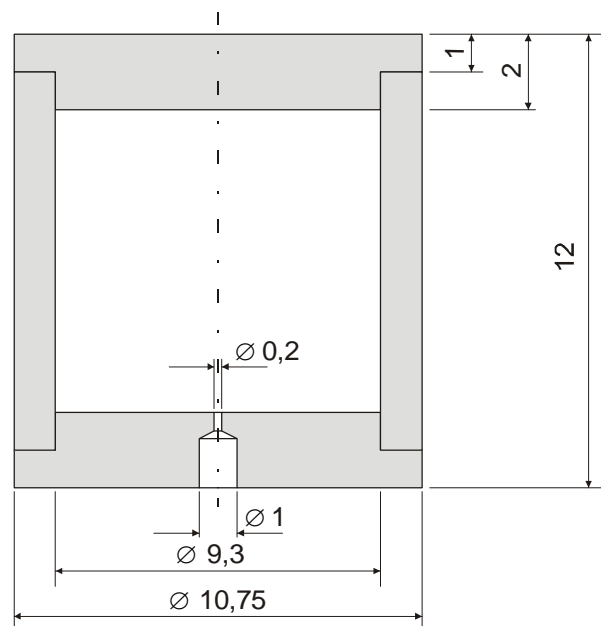


**Figure 5:** Specimen with closed bottom and top to prevent internal oxidation; left: macro photo after test 51216b, right: sketch with dimensions (in mm).

### 2.3 Test conduct

Argon was used as carrier gas and reference gas for mass spectroscopy in all tests. This will not be explicitly mentioned in the rest of the report. So, "tests in pure air or steam

atmosphere" have been conducted in air-argon and steam-argon mixtures, respectively. The use of argon may have some influence on gas diffusion, especially in pores and cracks. The investigation of this effect was not within the scope of the report.

### **BOX Rig**

At the beginning of a test series the furnace was heated to the desired temperature and all auxiliary heaters for tubing, valves, and flanges were switched on. The mass spectrometer was calibrated in parallel.

After inserting of the specimen, the air lock was connected to the furnace and flushed with argon. When the mass spectrometer indicated the removal of residual air in the furnace the sample was slowly pushed into the hot centre of the furnace and thermally equilibrated before the desired gas mixture was switched on. To avoid strong temperature overshooting at high temperatures ( $\geq 1200$  °C) the specimens were shifted into the furnace at (oxidising) atmosphere, kept at position at 1100 °C for one minute (giving a pre-oxidation of approx. 15  $\mu\text{m}$ ) and only then pushed to the hot zone. In any case, the gas flow was changed from the oxidising gas or gas mixture to pure argon at the end of the isothermal oxidation period. The specimen was pulled into the air lock, where it quickly cooled down and could be exchanged with a new one. Figure 6 gives an example of the conduct of a test series at 1000 °C under various air-steam mixtures.

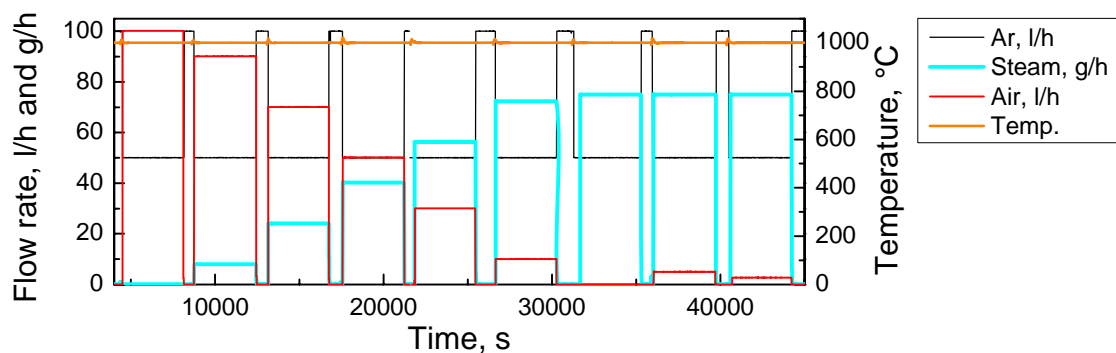


**Figure 6:** Test conduct of a series at 1000 °C under different air-steam mixtures in the BOX Rig, showing temperature and gas flow rates.

The flow rate of the reference gas argon was usually 50 l/h; the air and nitrogen flow rates varied between 0 and 100 l/h and steam was injected with 0-75 g/h. The exact test conditions for all tests are compiled in tables in Appendix A. Masses of the specimens were measured before and after all tests.

### **Thermal balance**

The specimens were heated with a rate of 30 K/min under argon to the desired temperature and 5 min thermally equilibrated. Then, the oxidising gas (mixture) was injected till approx.

25 wt% mass gain was obtained or for a pre-defined time. The tests were finished by switching off the oxidising gases and cooling the furnace as fast as possible with an argon atmosphere.

Complete oxidation of Zircaloy leads to a mass gain of 35 wt%. The target 25 wt% mass gain resulted in adequate test duration resulting in enough remaining metal phase for metallographic examinations.

The argon flow rate during all the tests was 10 l/h. Typical flow rates for oxygen, nitrogen and air were also 10 l/h. At 1400 °C some tests were conducted with 30 l/h air or oxygen to prevent oxygen starvation conditions. Pre-oxidation was partially done with 3 l/h oxygen.

Figure 7 shows a typical test conduct with pre-oxidation in oxygen and subsequent reaction in air. The main parameters of all tests conducted in the thermal balance are summarised in Appendix B. In [9] diagrams and descriptions of all tests performed in the frame of Ziegler's diploma thesis are given in detail.

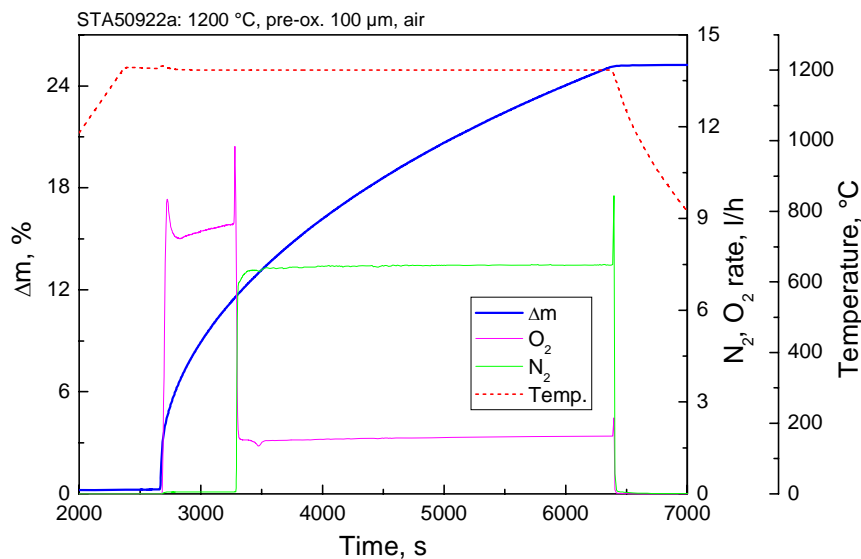


**Figure 7:** Example for test conduct in the thermal balance: Pre-oxidation in oxygen and subsequent oxidation in air at 1200 °C.

## 2.4 Post-test examinations (PTE)

Macro photos were taken of all specimens after the tests. Then the specimens were embedded in epoxy resin, cut, ground and polished for metallographic examinations by optical microscopy. Some specimens were investigated by SEM/EDX especially for the determination of nitride phases and some specimens were used for the analysis of hydrogen content in the metal and oxide phases by neutron radiography [11].

As already mentioned, most of the specimens were open and thus allowed inner and outer oxidation. Because the experimental conditions e.g. regarding gas flow are better defined for

the external surface of the tube segments it is recommended to focus attention on examination of external oxide scales.

## 3 Experimental Results

### 3.1 Simple tests in oxygen, nitrogen and air

#### *TG results*

Reference tests have been conducted in oxygen, nitrogen and air at 800, 1000, 1200, and 1400 °C in the thermal balance. Figure 8 gives an overview on the results of these experiments. They are shown in  $\Delta m = f(t)$  and  $(\Delta m)^2 = f(t)$  diagrams to make visible linear and parabolic reaction kinetics, respectively. Temperatures and specimen designations are given above the diagrams. Test parameters and results are compiled in Table A6 in Appendix B.

Generally, the reaction rate in nitrogen atmosphere is much lower (about two orders of magnitude) than in oxygen or air. This is why a magnified y-scale curve for the nitrogen is inserted in the diagrams, showing parabolic reaction kinetics at all investigated temperatures.

At 800 °C the oxidation kinetics in air and oxygen are parabolic and identical during about one hour. Then the reaction in air accelerates significantly and switches to linear behaviour. After about 3.5 hours the linear reaction coefficient again increases by a factor of two. The oxidation kinetics in oxygen remain parabolic for about 4.5 hours before a deviation to more linear behaviour is observed. The deviation from the parabolic kinetics is caused by the breakaway effect [12] which is strongly accelerated in air due to the influence of nitrogen. This is discussed in more detail in chapter 4.

The behaviour at 1000 °C is quite similar. The transition from parabolic to faster kinetics is earlier (about 200 and 2000 seconds for air and oxygen, respectively), but the kinetics in air are still remarkably faster, although less oxygen is available.

At 1200 °C the reaction in oxygen follows parabolic kinetics during the whole test (no breakaway at temperatures above 1050 °C). An initially slightly enhanced reaction rate is caused by a small temperature increase due to the strongly exothermic reaction. The reaction kinetics in air are somewhere between linear and parabolic. At beginning of the reaction it is slower than in pure oxygen due to the limited oxygen supply.

At 1400 °C the reaction kinetics are even more determined by different oxygen supply in the two gases, and the reaction in pure oxygen is faster than and finally equal to the reaction in air.

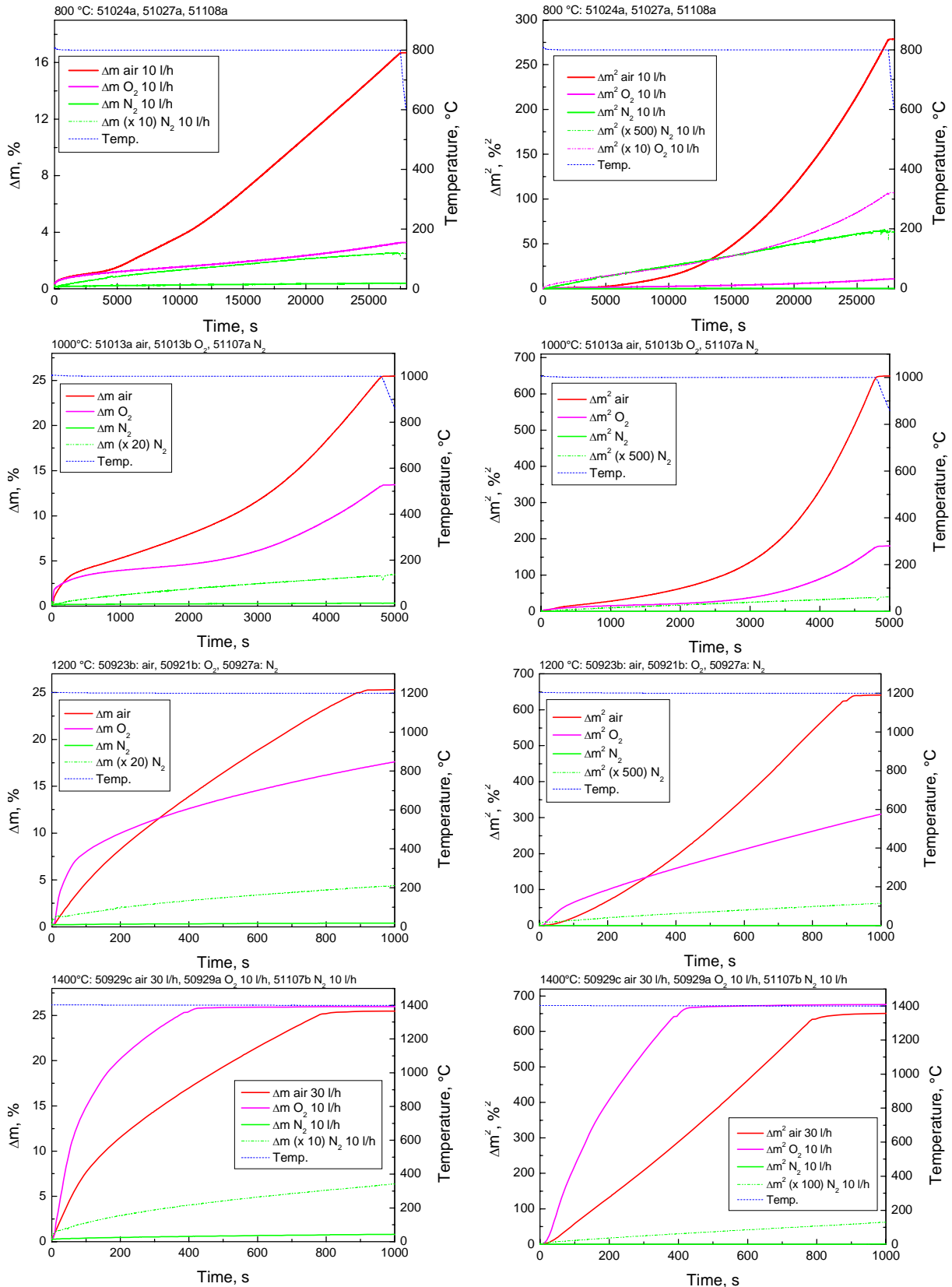


**Figure 8:** Thermo-gravimetric results for the reaction of Zircaloy-4 in oxygen, nitrogen, and air at 800, 1000, 1200, and 1400 °C. Left: mass gain versus time; right: squared mass gain versus time.

The above-mentioned behaviour is also clearly demonstrated by the first derivatives with respect to time, the reaction rates, shown in Fig. 9. Up to 1200 °C the reaction rate in air is always higher than in oxygen after a certain initial time. On the other hand, the oxidation rate in oxygen is higher and finally the same as in air at 1400 °C.

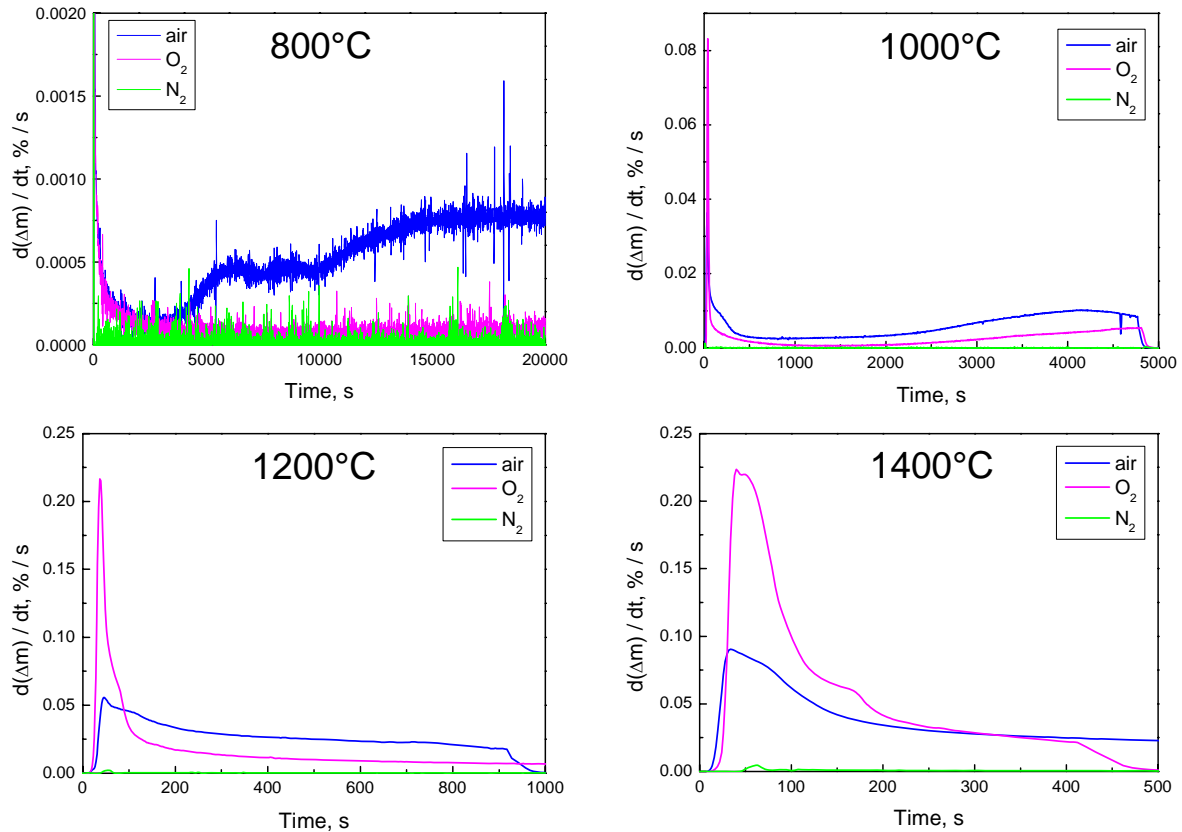


**Figure 9:** Reaction rates of Zircaloy-4 in air, oxygen and nitrogen at various temperatures.

### Post-test examinations

Figure 10 gives an overview on the post-test appearance of the specimens. The macro images reveal the strongest degradation for the specimens oxidised in air, whereas the samples reacted in nitrogen appear as almost unchanged metallic with a more or less golden colour.

A deeper insight can be obtained by the metallographic pictures shown in Fig. 11. Typical breakaway effects, like a wavy interface between metal and oxide phases and circumferential cracks in the oxide scale, are clearly to be seen at the specimens oxidised in air and oxygen at 800 and 1000 °C.

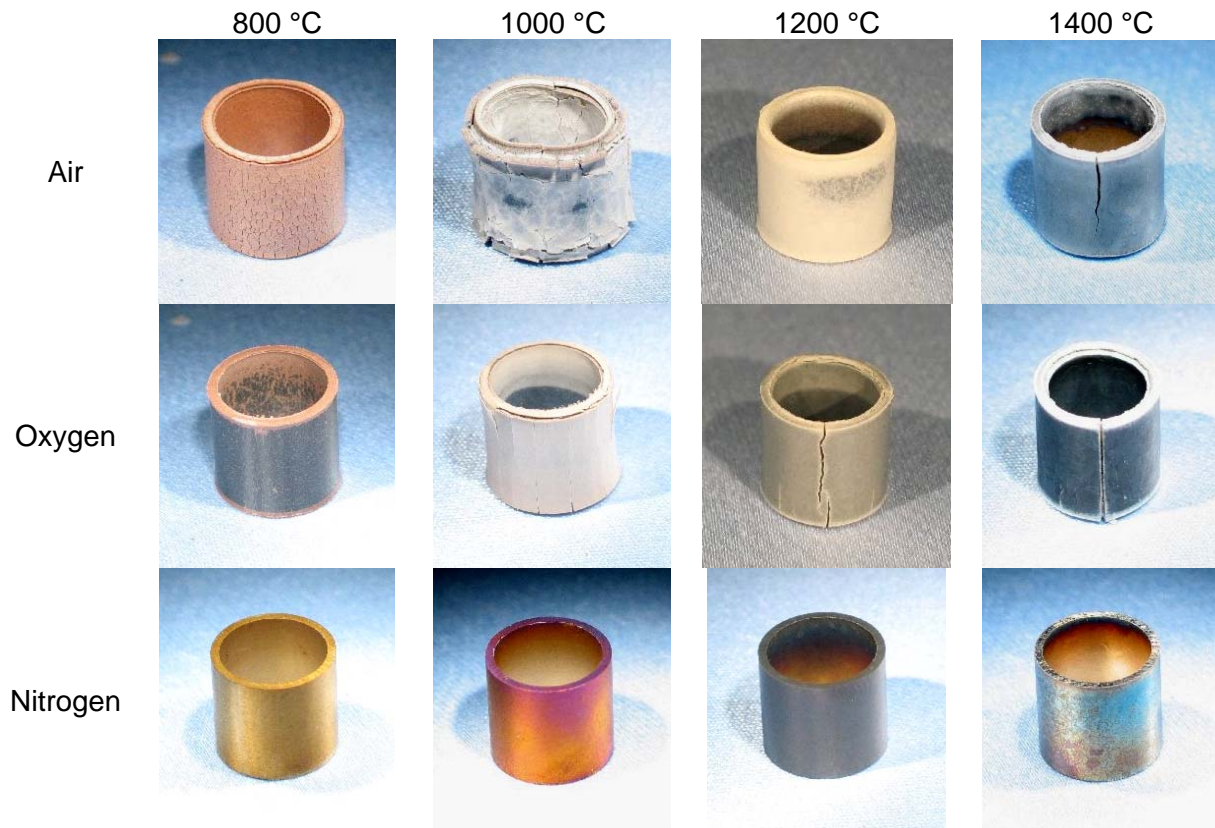


**Figure 10:** Appearance of the specimens after tests in pure atmospheres.

Gold-coloured nitride phases are observed after oxidation in air at all temperatures. Higher magnification is necessary to make visible the nitride at the phase boundary metal-oxide for the 800 °C specimen (see [9]). The specimen oxidised in air at 1400 °C showed only very local formation of nitride at locations where the oxide scale was defect, but was generally very similar to the specimen oxidised in oxygen at that temperature. This tendency of decreasing effect of nitrogen at higher temperatures ( $\geq 1400$  °C) was also confirmed in tests with mixed air-steam atmospheres in the BOX rig, presented below in chapter 3.2.

As already seen in the TG curves, the reaction of Zircaloy-4 with pure nitrogen is only marginal in comparison to air. No nitride at all was detected in such specimens, although they were macroscopically of golden colour. In accordance with the Zr-N phase diagram (see Appendix G) a superficial  $\alpha$ -Zr(N) layer formed at all specimens in pure nitrogen. Note, that the reaction times at 1200 and 1400 °C were much longer for the nitrogen samples in comparison to the ones in oxygen and air. At present, it is not clear if the  $\alpha$ -Zr(N) phase contains also oxygen which could e.g. slowly diffuse through the alumina reaction tube at the higher test temperatures.

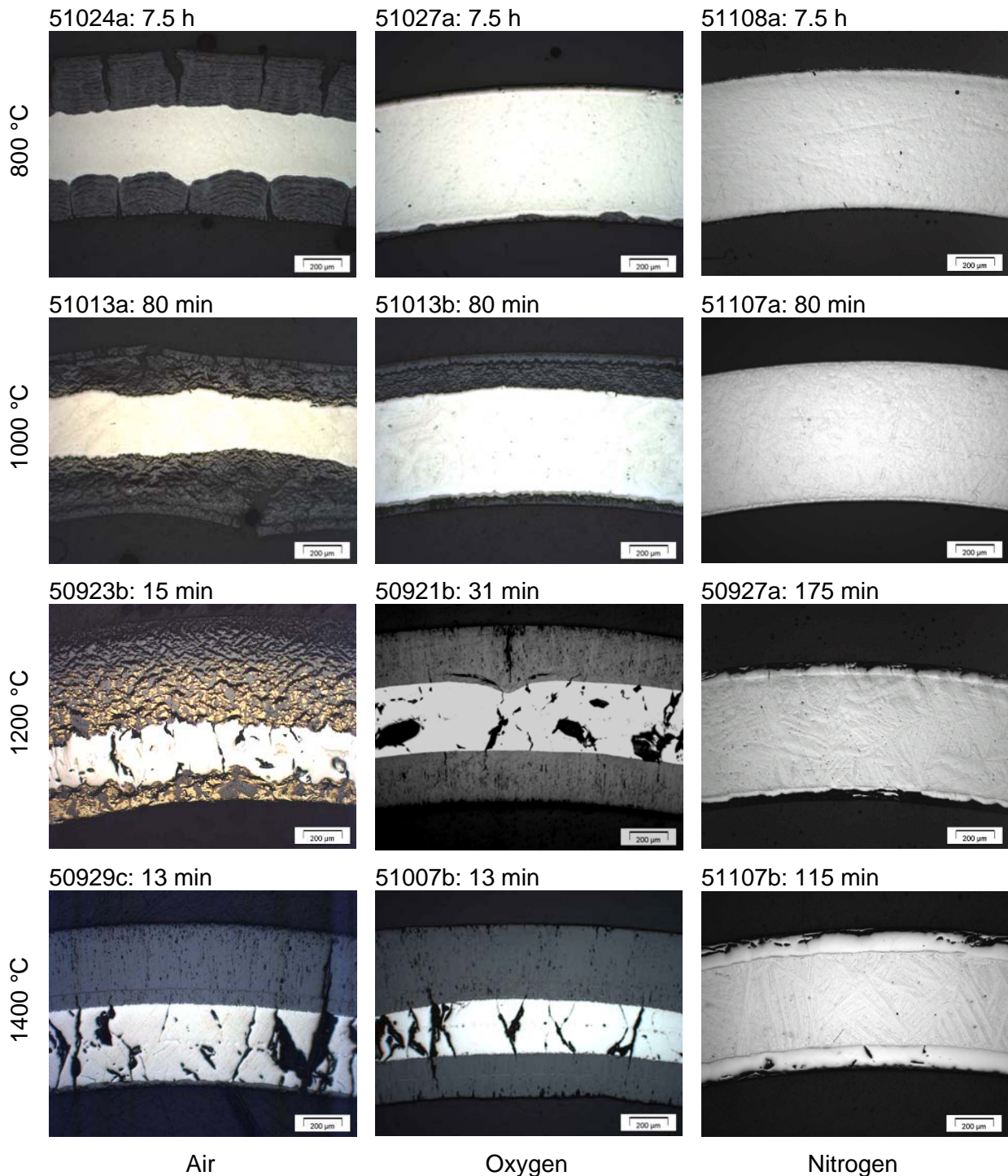


**Figure 11:** Metallographic images of the Zircaloy-4 specimens after reaction in pure atmospheres. The numbers above the pictures indicate test name and approx. time of reaction.

### 3.2 Tests in mixed air-steam atmospheres

An extensive study of the oxidation of Zircaloy-4 in mixed air-steam atmospheres has been conducted in the BOX rig. Between 800 and 1200 °C 1-hour isothermal tests and between 1200 and 1500 °C (with 100 K steps) 10-min isothermal tests under nine different

atmospheres each between and including pure air and pure steam were carried out, giving a total of 81 tests. Tables A1, A2 summarise the main parameters and results of these experiments.

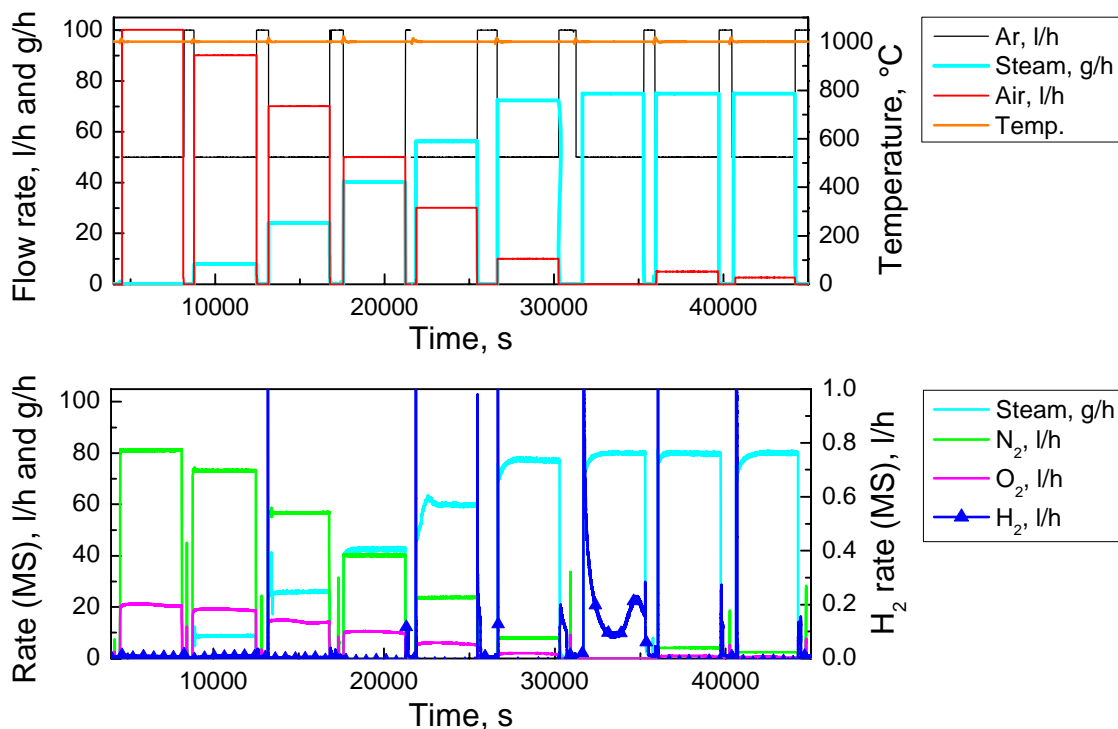
### Mass spectrometer measurements

During all tests the reaction gases in the off-gas system were analysed by mass spectroscopy. Figures 12-14 give some examples at various temperatures and atmospheres.

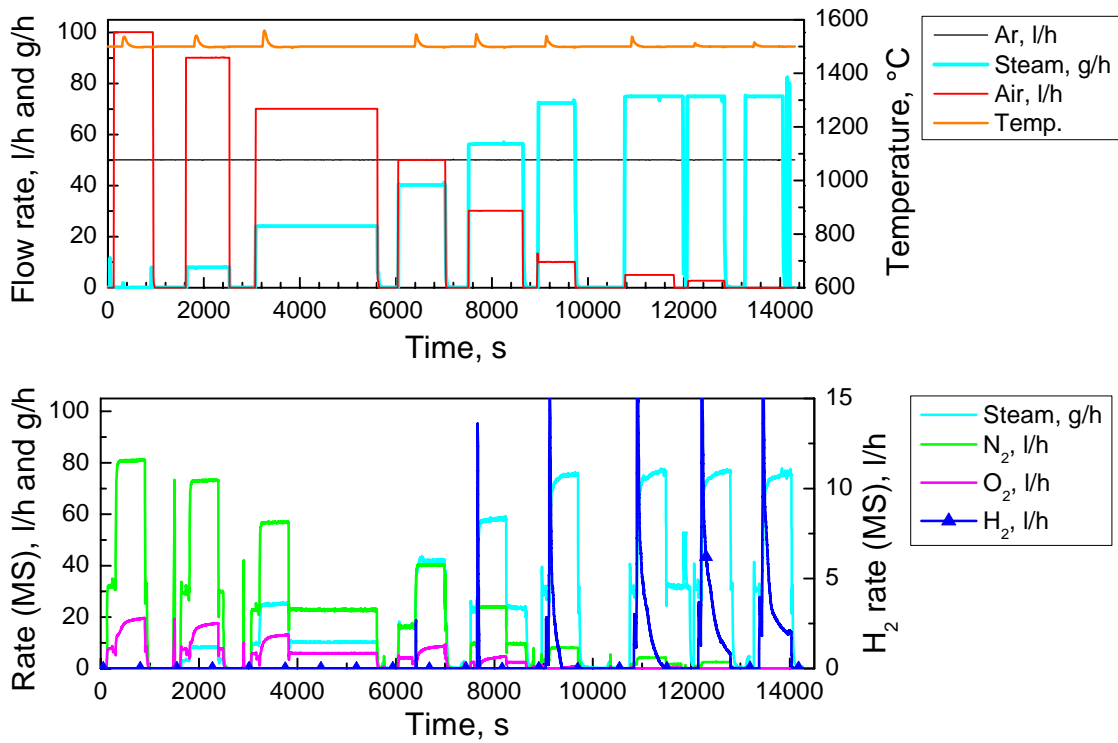
The first two figures show an overview of the test conduct and MS results of the series at 1000 and 1500 °C. At 1000 °C hydrogen is only produced during the test in pure steam; at 1500 °C hydrogen is released in all tests with less than 50 vol% air in the mixture. Under these conditions the oxygen is at least initially completely consumed and steam oxidation can take place. The lower right diagram in Fig. 14 reveals in more detail the transition from oxygen starvation conditions with hydrogen release to conditions with excess oxygen and corresponding suppression of hydrogen production.

Figure 14 also shows the discontinuities in the gas release curves at 1000 °C caused by the breakaway effect, i.e., the transition from dense, protective oxide scales to cracked and less protective oxide scales.

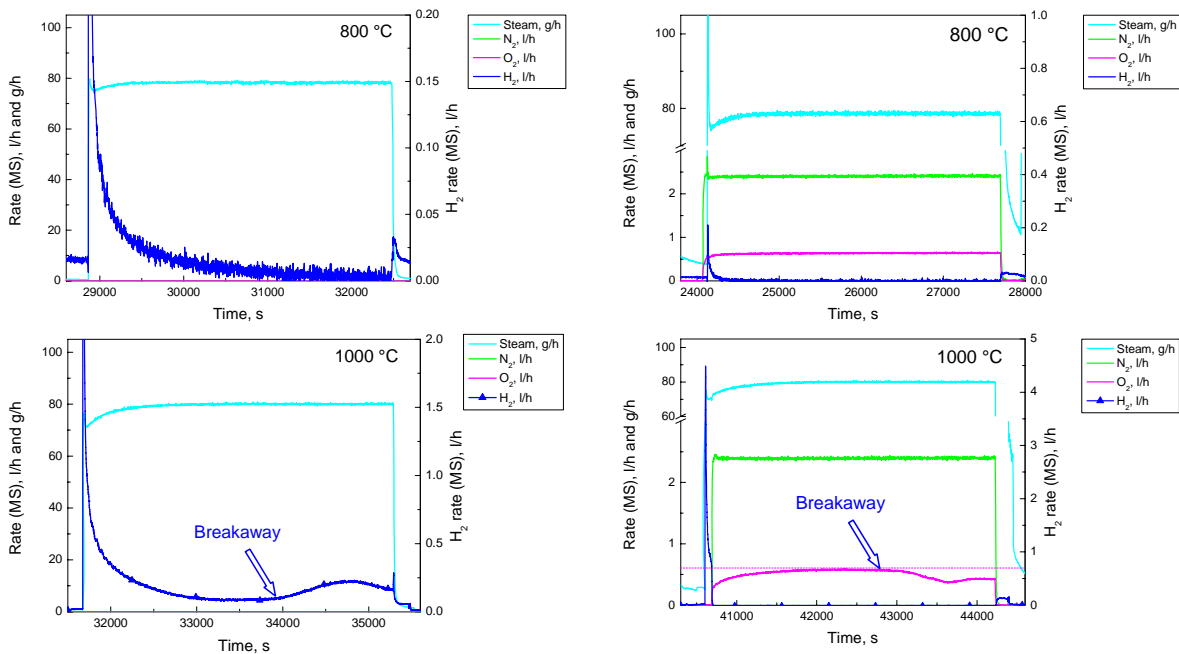
At the high temperatures, an initial temporary temperature increase could not be avoided even by the test procedure described in chapter 2.3 as could be seen in Fig. 13.



**Figure 12:** Test conduct showing gas and steam injection rates and temperature (top) and MS results with flow rates of steam, oxygen, nitrogen, and hydrogen in the off-gas (bottom) for the test series at 1000 °C.



**Figure 13:** Test conduct showing gas and steam injection rates and temperature (top) and MS results with flow rates of steam, oxygen, nitrogen, and hydrogen in the off-gas (bottom) for the test series at 1500 °C.



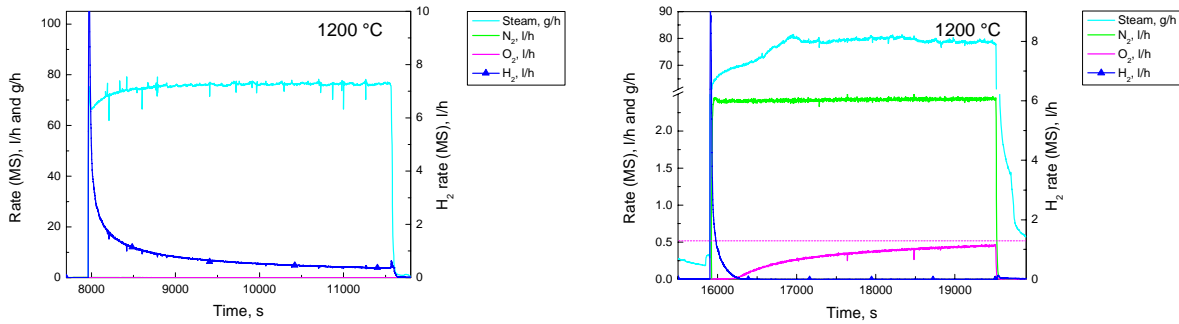


**Figure 14:** Detailed MS results of tests in pure steam (left) and in air-steam mixture with low air content at 800, 1000, and 1200 °C.

**Mass change**

For all tests the masses of specimens were measured before and after oxidation. For the reasons described above, hydrogen release could not be used as measure for the degree of oxidation as in experiments under pure steam, so, the mass gain is the only integral figure of oxidation.

At 800 °C, no influence of air in the mixture was observed except for pure air which caused a ca. twofold higher mass gain after 1 h isothermal oxidation. At 900 °C, a first influence of air was detected at 90% air. Figure 15 shows, that at higher temperatures a more continuous transition between pure steam and pure air is observed, i.e., even low amounts of steam in the mixture influence the oxidation kinetics. The breakaway effect causes the more scattered curve of the 1000 °C series, which is moreover higher than expected in comparison with the series at the other temperatures.

The curves of the 10-min test at the higher temperatures (Fig. 15, right) are continuous with maxima at approx. 80% air. The dependency of oxidation on composition of the atmosphere decreases with temperature and is remarkable small for the 1500 °C series.

These results are confirmed by and can be better understood by means of the post-test examinations presented in the next chapter.

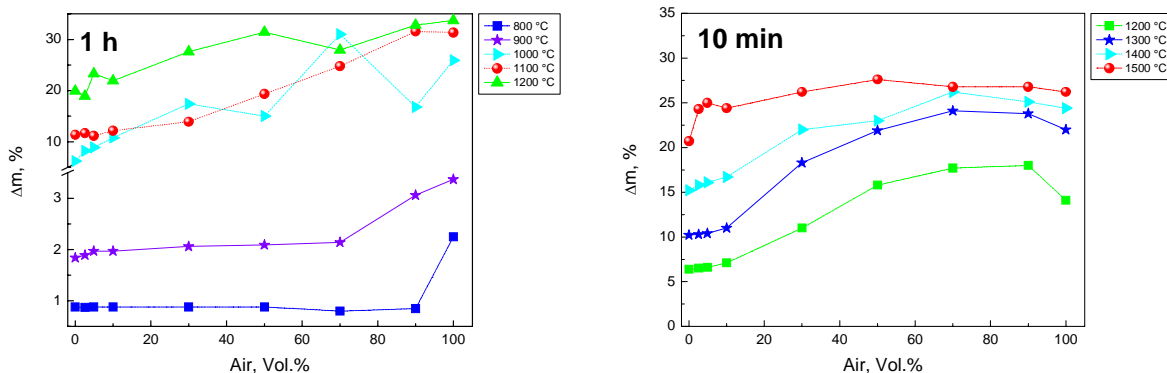


**Figure 15:** Mass gain of specimens after isothermal tests 1 h at 800-1200 °C (left) and 10 min at 1200-1500 °C (right) in dependence on the composition of the air-steam mixture.

### Post-test examinations

Macro-photographs as well as microscopic images of all 81 specimens are compiled in Appendix C. Here, only some characteristic images are shown for tests at various temperatures.

As already seen in the mass gain diagram (Fig. 15), there was no effect of air addition to steam on the oxidation of Zircaloy-4 during the one-hour isothermal tests at 800 °C. A significantly higher mass gain was only obtained for pure air which is also confirmed by the PTE. The oxide scale of that specimen is much thicker and more porous than of all other specimens of this series. Small amounts of gold-coloured nitride were observed in the oxide scale near the phase boundary metal-oxide (better seen with higher magnifications). No nitride at all was found in all other specimens oxidised at 800 °C. The wavy interface between metal ( $\alpha$ -Zr(O)) and oxide for the specimens with steam is typical for pre-breakaway conditions.

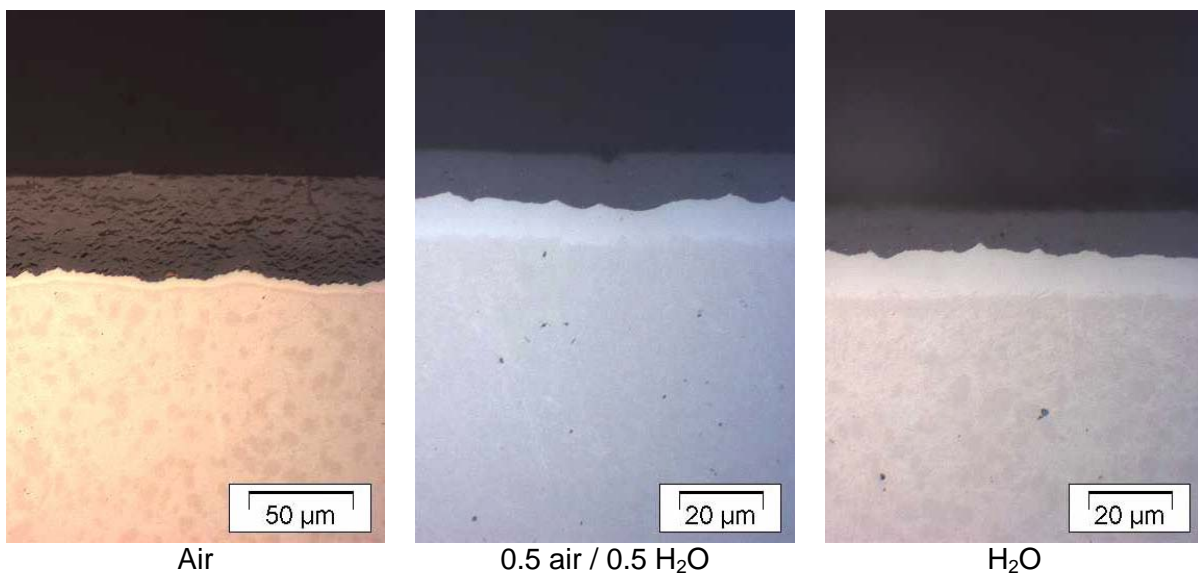


**Figure 16:** 1 h, 800 °C: Optical microscopy images of selected specimens.

The influence of air in the atmosphere is stronger at 900 °C. Here, locally significant nitride formation near the metal-oxide interface was observed for pure air as well as 90/10 (by volume) and 70/30 air-steam mixtures. Much smaller amounts of nitrides were seen down to 30 vol% air, whereas less air in the mixture had no effect on the quality of the oxide scale.

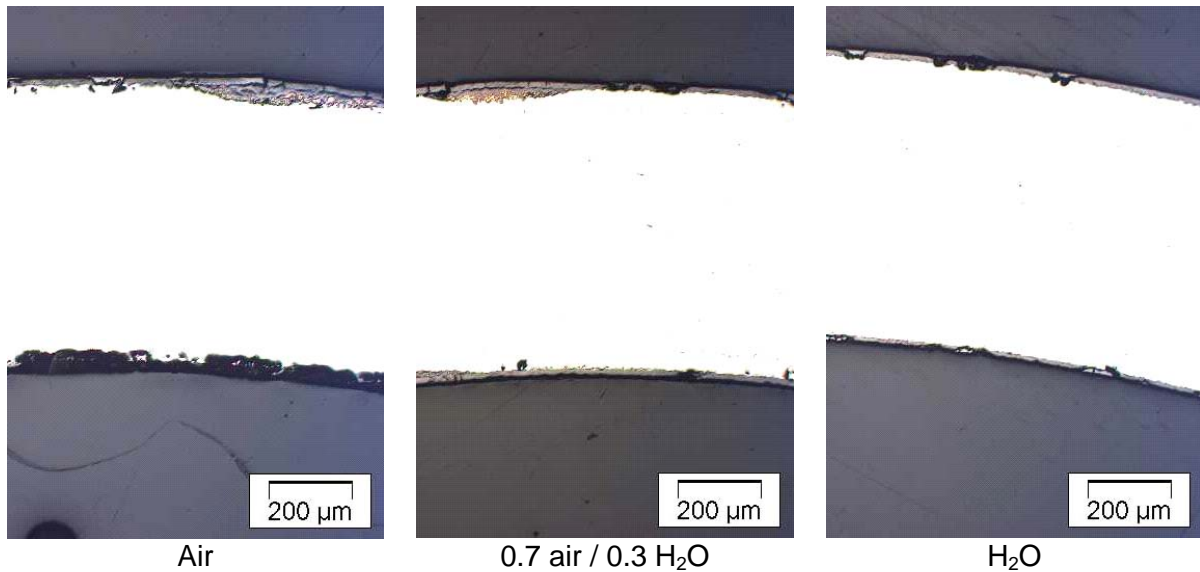


**Figure 17:** 1 h, 900 °C: Optical microscopy images of selected specimens.

At 1000 °C, the influence on air on the degradation of Zircaloy during oxidation increases dramatically. Nitride phases were found in all specimens except for that oxidised in pure steam. The image series in Appendix C shows that almost complete oxidation occurred in pure air and the 90/10 and 70/30 mixtures, but strongly enhances degradation was also found for the 50/50 mixture. The magnified photos (Fig. 18) again reveal nitride formation initiated at the oxide-metal interface for the specimens oxidised in pure air and the mixtures and the characteristic appearance for breakaway oxidation with wavy phase boundary and circumferential cracks in the oxide layer. The dark-field image in Fig. 19 demonstrates quite different oxide morphology near the metal and near the external surface. The latter is not mixed (anymore) with nitride and obtains a huge number of micro-cracks indicated by the bright contrast of the dark-field image. The outermost ca. 30 µm oxide scale is of columnar structure and was formed at first before the transition to breakaway and nitrogen attack.

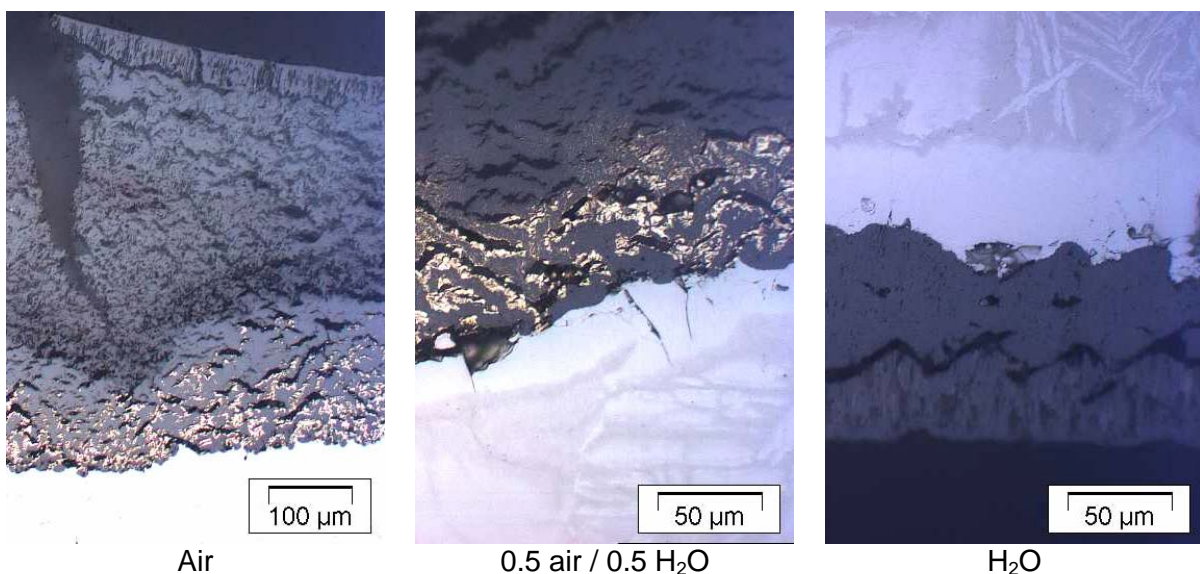


**Figure 18:** 1 h, 1000 °C: Optical microscopy images of selected specimens.

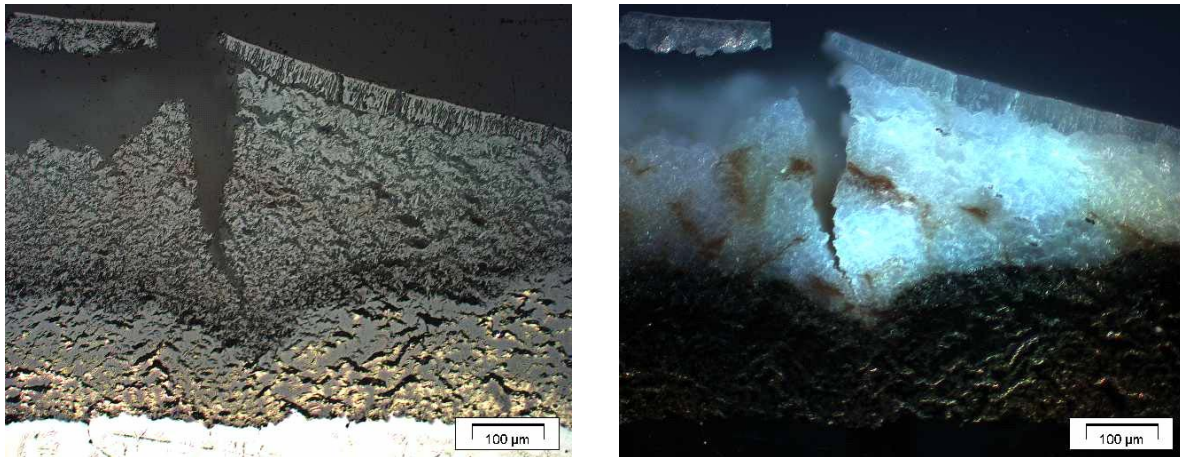


**Figure 19:** Bright-field (left) and dark-field (right) image of the same position of the specimen oxidised one hour at 1000 °C in air.

The specimens are completely oxidised in air and in mixtures with high air content after the one-hour tests at 1100 and 1200 °C (see Appendix C). At these and higher temperatures breakaway does not occur and the metal-oxide interface of the specimens with less than 50% air at 1100 °C and less than 30% at 1200 °C in the mixture is smooth and no nitrides were observed.

The attack of nitrogen takes place locally at cracks or other imperfections in the oxide scale as can be seen from the images of the short-time tests in Appendix C and Fig. 20. After 10 min at 1300 °C in 30/70 air-steam mixture (here as an example) local defects caused by nitrogen attack could be seen at different positions of the same specimen at different states of development. Obviously the first access of nitrogen via defects in the oxide occurred at different times. The degraded areas consist of oxide-nitride mixtures or in the later stage (right image in Fig. 20) only of porous oxide formed by re-oxidation of nitride.

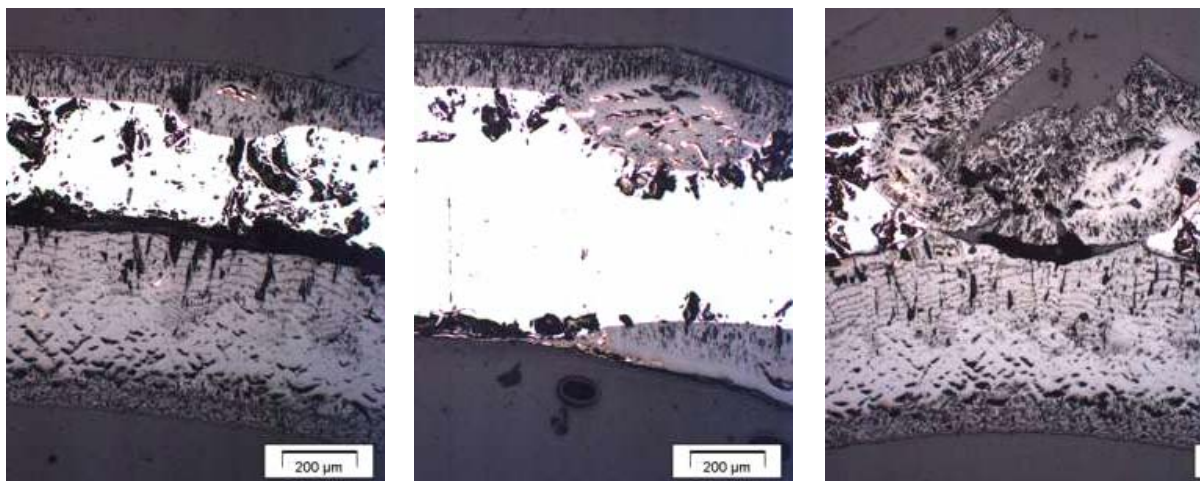


**Figure 20:** 10 min, 1300 °C: Three images at different positions of the specimen after oxidation in 30% air and 70% steam.

The local initiation of nitrogen attack and the transition of the specimens to a layer-like structure with increasing temperature (or time) is also demonstrated in Fig. 21 showing

specimens after 10 min oxidation in pure air at 1200-1500 °C. Even more interestingly, this series of images shows a coarsening of morphology of the oxide with temperature and finally a reversal of the trend of increasing degradation with raising temperatures at 1500 °C. Here, the oxide scale is dense and looks very similar to that obtained in pure steam. This tendency was already observed in the thermo-gravimetric experiments described in chapter 3.1 and is confirmed by the results given in Table 1 which gives a summary of the metallographic images compiled in Appendix C. With increasing temperature up to 1300 °C less air is necessary to detrimentally influence the oxide scale growth, at 1400 °C this tendency is stopped, and at 1500 °C no detrimental effect of nitrogen was seen at all – at least during the test duration of 10 min.

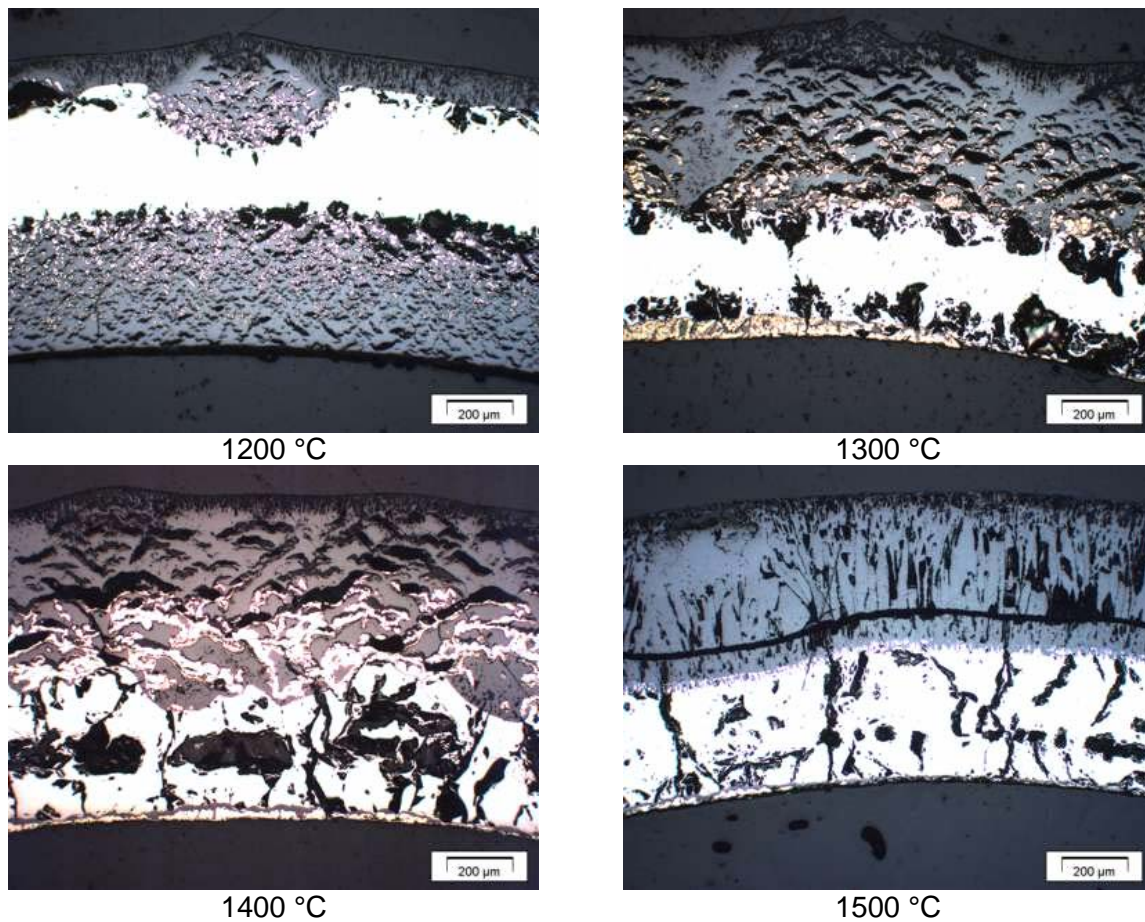


**Figure 21:** Comparison of specimens oxidised 10 min in pure air at various temperatures.

**Table 1:** Influence of temperature and composition of the atmosphere on the degradation of the oxide scale.

Time, min	Temperature, °C	Transition to strongly degraded oxide scale at air content in mixture*
1 h	800	0.9 – 1.0
	900	0.5 – 0.7
	1000	0.1 – 0.5
	1100	0.3 – 0.5
	1200	0.1 – 0.3
10 min	1200	0.1 – 0.3
	1300	0.1 – 0.3
	1400	0.3 – 0.5
	1500	no

\* The oxide scale is intact or only slightly degraded at the lower value and strongly degraded at the higher value.

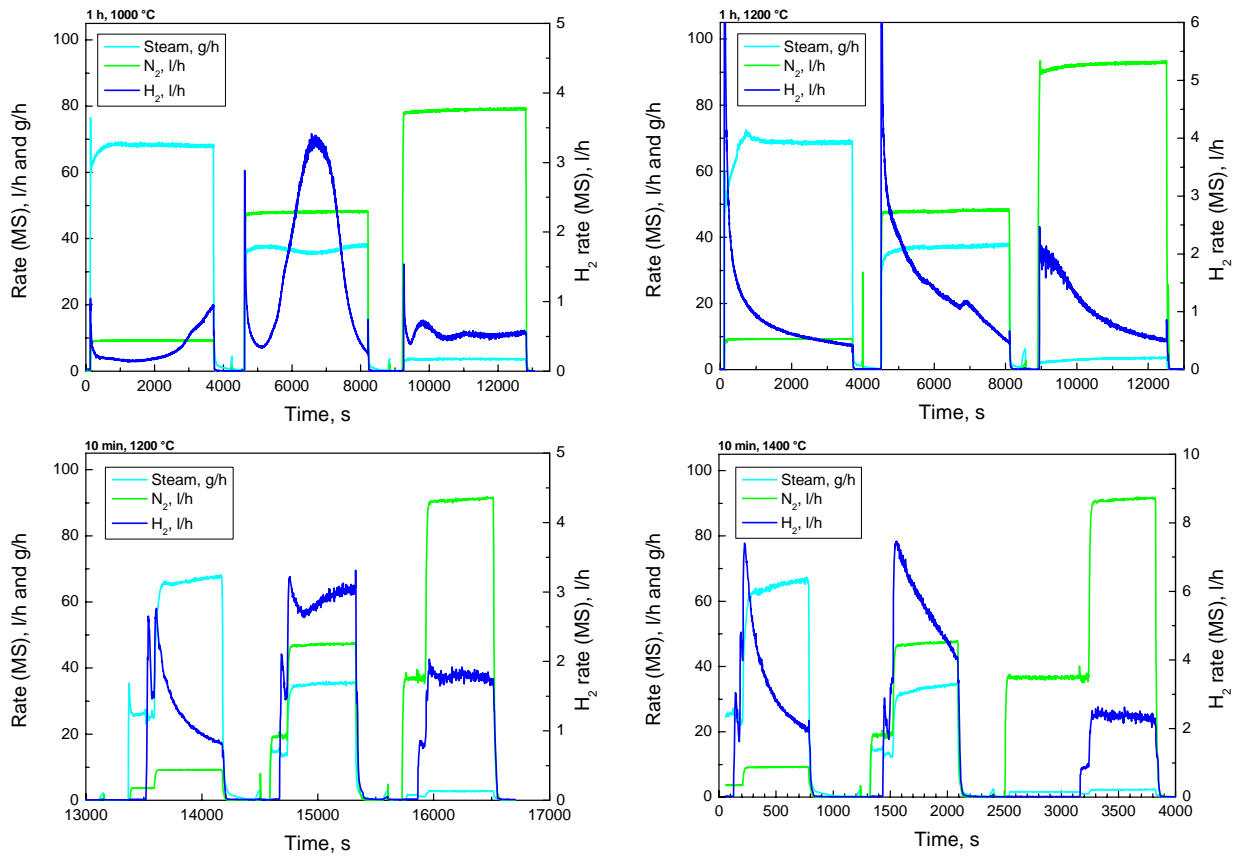
### 3.3 Tests in mixed nitrogen-steam atmospheres

Similar tests like described in the previous chapter have been performed in nitrogen-steam mixtures. Such atmospheres may be present 1) when all oxygen is consumed in the lower part of a fuel bundle, i.e. under oxygen starvation conditions or 2) in BWRs where containments are filled with nitrogen for inerting and safety injection systems are pressurised by nitrogen.

This test series was less extensive than the previous one; isothermal tests have been conducted at 1000 °C (1 h), 1200 °C (1 h, 10 min), and 1400 °C (10 min) in mixtures with 0, 10, 50, 95, and 100 vol% nitrogen in the mixture. Detailed test parameters and results are compiled in Table A3.

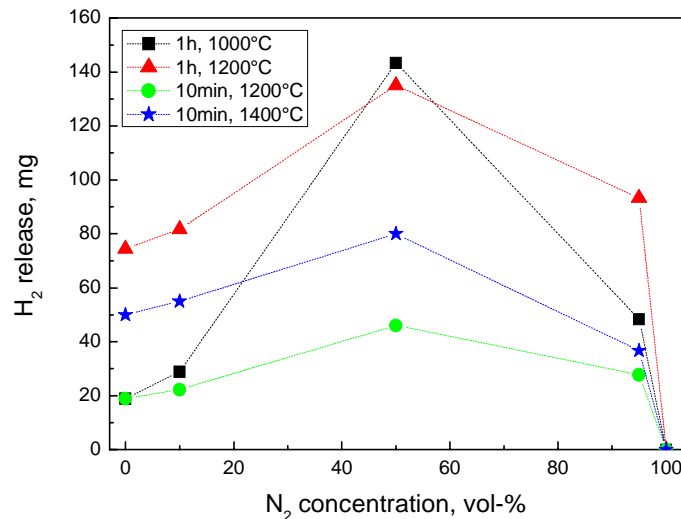
#### **MS measurements**

Figure 22 summarises the MS results of all test in mixed nitrogen-steam atmospheres. The main gas of interest is hydrogen, because it is an indicator for the reaction kinetics. At 1000 °C and high and medium steam content, the reaction starts with a parabolic kinetics which turns into a much faster one after 33 and 9 min, respectively. This is caused by the breakaway effect accelerated by the presence of nitrogen. A more or less linear behaviour is observed for the mixture with 95% nitrogen in the mixture. As expected, no breakaway related effect was seen at the higher temperatures. The reaction kinetics are somewhere between parabolic and linear with the tendency to more linear behaviour for low steam contents in the mixture.



**Figure 22:** Off-gas analyses by MS during tests in mixed nitrogen steam atmospheres.

Interestingly, the highest amounts of hydrogen were produced in tests with 50/50 mixtures. In most test series more hydrogen was produced even during tests with only 5% steam and 95% nitrogen than in tests under pure steam, as could be seen from Fig. 23.



**Figure 23:** Integral hydrogen release during isothermal reaction of Zircaloy-4 in nitrogen-steam mixtures.

### Mass change

The diagram with the mass gain vs. nitrogen concentration in the gas mixture (Fig. 24) looks very similar to the one with hydrogen release (Fig. 23). Again, maximum values are obtained for the 50/50 mixture. The comparison of the data of these two diagrams also reveals that a significant fraction of the mass gain (up to 50%) must have been caused by the uptake of nitrogen.

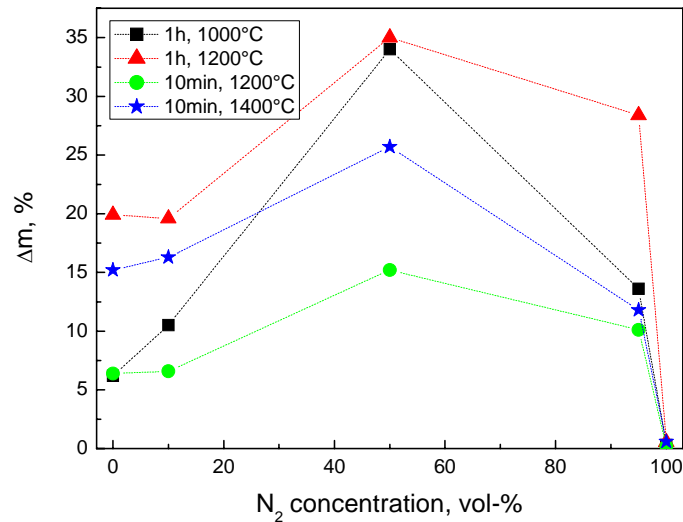


**Figure 24:** Mass gain of Zircaloy-4 samples after reaction in mixed nitrogen-steam atmosphere.

### Post-test examinations

The macro-photos and microscopic images of all specimens are compiled in Appendix D. The reference test series with specimens reacted in pure nitrogen was conducted separately; please note that the magnification of these photos is slightly different from the others.

No pictures were taken of the specimens reacted in pure nitrogen, because after the very small mass gains no interesting features were expected. Reference is made to Fig. 11 for samples after reaction in nitrogen.

As already seen in Figs. 23 and 24 the strongest degradation of the specimens occurred during tests in 50/50 mixtures. The Zry-4 tube segment after the test 1 h at 1000 °C was strongly swollen by more than 30%, and the one after the 1200 °C test (1 h) was so brittle, that it broke in pieces during handling. Both specimens were almost completely oxidised. Though less pronounced, this tendency was also seen after the 10-min tests at 1200 and 1400 °C where the specimens after annealing in 50/50 mixtures featured the most degraded (bumpy and spotty) surface.

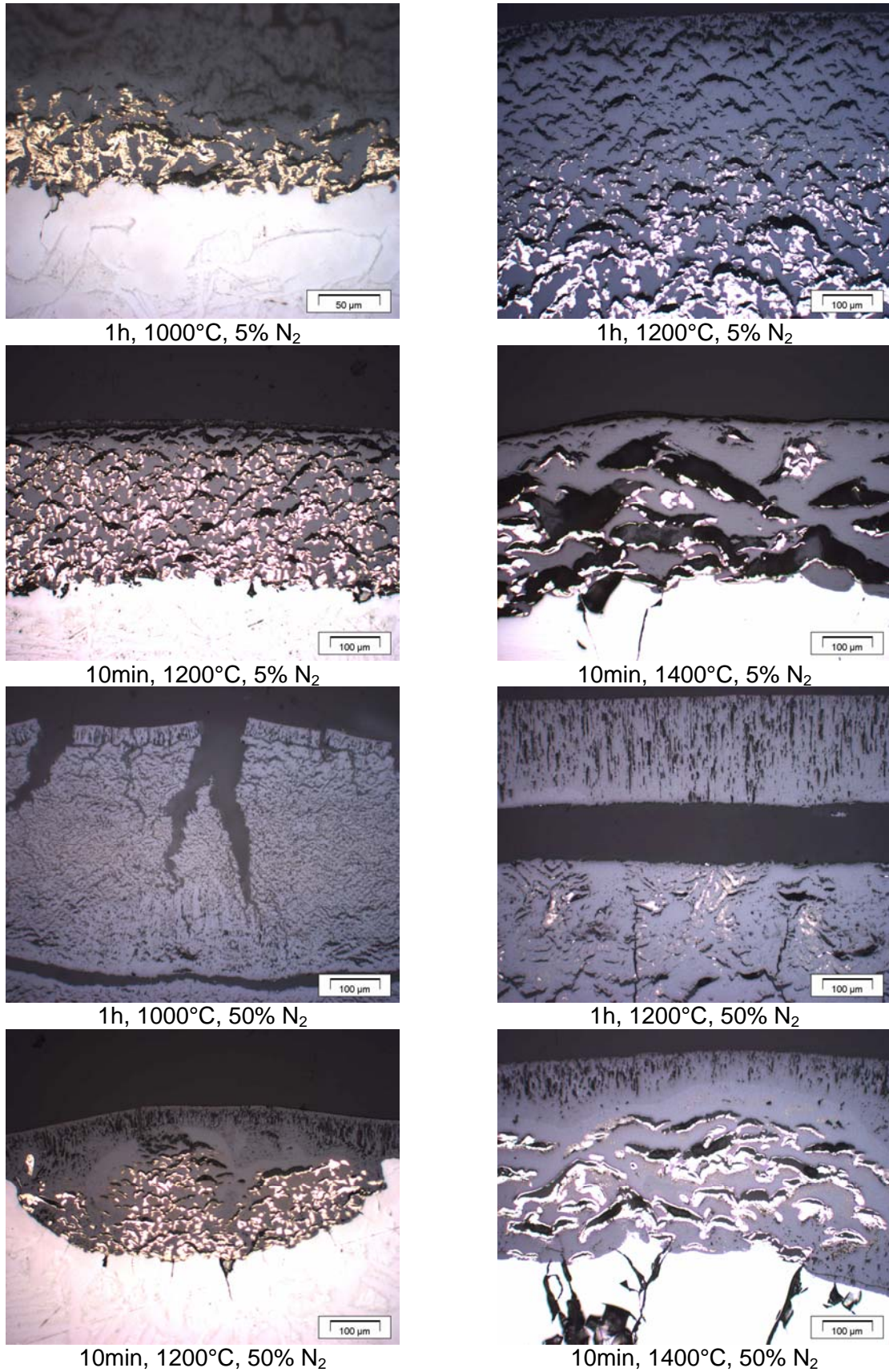


**Figure 25:** Microscopic details of oxidised Zircaloy-4 specimens after reactions in 5/95 and 50/50 nitrogen-steam mixtures.

The metallographic images look quite similar to the ones in mixed air-steam atmospheres. The degradation of the oxide scales is even more pronounced after treatment of Zircaloy-4 in nitrogen-steam mixtures in comparison to air-steam, especially at 1000 °C. Except for the high temperatures (1200, 1400 °C) and low nitrogen content (10%) the oxide scales are very porous and cracked. Nitride precipitations are found in the oxide scale near the phase boundary metal-oxide. Local nitrogen attack is observed especially after the short-time tests. Furthermore, also here a coarsening of the oxide microstructure is observed with raising temperature. Figure 25 gives some more detailed metallographic images.

### **3.4 Influence of pre-oxidation on subsequent oxidation in air and nitrogen**

The direct access of air to metallic cladding during any kind of hypothetical accidents in nuclear reactors, storage pools, or transport casks is very unlikely. In any case, the cladding tubes will have been oxidised in water/steam during operation and/or the initial phase of the accident. Therefore, a separate-effects test (SET) program on the influence of pre-oxidation on the reaction in air and nitrogen has been performed. Of special interest was to which extent an oxide scale formed in steam can protect the cladding from nitrogen attack and the associated strong degradation described in the previous chapters.

Most of the work was performed in the frame of a diploma thesis and is well documented in the corresponding report [9]. So, here a summary of this work will be given together with some results obtained in preparation of the diploma task and arising from results of the thesis.

The majority of the experiments were conducted in the thermal balance with pre-oxidation in argon-oxygen mixtures. Only one test series at 1200 °C was performed in the BOX rig with pre-oxidation in steam to confirm the similarity between steam and oxygen. Tests have been conducted without and with pre-oxidation with the degree of pre-oxidation as parameter. The tests were aimed at maximum 25% mass gain to allow for meaningful metallographic post-test examinations including metal, oxide, and nitride phases.

#### ***First tests at 1000 and 1100 °C***

A series of 80 min isothermal tests at 1100 °C has been performed under oxygen, air, and nitrogen, with and without pre-oxidation together with one test with pre-oxidation and subsequent oxidation in air at 1000 °C for comparison. The atmosphere was switched from pure oxygen to air when a mass gain of 2%, corresponding to about 20 µm oxide, was obtained. Actually, the pre-oxidation phase lasted slightly longer due to the delay in gas exchange in the tubing and furnace.

Figure 26 gives one example of test conduct in the thermal balance showing temperature, mass gain, and off-gas composition for the test with pre-oxidation and succeeding reaction in air. Relevant test parameters and the main results of all tests are compiled in Table A5 in Appendix B.

The TG curves of all tests of this series are shown in Fig. 27. The results obtained in the tests without pre-oxidation are in agreement with the results presented in chapter 3.1, i.e.

oxidation in air is much faster (and non-parabolic) than in oxygen; and reaction rates in nitrogen are much lower than in the oxygen containing gases. The results of the experiments with pre-oxidation are quite opposite: on the one hand, pre-oxidation causes equalisation of the air curve to the one in pure oxygen. Obviously, the pre-existing oxide scale suppresses the detrimental effect of nitrogen in the air. Reaction kinetics in both tests are parabolic. On the other hand, pre-oxidation leads to an acceleration of the reaction in nitrogen by more than a factor of 10. The observed even faster than linear reaction kinetics in the test with pre-oxidation, after an initial parabolic period, and subsequent reaction in air at 1100 °C, can be explained by the already-mentioned breakaway effect in combination with nitrogen attack.

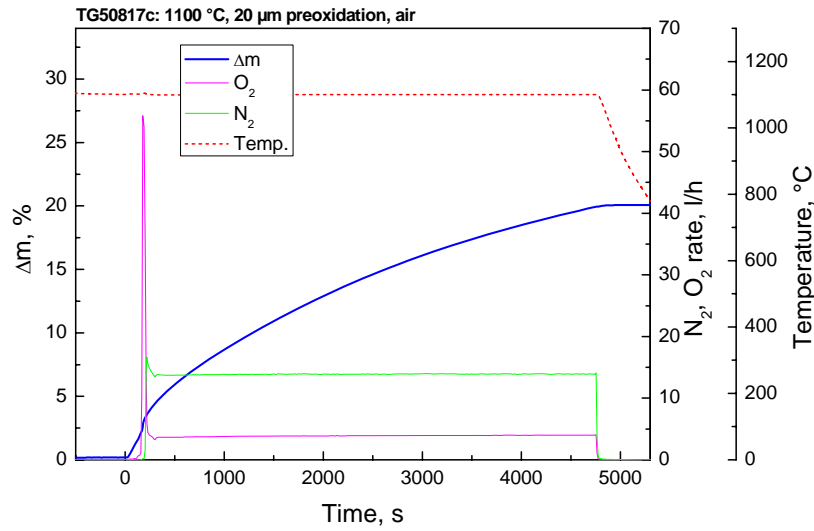


**Figure 26:** Test conduct and results of an isothermal test at 1100 °C with pre-oxidation in oxygen and succeeding reaction in air.

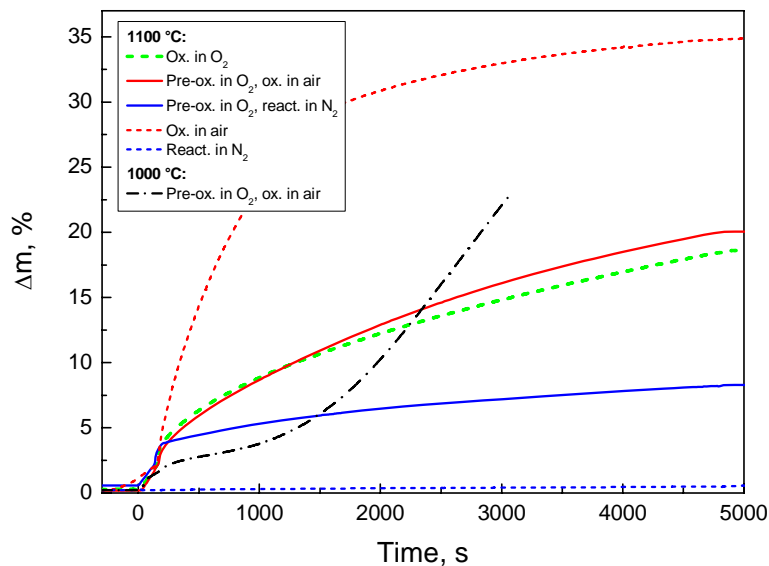


**Figure 27:** Mass gain of Zircaloy-4 specimens during oxidation in oxygen, nitrogen and air, with and without pre-oxidation in oxygen.

The results shown in Fig. 27 are impressively confirmed and illustrated by the metallographic images compiled in Fig. 28. The through-wall cross-sections of the specimens without pre-oxidation and under the same conditions regarding temperature and time, look completely different from each other as already seen in Fig. 11.

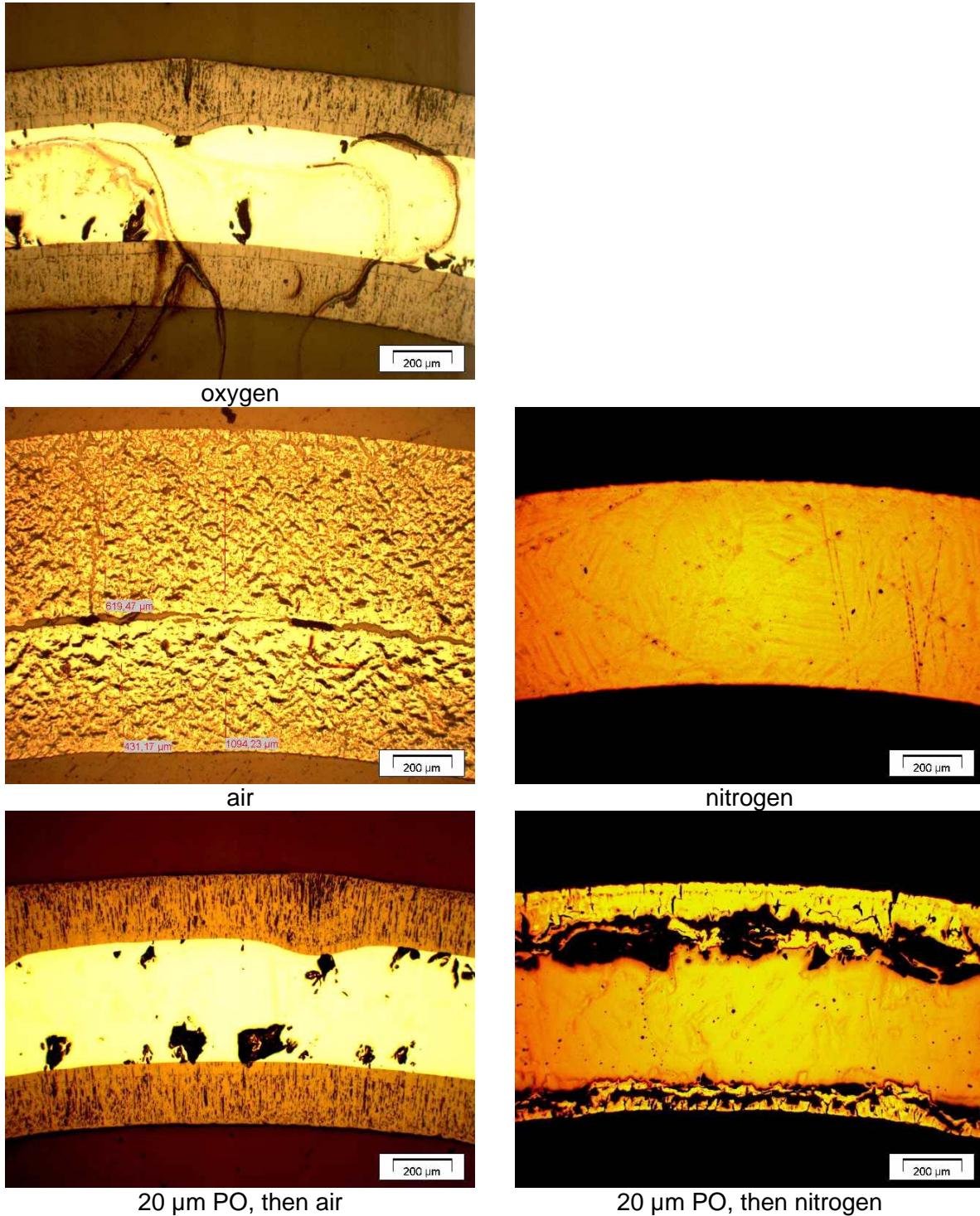


**Figure 28:** Metallographic images of Zry-4 specimens after 80 min reaction in oxygen, air, and nitrogen, with and without pre-oxidation (PO).

The oxide scale formed in oxygen is dense and protective; self-healing effects can be observed at a radial crack and about 330  $\mu\text{m}$  metal phase is left. The specimen oxidised in air is completely oxidised as could be expected from the mass gain of 35 wt%. The oxide is very porous; cracks are mainly aligned circumferentially. No scale formation at all could be observed at the sample reacted in nitrogen atmosphere.

Pre-oxidation obviously leads to a further growth of the dense oxide scale in case of subsequent air oxidation. The oxide layers obtained in oxygen and air after pre-oxidation look very similar. Strong formation of external nitride is found for the pre-oxidised specimen after annealing in pure nitrogen. So, as already recognised from the TG curves, from the degradation point of view, pre-oxidation has a positive effect in case of subsequent air ingress, but a negative one in case of subsequent nitrogen access.

### ***Summary of tests at 800, 1000, 1200, and 1400 °C***

A large number of systematic experiments on the influence of pre-oxidation in oxygen on the subsequent reaction in air and nitrogen, respectively, at temperatures 800, 1000, 1200, and 1400 °C have been conducted using the thermal balance in the frame of Ziegler's diploma thesis [9]. Here, the main results of this work are summed up. Metallographic images of all relevant tests are compiled in Appendix E.

Most of the experiments were done with open specimens. Due to different behaviour of the inner and outer surfaces of these specimens especially after short pre-oxidation times, some tests were conducted with specially prepared closed specimens (see chapter 2.2).

At 800 and 1000 °C, i.e. in the breakaway regime, pre-oxidation caused a delay of the transition from parabolic to linear or even faster kinetics. The left diagram in Fig. 29 shows that the TG curves in air initially follow the curve obtained in pure oxygen. After a delay time of about 5000 sec the reaction rates increase and conform to the curve obtained in pure air. The metallographic images (Appendix E) show strongly degraded oxide scales with a dense external layer which was initially formed and nitride precipitates near the boundary oxide-metal. Nitrogen attack obviously occurred due to the breakaway effect.

At higher temperatures (1200, 1400 °C) pre-oxidation prevents nitrogen attack and the oxidation kinetics continue to be parabolic even after change from oxygen to air flow as it is demonstrated on the right diagram in Fig. 29. The pre-oxidation phase in these tests was very short in comparison with the total duration of the experiments.

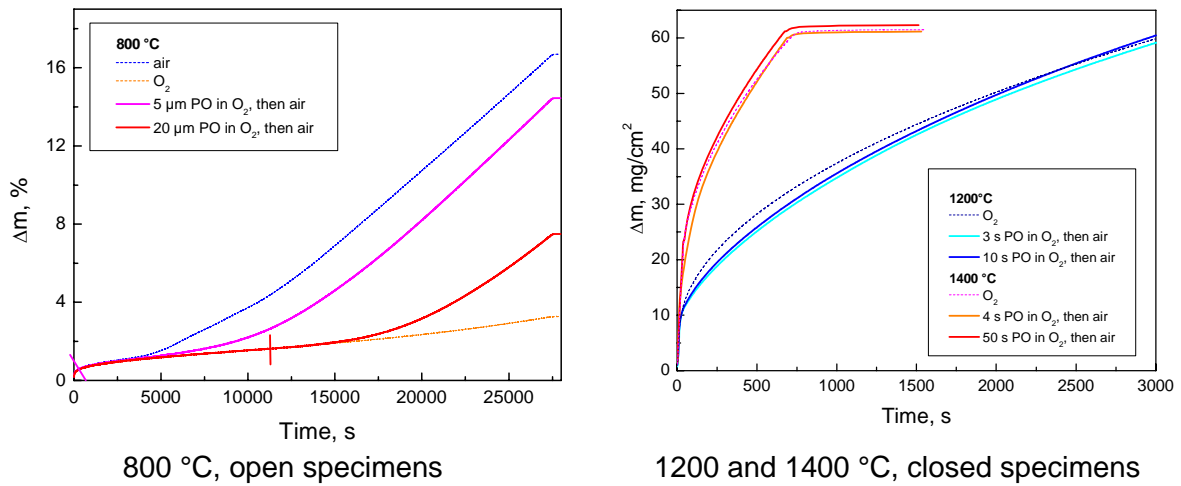


**Figure 29:** Influence of pre-oxidation on subsequent oxidation in air. The vertical lines indicate the transition from pre-oxidation to reaction in air.

Reaction rates in nitrogen are significantly higher after pre-oxidation in oxygen in comparison to fresh metal, but seem to be independent on the degree of pre-oxidation as can be seen in Fig. 30. The diagram compares reaction rates  $dm/dt$  of Zircaloy-4 in pure nitrogen in dependence on the degree of pre-oxidation at 1200 °C as an example. Such behaviour was observed at all temperatures investigated. Contrary to the tests in air, nitride phases were formed mainly at the external surface of the oxide layer (see images in Appendix E).

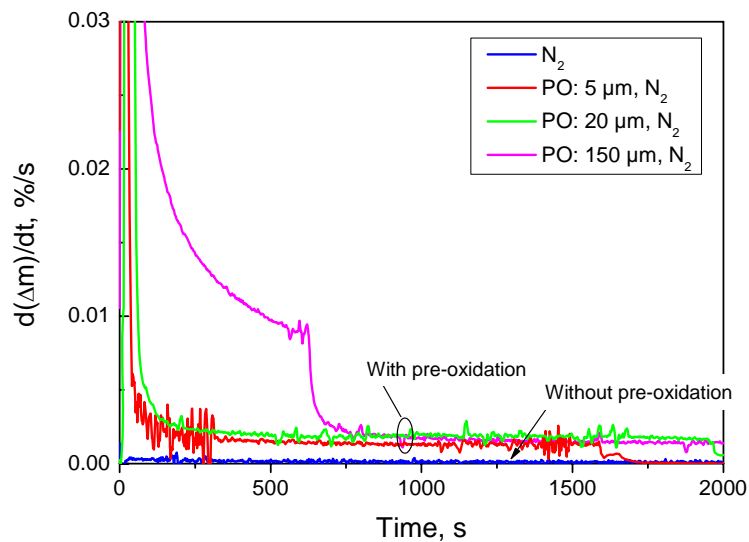


**Figure 30:** Influence of pre-oxidation on subsequent oxidation in nitrogen.

Some words have to be said about the metallographic images of the open specimens after tests at 1200 and 1400 °C and short PO times (see Appendix E). A completely different appearance was observed for the external and internal surfaces of the open specimens. Short pre-oxidation in oxygen and subsequent oxidation in air led to a more or less dense external oxide scale and a very porous internal oxide mixed with nitride. Reaction of pre-oxidised specimens in nitrogen caused the formation of an external nitride on oxide layer and only a thin  $\alpha$ -Zr(N) phase internally. So, in both cases the external surfaces behaved like pre-

oxidised ones and the internal like fresh metal surfaces. Obviously, the special configuration of the specimens on the sample plates and the gas flow from the bottom to the top caused only significant oxidation of the outer surfaces and let the inner surfaces un-oxidised for short pre-oxidation phases. These "mixed effects" were the main reason to manufacture closed specimens to repeat some of the tests under better defined boundary conditions. The images on the last page of Appendix E clearly demonstrate that even a short period of pre-oxidation effectively prevents detrimental effects during subsequent oxidation in air. In fact, only for one specimen of this series (1400 °C, 4 sec PO) local formation of nitride at the metal-oxide interface was observed.

### ***Test with pre-oxidation in steam at 1200 °C***

One experimental series at 1200 °C was performed in the BOX rig with pre-oxidation in steam and following reaction in air and nitrogen, respectively, to check the assumption that pre-oxidation in oxygen and steam are very similar. All tests took 50 min with 0, 1, and 5 min pre-oxidation in steam. For comparison, three specimens were only oxidised in steam 1, 5, and 50 min. Figure 31 gives an example for the test conduct by means of the mass spectrometer measurements. Post-test appearances as well as microscopic images (with bright-field, dark-field, and polarised light illumination) of all specimens are shown in Appendix F.

The results of this test series confirm the results obtained in the thermal balance with pre-oxidation in oxygen. On the one hand, the oxide scale formed during pre-oxidation protects the metal from being attacked by nitrogen in case of subsequent reaction in air. On the other hand, pre-oxidation and following reaction in nitrogen leads to a strongly degraded oxide scale, almost completely converted into nitride.

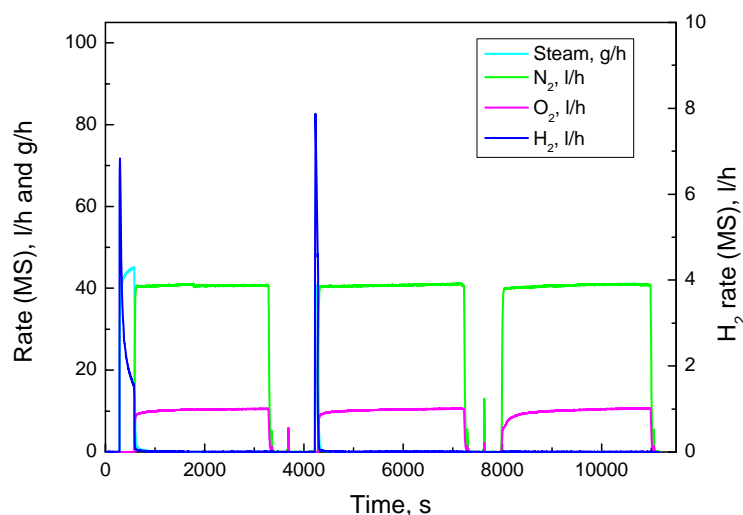


**Figure 31:** Off-gas analysis by MS for the tests with 5, 1, and 0 min PO in steam and following oxidation in air at 1200 °C.

Figure 32 clearly illustrates this behaviour. The mass gain decreases with increasing time of pre-oxidation for the experiments in air and increases for the test in nitrogen. The difference

between the two tests with PO in air results from the enhanced internal oxidation due to insufficient pre-oxidation of the inner surface during the short PO phase, as already discussed above. A similar, but opposite behaviour was observed for the tests in nitrogen. Here, the insignificant inner oxidation during 1 min PO suppressed the formation of nitrides and thus lead to less mass gain as after the 5 min PO test. The metallographic images of the specimen after 5 min PO and air oxidation looks almost identical to those of the specimen oxidised for 50 min in steam.

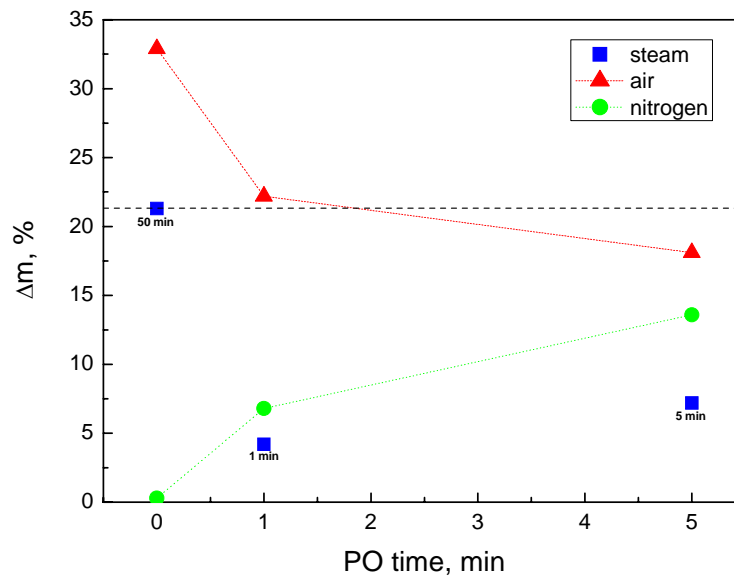
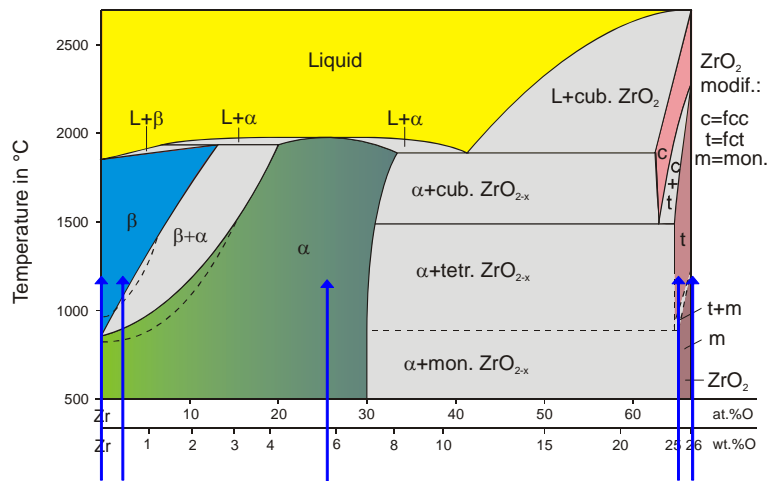


**Figure 32:** Mass gain of Zircaloy-4 specimens after 0, 1, and 5 min pre-oxidation in steam and subsequent reaction in air and nitrogen. For comparison, results of reference tests in only steam are also shown.

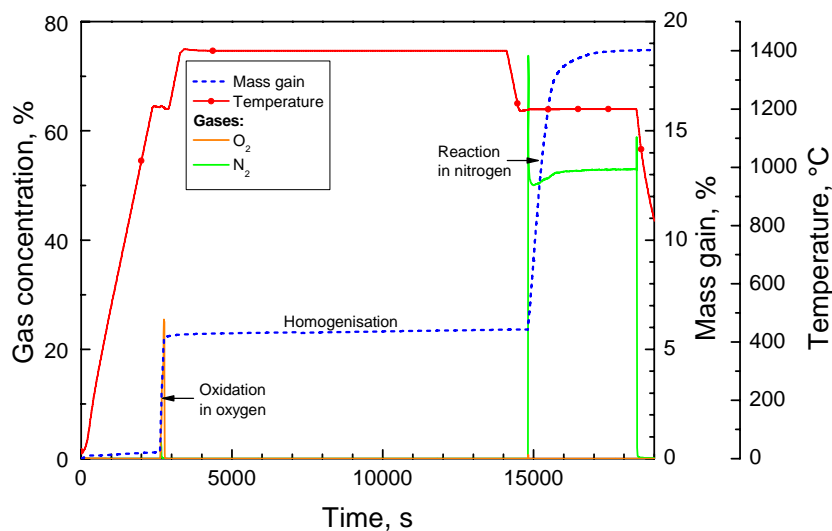
### 3.5 Tests on the mechanisms of nitrogen attack

The results presented in the previous sections indicate that significant nitrogen attack only occurs in the absence of oxygen in the gas phase (local or global oxygen starvation, see below) and in the presence of oxygen in the solid phase. From the thermo-chemical point of view, stoichiometric zirconia should be stable in nitrogen atmosphere. So the assumption was that nitrogen attacks sub-stoichiometric oxide or zirconium with dissolved oxygen. Oxygen stabilises the hexagonal  $\alpha$ -Zr(O) phase which is able to dissolve up to about 30 at% oxygen, as it is shown in Fig. 33.

Five Zircaloy-4 specimens with different oxygen contents were annealed in nitrogen at 1200 °C to check which phase is accessible for nitrogen reaction: pure Zry-4,  $\beta$ -Zr with about 3 at% oxygen,  $\alpha$ -Zr(O) with about 26 at% oxygen, sub-stoichiometric oxide  $ZrO_{1.9}$  and stoichiometric  $ZrO_2$ , as indicated by the arrows in Fig. 33. They were prepared in the thermal balance by 1) slow oxidation at 1200 °C till the desired mass gain was obtained, 2) 3 h homogenisation in argon at 1400 °C and 3) 1 h reaction at 1200 °C in nitrogen. Reference specimens were prepared by cooling down the TG furnace after step 2. Figure 34 gives an example of test conduct and TG signal for the  $\alpha$ -phase specimen.



**Figure 33:** Phase diagram Zr-ZrO<sub>2</sub>. The arrows indicate compositions of specimens prepared and investigated.



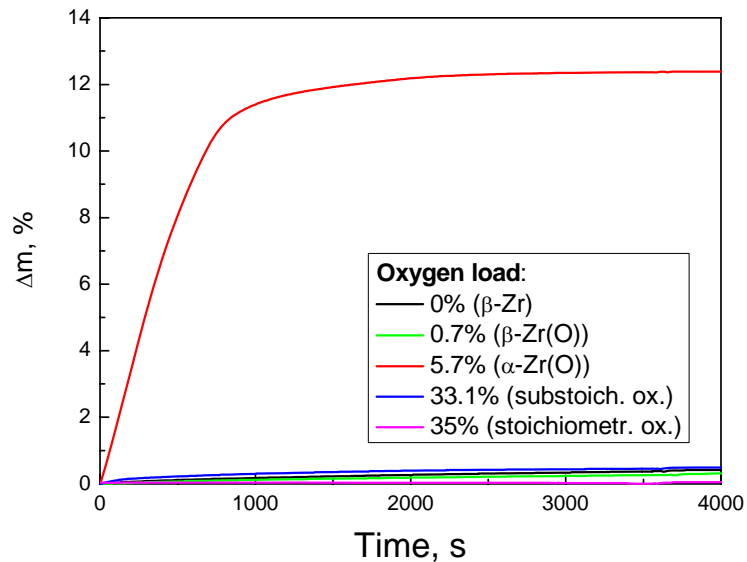
**Figure 34:** Example for conduct and results of the test series on the mechanism of nitrogen attack. Here: pre-oxidation in oxygen till 5.7% mass gain at 1200 °C, homogenisation at 1400 °C and reaction in nitrogen at 1200 °C.

Figure 35 compares the TG signals of all tests with nitrogen access starting with initiation of nitrogen injection. The highest mass gain by far was obtained with the  $\alpha$ -Zr(O) sample. Saturation was reached after about 1000 sec for this specimen. The second-fastest reaction was observed for the sub-stoichiometric oxide. By nature, the capacity for further nitrogen uptake was limited. A nitride scale covered the surface of the specimen and open cracks.

Both specimens were finally completely "oxidised", i.e. no metal was left. The mass gain of  $\alpha$ -Zr(O) was 5.7% during the oxidation and 12.8% during the nitrogen phase, meaning a final composition of "ZrO<sub>0.325</sub>N<sub>0.881</sub>". The metallographic images in Figs. 36 and 37 reveal

formation of a  $\text{ZrO}_2\text{-ZrN}$  two phase mixture, i.e. the final composition of the specimen is rather  $0.16 \text{ ZrO}_2 + 0.88 \text{ ZrN}$ , whereby a small mutual dissolution cannot be excluded.

As already seen below, pure Zry-4 only insignificantly reacts with nitrogen; the same was observed for the  $\beta\text{-Zr(O)}$  specimen. As expected, the stoichiometric oxide did not change during the annealing in nitrogen. The images in the left column in Fig. 36 confirm a complete homogenisation of the specimens during the three hours at  $1400 \text{ }^\circ\text{C}$ , except for the sub-stoichiometric oxide where a locally residual metal phase was observed.



**Figure 35:** Mass gain of pre-oxidised and homogenised Zircaloy-4 specimens during annealing in nitrogen at  $1200 \text{ }^\circ\text{C}$ .

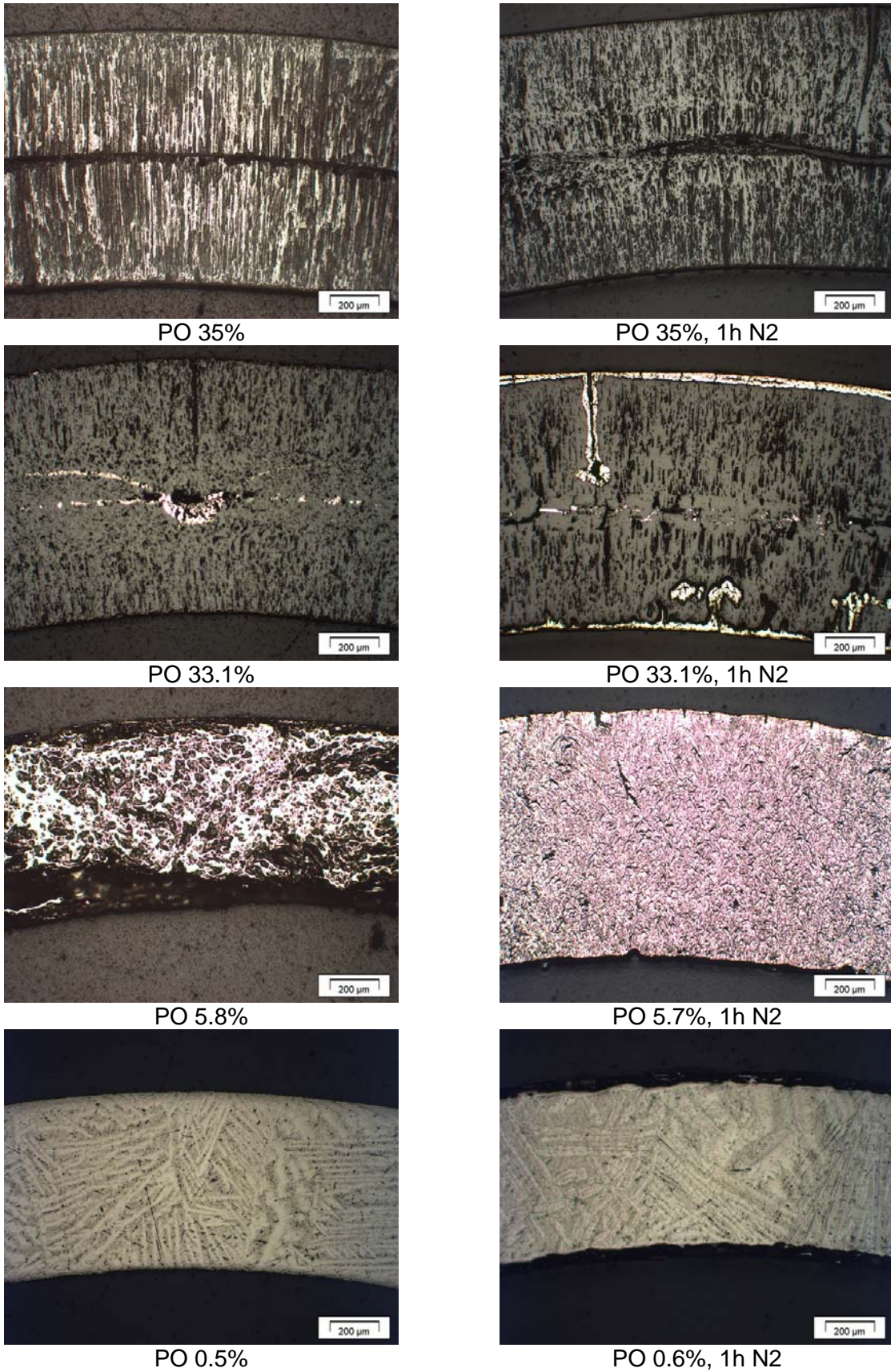


**Figure 36:** Micro images of specimens pre-oxidised in oxygen (PO), homogenised, and partly (right column) annealed in nitrogen at 1200 °C.

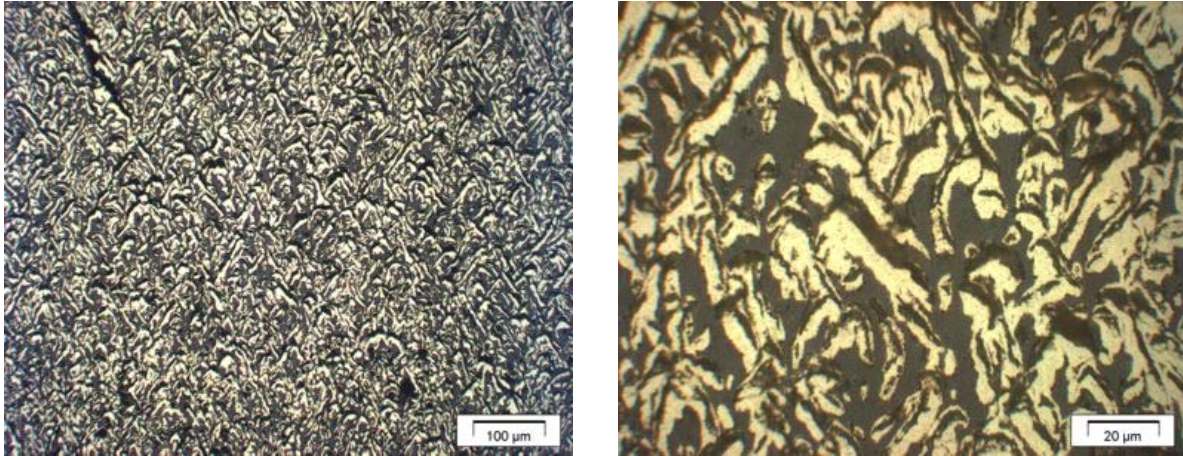


**Figure 37:** Magnified images of the specimen with 5.7% PO and subsequent annealing in nitrogen shown in Fig. 36.

## 4 Discussion

The experimental results presented in chapter 3 have clearly shown the strong effect of air and especially of nitrogen on the oxidation and degradation of Zircaloy cladding. Generally, air in the atmosphere can dramatically increase degradation, so, that the cladding barrier effect against the release of fission products is lost much earlier than under pure steam conditions.

The reaction kinetics in the pure gases oxygen, nitrogen, and air are very different from each other. The oxidation of zirconium alloys in oxygen is similar to steam, characterised by the formation of a protective oxide scale and thus controlled by diffusion of oxygen through the growing oxide layer giving parabolic kinetics. At temperatures below 1100 °C this is true only for the initial period, before, due to breakaway of the oxide scale, a transition to a faster, more complicated, but rather linear kinetics occurs. In air this transition occurs much earlier and the kinetics are much faster than in steam and it is not limited to the breakaway regime. Interestingly, a reversal of the increasing degradation with temperature in air is observed at temperatures 1400-1500 °C. This could be explained by increasing plasticity of the oxide with temperature, so that stresses build-up by initial nitride formation could be relieved not only by crack formation.

The reaction kinetics in nitrogen were parabolic at all temperatures investigated, but much slower than in the oxygen containing gases. Nitride phases have never been detected by metallographic post-test analyses, only a comparably thin  $\alpha$ -Zr(N) phase was observed at specimens annealed in pure nitrogen.

A considerable nitrogen attack, i.e. extremely porous oxide layers with nitride precipitations, was also observed for the air-steam and nitrogen-steam mixtures over a large composition range. The degradation increased with increasing temperature (at least till 1300 °C) and increasing content of air in the mixture. The maximum degradation of Zry cladding in nitrogen-steam was found for 50/50 mixtures.

Nitride formation in these tests was always observed in the oxide near the metal-oxide boundary. The attack starts locally at defects in the oxide scale, where the air can diffuse e.g. through cracks to the oxide-metal interface. There, the oxygen is consumed first and a pure nitrogen atmosphere remains which is then able to react either with the  $\alpha$ -Zr(O) phase or the sub-stoichiometric oxide, both available at that place. So, here nitride forms under local oxygen starvation. As the oxide scale further grows, the formed nitride "moves" outwards where it is re-oxidised by fresh air flowing from the external surface to the metal. Due to the lower density of  $\text{ZrO}_2$  ( $5.6 \text{ g/cm}^3$ ) in comparison to  $\text{ZrN}$  ( $7.1 \text{ g/cm}^3$ ) this reaction is connected with a significant volume increase (48%) leading to high compressive stresses which can be only relieved by the formation of cracks. Incidentally, a volume mismatch already occurs during nitride formation leading to the formation of pores.

Figure 38 illustrates this mechanistic approach. One can clearly distinguish two or even three regions in the oxide layers. The internal one with nitride precipitates is characterised by macro-cracks formed during breakaway and/or nitride formation and the external part is interspersed with micro-cracks visualised by the dark-field illumination. The outermost, about  $30 \mu\text{m}$  thick, oxide layer is of columnar structure and was formed first during the pre-oxidation period before the transition to breakaway and nitrogen attack.

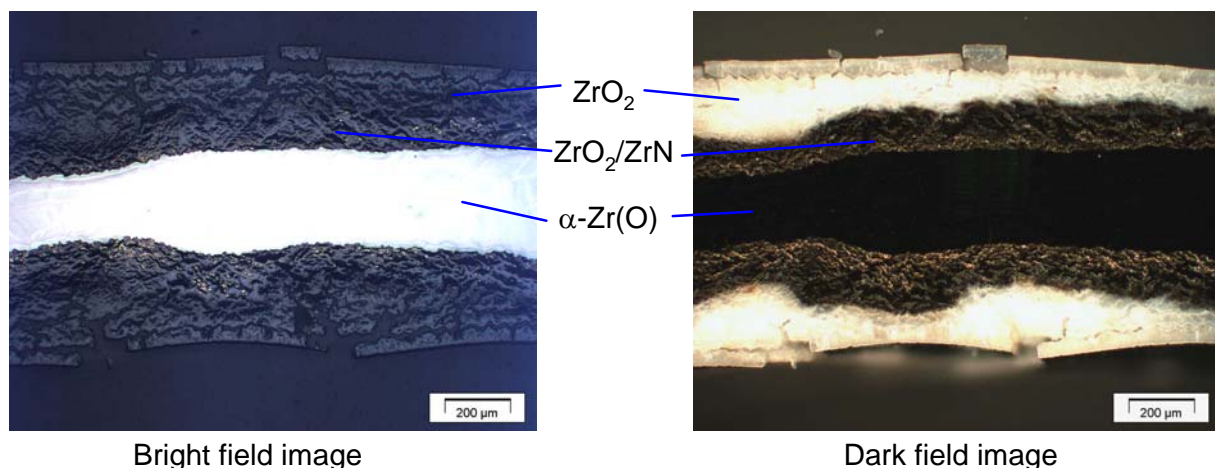


**Figure 38:** Microscopic images of a Zry-4 cladding after pre-oxidation in oxygen and oxidation in air at  $1000 \text{ }^\circ\text{C}$  under two different illuminations. The dark-field image clearly shows the formation of micro-cracks in the external part of the oxide where the nitride already has been re-oxidised.

Below  $1100 \text{ }^\circ\text{C}$  breakaway and nitride formation accelerate each other. Breakaway-induced failures in the oxide scale allow early access of the nitrogen to the metal-oxide interface leading to the formation of nitrides as discussed above. This effect is specially pronounced at the  $800 \text{ }^\circ\text{C}$  tests described in chapter 3.1 where mass gain is by far larger and oxide scale dramatically thicker in air than in oxygen annealed samples. By the way, the mechanisms of breakaway and air attack are quite similar. Both are connected with volume mismatches, caused by the phase transition tetragonal-monoclinic during "pure" breakaway [12] and by formation and re-oxidation of nitride during reaction in air.

Generally, nitrogen attack takes place locally, namely at places where the oxide is defective and thus allows access of air/nitrogen to the metal. This is well seen e.g. in the micrographs of the 10-min tests at 1200 -1400 °C in mixed atmospheres (Figs. 20, 21 and Appendix C). First nitrogen attack causes fast (with temperature and time increasing) proliferation of the affected area finally leading to the complete degradation of the scale. Local defects can also be seen in the macro-images of these specimens by bumps and spots at the surface. At temperatures below 1100 °C the degradation of the oxide layer of specimens annealed in air containing atmosphere is more layer-like because the crack network caused by breakaway offers a more homogeneous area of attack for nitrogen.

An intact oxide scale, even a thin one, formed before air ingress could effectively protect the cladding from nitrogen attack and corresponding degradation. During annealing in air the scale continues growing as before in oxygen as long as the access of nitrogen to the metal is blocked and as long as oxygen is available. A protective oxide scale is of course only formed beyond the breakaway regime, i.e. above ca. 1050 °C.

Global oxygen starvation, i.e. the absence of oxygen or other oxidising gases in the atmosphere, changes the situation dramatically. In experiments with pre-oxidised Zircaloy specimens in pure nitrogen, significant amounts of nitrides were formed externally at the oxide scale independent on the degree of pre-oxidation. Stuckert [13] has shown that oxygen diffusion from the oxide to the metal occurs during steam starvation condition leading to sub-stoichiometric oxide,  $\alpha$ -Zr(O) precipitations in the oxide and even external  $\alpha$ -Zr(O) layers at the oxide. Although the oxide is thermodynamically much more stable than the nitride, nitrogen can react with sub-stoichiometric oxide and the  $\alpha$ -Zr(O) phase as it was shown in chapter 3.5.

The results of these experiments gave also an explanation why pure metal only insignificantly reacts with nitrogen, but strong nitride formation is observed during reaction of Zircaloy in air. At the interface metal-oxide  $\alpha$ -Zr(O) and  $ZrO_{2-x}$  are available which both rapidly reacted with nitrogen in the separate-effects tests described in chapter 3.5. In these experiments it was also shown, that  $\beta$ -Zr with no or low oxygen content only insignificantly reacts with nitrogen. The reason for that behaviour is not yet clear. It is assumed that nitrogen occupies lattice defects in the sub-stoichiometric oxide or the Zr-O solution resulting in the formation of nitride seed crystals.

Table 2 gives a simplified summary of the influence of pre-oxidation on the subsequent reaction in air or nitrogen. This is only valid at temperatures above 1050 °C; and especially for reactions in air deviations from the linear kinetics in both directions were found.

**Table 2:** Reaction kinetics of Zircaloy-4 in oxygen, air, and nitrogen with and without pre-oxidation in steam or oxygen (simplified).

Reaction in	Oxygen	Air	Nitrogen
without pre-oxidation	parabolic	linear (fast)	parabolic (slow)
with pre-oxidation		parabolic	linear

## 5 Summary and Conclusions

The report presents the results of extensive experimental work on the oxidation of Zircaloy-4 in air at high temperatures. The experimental program was aimed at the mechanistic phenomenology of the reaction between Zircaloy and air and the investigation of air attack under prototypical conditions for air ingress during an hypothetical severe nuclear reactor accident, i.e. at temperatures 800-1500 °C and consideration of mixed air(nitrogen)-steam atmospheres and pre-oxidation.

The oxidation in air as well as in air and nitrogen-containing atmospheres leads to strong degradation of the cladding material. The main mechanism for this process is the formation of zirconium nitride and its re-oxidation. The different densities of Zr, ZrO<sub>2</sub>, and ZrN cause volume mismatches, compressive stress build-up and relief by crack formation leading to porous, non-protective oxide scales. From a safety point of view, the barrier effect of the fuel cladding is lost much earlier than during accident transients under only steam atmosphere.

Significant formation of ZrN was obtained under local or global oxygen starvation conditions, i.e. in the absence of oxygen/steam in the gas phase, and the presence of oxygen in the solid phase. Alpha-Zr(O) and to a limited extent sub-stoichiometric oxide ZrO<sub>2-x</sub> then react with nitrogen to form zirconium nitride.

Pre-oxidation in steam prevents air attack as long as the oxide scale is intact, i.e. at temperatures above 1050 °C (beyond breakaway regime) and as long as oxidising gases are available (no steam starvation conditions).

Under steam/oxygen starvation conditions the oxide scale is reduced (both chemically and with respect to its thickness) and significant external nitride formation takes place. From a safety point of view, during reflood with water this nitride may very rapidly re-oxidise and lead to temperature escalations in later phases of the accident.

More generally, the high exothermal energy of the oxidation of zirconium alloys in air on the one hand and low cooling effect of air compared to steam on the other hand cause early temperature escalations from comparably low temperatures as was seen during the preparation and conduct of the QUENCH-10 bundle test on air ingress [10].

Regarding modelling of air ingress in severe accident computer codes one conclusion is that parabolic correlations for oxidation in air may be applied only for high temperatures (>1400 °C) and for pre-oxidized cladding (≥ 1100 °C). For all other conditions, faster, i.e. more linear reaction kinetics should be applied.

The results presented in this report are mainly of a phenomenological nature. So, in the test series with mixed air(nitrogen)-steam atmospheres only one data point per temperature and gas composition was obtained. Therefore, the program will be extended by selected experiments aimed at the determination of kinetic correlations.

## Acknowledgements

The work presented in the report is sponsored by the HGF Programme NUKLEAR at Forschungszentrum Karlsruhe. The authors would like to thank P. Severloh (FZK-IMF I) for performing metallographic examinations, G. Schanz (FZK-IMF III) for very fruitful discussions, and T. Haste (PSI) for careful review of the report.

## References

- [1] D.A. Powers, L.N. Kmetyk, R.C. Schmidt, A Review of Technical Issues of Air Ingression during Severe Reactor Accidents, Report NUREG/CR-6218, SAND94-0731, Sandia National Lab., 1994.
- [2] I. Shepherd et al., Oxidation Phenomena in Severe Accidents (OPSA), Final Report, INV-OPSA(99)-P008, 2000.
- [3] I. Shepherd et al., Investigation of Core Degradation (COBE), Nucl. Eng. Design 209, 107-16, 2001.
- [4] K. Natesan, W.K. Soppet, S. Basu, Low Temperature Air Oxidation Experiments at ANL, CSARP Meeting, Crystal City, VA, May 3-4, 2004.
- [5] P. Giordano, C. Séropian, The Air Ingress Issue for PWRs, 5th Technical Seminar on the Phebus FP Programme, Aix-en-Provence, June 2003.
- [6] C. Duriez, T. Dupon, D. Drouan, The MOZART Program on Air Cladding Oxidation: Results on Bare Zircaloy-4 in the Range 600-1000 °C, ISTP Report N°7, DPAM/SEREA/06-001, 2006.
- [7] M. Steinbrück et al., Experiments on Air Ingress during Severe Accidents in LWRs, Nucl. Eng. Design 236, 1709-1719, 2006.
- [8] M. Steinbrück, Prototypical Experiments on Air Oxidation of Zircaloy Cladding at High Temperatures, ANS Annual Meeting Reno, NV, June 4-8, 2006.
- [9] T. Ziegler, Sequentielle Oxidation von Zircaloy-4-Brennstabhüllen in Ar/O<sub>2</sub> and Ar/Luft Atmosphäre, Forschungszentrum Karlsruhe, internal report NUKLEAR-3407, 2006.
- [10] G. Schanz et al., Results of the QUENCH-10 Experiment on Air Ingress, Forschungszentrum Karlsruhe, Report FZKA 7087, 2006.
- [11] M. Große, FZK, private communication to M. Steinbrück, 2006.
- [12] Schanz, G., Leistikow, S., Microstructural Reasons for Mechanical Oxide Degradation (Breakaway Effect) and Resulting Kinetic Anomalies of Zircaloy-4/Steam High-

Temperature Oxidation, 8th International Congress on Metallic Corrosion, Mainz, Germany, ICC/EFC Proceedings Vol.2, DECHEMA, 1712-1717, 1981.

- [13] J. Stuckert, M. Steinbrück, U. Stegmaier, Development of the Metallic Layer on the Surface of Oxidised Zry-Cladding under Steam Starvation Conditions. ISTC/WTZ Progress Meeting, Moscow, July 03-06, 2006, CD-ROM.

## **Appendix A Test parameters and main results of the tests in the BOX rig**

**Table A 1:** Test matrix of 1 h isothermal experiments in mixed air-steam atmospheres at 800, 900, 1000, 1100, and 1200 °C.

Test	T, K	Steam, g/h	Air, l/h	Ar, l/h	$\Delta m$ , %	ZrO <sub>2</sub> , $\mu\text{m}$	$\alpha$ -Zr(O), $\mu\text{m}$	ZrN?
40930b1	800	0	100	50	2.25	40	6	n
41001a1	800	8.04	90	100	0.85	10	11	n
41001a2	800	24.1	70	50	0.80	10	11	n
41001a8	800	40.18	50	100	0.88	10	10	n
41001a3	800	56.25	30	50	0.88	10	11	n
41001a4	800	72.3	10	50	0.88	11	11	n
41001a5	800	75	4.9	50	0.88	12	10	n
41001a6	800	75	2.6	100	0.87	10	11	n
41001a7	800	75	0	100	0.88	10	10	n
40927a1	1000	0	100	50	25.9	455	20	y
40927a2	1000	8.04	90	50	16.8	295	20	y
40927a3	1000	24.1	70	50	31.0	490	35	y
40927a4	1000	40.18	50	50	15.0	225	30	y
40928a1	1000	56.25	30	50	17.4	160	25	y
40928a2	1000	72.3	10	50	10.8	90	45	?
40928a4	1000	75	4.9	50	8.9	90	45	n
40928a5	1000	75	2.6	50	8.2	105	30	n
40928a3	1000	75	0	50	6.2	75	50	n
40929a1	1200	0	100	50	33.7	560	-	?
40929a3	1200	8.04	90	50	32.8	935	-	y
40929a5	1200	24.1	70	50	27.9	915	-	?
40929a4	1200	40.18	50	50	31,4	1075	-	?
40929a6	1200	56.25	30	50	27.6	280	50	y
40930a1	1200	72.3	10	50	21.9	285	320	n
40930a2	1200	75	4.9	50	23.3	290	290	n
40930a3	1200	75	2.6	50	18.9	255	415	n
40929a2	1200	75	0	50	19.9	250	395	n

Test parameters and main results of the tests in the BOX rig

---

41129a1	900	0	100	50	3.37	26	30	y
41129a2	900	8.04	90	100	3.06	30	40	y
41130a1	900	24.1	70	50	2.14	25	40	y
41130a2	900	40.18	50	50	2.09	23	36	n
41130a3	900	56.25	30	50	2.06	22	36	n
41130a4	900	72.3	10	50	1.97	24	36	n
41130a5	900	75	4.9	50	1.97	24	40	n
41130a6	900	75	2.6	50	1.89	22	36	n
41130a7	900	75	0	50	1.84	21	36	n
41201a1	1100	0	100	50	31.33	compl.	-	y
41201a2	1100	8.04	90	50	31.55	compl.	-	y
41201a3	1100	24.1	70	50	24.73	176	200	y
41201a4	1100	40.18	50	50	19.34	155	250	y
41201a5	1100	56.25	30	50	13.91	158	100	y
41201a6	1100	72.3	10	50	12.17	161	100	n
41202a1	1100	75	4.9	50	11.16	152	100	n
41202a2	1100	75	2.6	50	11.70	160	100	n
41202a3	1100	75	0	50	11.38	148	100	n

**Table A 2:** Test matrix of 10 min isothermal experiments in mixed air-steam atmospheres at 1200, 1300, 1400, and 1500 °C.

Test	T, K	Steam, g/h	Air, l/h	Ar, l/h	$\Delta m$ , %	ZrO <sub>2</sub> , $\mu\text{m}$	$\alpha$ -Zr(O), $\mu\text{m}$	ZrN ?	Remarks
50627a1	1200	0	100	50	14.1	100-400	100	y	
50627a2	1200	8.04	90	50	18.0	100-450	50	y	
50627a3	1200	24.1	70	50	17.7	65-400	75	y	
50627a4	1200	40.18	50	50	15.8	75-450	90-200	y	
50628a1	1200	56.25	30	50	11.0	84	100	y	leaky O-ring sealing
50628a2	1200	72.3	10	50	7.1	82	90	n	11 instead of 10 min
50628a3	1200	75	4.9	50	6.6	76	90	n	
50628a4	1200	75	2.6	50	6.5	72	90	n	
50628a5	1200	75	0	50	6.4	74	100	n	
50628b1	1300	0	100	50	22.0	350-550	100	y	
50628b2	1300	8.04	90	50	23.8	425-550	100-125	y	
50628b3	1300	24.1	70	50	24.1	130-550	100	y	
50628b4	1300	40.18	50	50	21.9	125-500	180	y	
50628b5	1300	56.25	30	50	18.3	120	200	y	
50628b6	1300	72.3	10	50	11.0	115	150-190	y	
50628b7	1300	75	4.9	50	10.4	111	150	n	
50628b8	1300	75	2.6	50	10.3	110	150	n	
50629a1	1300	75	0	50	10.2	110	150	n	
50629b1	1400	0	100	50	24.4		200	y	
50629b2	1400	8.04	90	50	25.1	590	no $\beta$	y	
50629b3	1400	24.1	70	50	26.2	450	no $\beta$	y	sample 1cm displaced
50629b4	1400	40.18	50	50	23.0	200-400	no $\beta$	y	sample 1cm displaced
50629b5	1400	56.25	30	50	22.0	210	175-350	y	sample 1cm displaced
50629b6	1400	72.3	10	50	16.7	173	200	n	sample 1cm displaced
50630a1	1400	75	4.9	50	16.1	174	200-240	n	
50630a2	1400	75	2.6	50	15.8	176	200-240	n	sample 1cm displaced
50630a3	1400	75	0	50	15.2	169	no $\beta$	n	

Test parameters and main results of the tests in the BOX rig

50630b1	1500	0	100	50	26.2	508	no $\beta$	y	sample 2cm displaced
50630b2	1500	8.04	90	50	26.8	486	no $\beta$	y	sample 2cm displaced
50630b3	1500	24.1	70	50	26.8	310-500	no $\beta$	y	sample 2cm displaced
50630b4	1500	40.18	50	50	27.6	300-515	no $\beta$	y	sample 2cm displaced
50630b5	1500	56.25	30	50	26.2	300	no $\beta$	y	sample 2cm displaced
50630b6	1500	72.3	10	50	24.4	295	no $\beta$	n	sample 2cm displaced
50630b7	1500	75	4.9	50	25.0	286	no $\beta$	n	sample 1cm displaced
50630b8	1500	75	2.6	50	24.3	280	no $\beta$	n	
50630b9	1500	75	0	50	20.7	278	no $\beta$	n	

**Table A 3:** Test matrix of experiments in mixed nitrogen-steam atmospheres at 1000 and 1200 °C.

Test	T, °C	Time, min	Steam, g/h	N <sub>2</sub> , l/h	Ar, l/h	$\Delta m$ , %	Remarks
51205b1	1000	60	73.3	10	50	10.5	
51205b2	1000	60	40.18	50	50	34.0	Sample strongly swollen
51205b3	1000	60	4.02	95	50	13.6	
51206a1	1200	60	73.3	10	50	19.6	
51206a2	1200	60	40.18	50	50	30.4	Oxide scale partially spalled
51206a4	1200	60	4.02	95	50	28.2	
51206a5	1200	10	73.3	10	50	6.6	
51206a6	1200	10	40.18	50	50	15.2	
51206a7	1200	10	4.02	95	50	10.1	
51206b1	1400	10	73.3	10	50	16.3	
51206b2	1400	10	40.18	50	50	25.7	
51206b3	1400	10	4.02	95	50	11.8	
60103a	1000	60	0	100	50	0.31	
60103b1	1200	10	0	100	50	0.19	
60103b2	1200	60	0	100	50	0.56	
60103c	1400	10	0	100	50	0.60	

**Table A 4:** Tests on influence of pre-oxidation in steam on subsequent reaction in air and nitrogen.

Test	T, °C	Steam, min (50 g/h)	Air, min (50 l/h)	N <sub>2</sub> , min (50 l/h)	Ar, min (50 l/h)	Δm, %	ZrN?
60629a1	1200	50			50	21.3	n
60629a2	1200	5			50	7.2	n
60629a3	1200	1			50	4.2	n
60629b1	1200	5	45		50	18.1	n
60629b2	1200	1	49		50	22.2	(y)
60629b3	1200	0	50		50	32.9	y
60630a1	1200	5		45	50	13.6	y
60630a2	1200	1		49	50	6.8	y
60630a3	1200	0		50	50	0.3	(n)

## Appendix B Test parameters and main results of the tests in the thermal balance

**Table A 5:** Test matrix of first TG experiments at 1000 and 1100 °C.

Sample	Temperature, °C	Pre-oxidation	Reaction in	$\Delta m$ , %	$\Delta m(TG)$ , %	Remarks
50816a	1000	Ar/O <sub>2</sub> , 20 $\mu$ m	Ar/air	>30	33.4*	ZrO <sub>2</sub> spalling
50817a	1000	Ar/O <sub>2</sub> , 20 $\mu$ m	Ar/air	22.7	22.7	Repetition of 50816a with less O <sub>2</sub> during PO and shorter duration
50817c	1100	Ar/O <sub>2</sub> , 20 $\mu$ m	Ar/air	19.8	19.9	
50818a	1100	Ar/O <sub>2</sub> , 20 $\mu$ m	Ar/O <sub>2</sub>	18.5	18.3	
50822a	1100	Ar/O <sub>2</sub> , 20 $\mu$ m	Ar/N <sub>2</sub>	7.8	7.7	
50823a	1100	-	Ar/air	34.7	34.4	Stop of air injection only during cooldown
50823b	1100	-	Ar/N <sub>2</sub>	0.9	0.8	Change of N <sub>2</sub> injection during test
50824a	1100	-	Ar/N <sub>2</sub>	0.4	0.3	Repetition of 50823b with right N <sub>2</sub> injection
50824b	1100	-	Ar/N <sub>2</sub>	0	0.1	<b>Reference test with Al<sub>2</sub>O<sub>3</sub> tube segment</b>

- duration of all tests at 1100 °C was 80 m in

- initially lower oxygen rates during PO till about 2% mass gain

\* spalled oxide considered

**Table A 6:** Test parameters and results of TG experiments on influence of pre-oxidation on subsequent reaction in air and nitrogen.

Sample	Temp. °C	gas rates l/h	O <sub>2</sub> injection time	air injection time	N <sub>2</sub> injection time	Δm %	ZrO <sub>2</sub> μm	ZrN
<b>open samples</b>								
50920a	1200	10 O <sub>2</sub> 10 Air	10s	31min 3s		24.60	230	+
50921a	1200	10 O <sub>2</sub> 10 N <sub>2</sub>	10s		31 min 3s	8.89	200	+
50921b	1200	10 O <sub>2</sub>	31min13s			22.90	300	-
50922a	1200	10 O <sub>2</sub> 10 Air	10min	52min		24.98	325	+
50922b	1200	10 O <sub>2</sub> 10 N <sub>2</sub>	10min		52min	20.05	325	+
50923a	1200	10 O <sub>2</sub> 10 Air	10min	25min 54s		25.00	310	+
50923b	1200	10 Air		14min 54s		25.20	540	+
50926a	1200	10 O <sub>2</sub> 10 Air	3s	26min 39s		25.38	230	+
50926b	1200	10 O <sub>2</sub> 10 N <sub>2</sub>	3s		26min 39s	6.94	175	+
50927a	1200	10 N <sub>2</sub>			175min	0.85	-	-
50927b	1400	10 O <sub>2</sub> 10 Air	4s	15min 28s		25.62	320-500	+
50928a	800	10 N <sub>2</sub>			175min	0.33	2	+
50928b	1400	10 O <sub>2</sub> 10 N <sub>2</sub>	4s		15min 28s	8.81	200-300	+
50929a	1400	10 O <sub>2</sub>	6min 30s			25.80	350	-
50929b	1400	10 Air		15min 10s		25.37	520	+
50929c	1400	30 Air		13min 10s		25.43	420	+
50930a	1400	30 O <sub>2</sub> 30 Air	4s	21min 30s		24.45*	530-620	+
51004a	1400	30 O <sub>2</sub> 10 N <sub>2</sub>	4s		21min 30s	12.04*	500-700	+
51004b	1400	30 O <sub>2</sub>	13min 30s			25.01	550	-
51005a	1400	10 O <sub>2</sub> 30 Air	50s	10min 20s		25.55	400	+
51005b	1400	10 O <sub>2</sub> 30 N <sub>2</sub>	50s		10min 20s	16.49	300	+
51006a	1400	10 O <sub>2</sub> 30 Air	4min 30s	1min 40s		25.81	400	+
51006b	1400	10 O <sub>2</sub> 30 Air	4s	10min 30s		25.31	400	+
51007a	1400	10 O <sub>2</sub> 30 O <sub>2</sub>	4s / 5min 45s			25.39	430	-
51007b	1400	10 O <sub>2</sub> 30 O <sub>2</sub>	10m15s/2m 45s			25.58	400	-
51007c	1400	10 O <sub>2</sub> 30 O <sub>2</sub>	50s/10m20s			22.88	290	-
51010a	1400	10 O <sub>2</sub> 30 N <sub>2</sub>	4s		10min 30s	8.77	50-100	+
51010b	1200	10 O <sub>2</sub>	3s			3.59	50	-

## Test parameters and main results of the tests in the thermal balance

	Temp.	gas rates	O <sub>2</sub> injection	air injection	N <sub>2</sub> injection	Δm	ZrO <sub>2</sub>	ZrN
51011a	1400	10 O <sub>2</sub> 30 N <sub>2</sub>	8min 20s		short	24.2	350	+
51011b	1400	10 O <sub>2</sub> 30 N <sub>2</sub>	3min 45s		1min 40s	24.27	350	+
51012a	1000	10 Air		79min 16s		28.48	150-400	+
51013a	1000	10 Air		79min 42s		25.31	120-400	+
51013b	1000	10 O <sub>2</sub>	79min 42s			13.27	200	-
51014a	1200	10 N <sub>2</sub>			175min	0.8	-	-
51017a	1000	10 O <sub>2</sub> 10 Air	1min	84min 25s		24.79	200-350	+
51017b	1000	10 O <sub>2</sub> 10 N <sub>2</sub>	1min		25min	3,25 abg.	50	+
51018a	1000	10 O <sub>2</sub> 10 N <sub>2</sub>	1min		84min 25s	3.41	50	+
51019a	1000	10 O <sub>2</sub> 10 Air	20min	70min 23s		26.74	550-850	+
51019b	1000	10 O <sub>2</sub> 10 N <sub>2</sub>	20min 23s		70min 23s	4.49	50	+
51020a	1000	10 O <sub>2</sub> 10 Air	60min 20s	45min 40s		24.47	450-600	+
51020b	1000	10 O <sub>2</sub> 10 N <sub>2</sub>	66min		45min 40s	7.94	140-150	+
51021a	1000	10 O <sub>2</sub> 10 Air	60min 20s	45min 40s		24.22	350-650	+
51024a	800	10 Air		7h 38min		16.47	280-300	+
51027a	800	10 O <sub>2</sub>	7 h 38min			3.05	15	-
51028a	800	10 O <sub>2</sub> 10 Air	6min 30s	7h 31min 30s		14.22	150-250	+
51102a	800	10 O <sub>2</sub> 10 N <sub>2</sub>	6min 30s		7h 31min 30s	1.27	15-20	+
51103a	800	10 O <sub>2</sub> 10 Air	3 h 13min	4 h 25min		7.33	20-140	+
51104a	800	10 O <sub>2</sub> 10 N <sub>2</sub>	3 h 13min		4 h 25min	1.8	20	+
51107a	1000	10 N <sub>2</sub>			1h 19min 42s	0.18	-	+
51107b	1400	10 N <sub>2</sub>			1 h 55min	1.64	-	-
51108a	800	10 N <sub>2</sub>			7 h 38min	0.18	-	-
51110b	1400	10 O <sub>2</sub> 30 Air	50s	10min 20s		Al <sub>2</sub> O <sub>3</sub>	-	-
51121a	1400	10 O <sub>2</sub>	4s			4.28	80-100	-
51121b	800	10 N <sub>2</sub>			some min	0.27	-	-
51121c	800	10 N <sub>2</sub>			15 h 40min	0.31	n.m.	n.m.
51122a	1400	10 N <sub>2</sub>			2 h 30min	1.83	n.m.	n.m.
<b>closed samples</b>								
51214a	1200	10 O <sub>2</sub> 10 Air	3s	25min		7.71	-	-
51215a	1200	10 O <sub>2</sub> 10 Air	3s	50min		9.72	300	-

Test parameters and main results of the tests in the thermal balance

	Temp.	gas rates	O <sub>2</sub> injection	air injection	N <sub>2</sub> injection	Δm	ZrO <sub>2</sub>	ZrN
51215b	1200	10 O <sub>2</sub> 10 Air	10s	50min		9.91	320	-
51216a	1400	10 O <sub>2</sub> 30 Air	4s	11min 30s		10.22	350	+
51216b	1400	10 O <sub>2</sub> 30 Air	50s	10min 30s		10.33	350	-
51219a	1200	10 O <sub>2</sub>	50min			9.96	300	-
51219b	1400	10 O <sub>2</sub>	20min 30s			10.14	300	-
60217a	1400	10 O <sub>2</sub>	12min			10.15	n.m.	n.m.
<b>open samples</b>								
51220a	1400	10 O <sub>2</sub> 30 Ar	4s dann Ar			4.74	20-50	-
51220b	1400	10 O <sub>2</sub> 40 Ar	4s dann Ar			5.31	n.m.	n.m.
51221a	1400	10 O <sub>2</sub>	4s			1.36	n.m.	n.m.

\* Sample partly broken after test, therefore TG was used to determine Δm

n.m.: not measured

yellow lines: these specimens oxidised slower than expected

green lines: rerun under same conditions

## **Appendix C Post-test results for the specimens oxidised in mixed air-steam atmosphere**



H<sub>2</sub>O



0.03 air / 0.97 H<sub>2</sub>O



0.05 air / 0.95 H<sub>2</sub>O



0.1 air / 0.9 H<sub>2</sub>O



0.3 air / 0.7 H<sub>2</sub>O



0.5 air / 0.5 H<sub>2</sub>O



0.7 air / 0.3 H<sub>2</sub>O

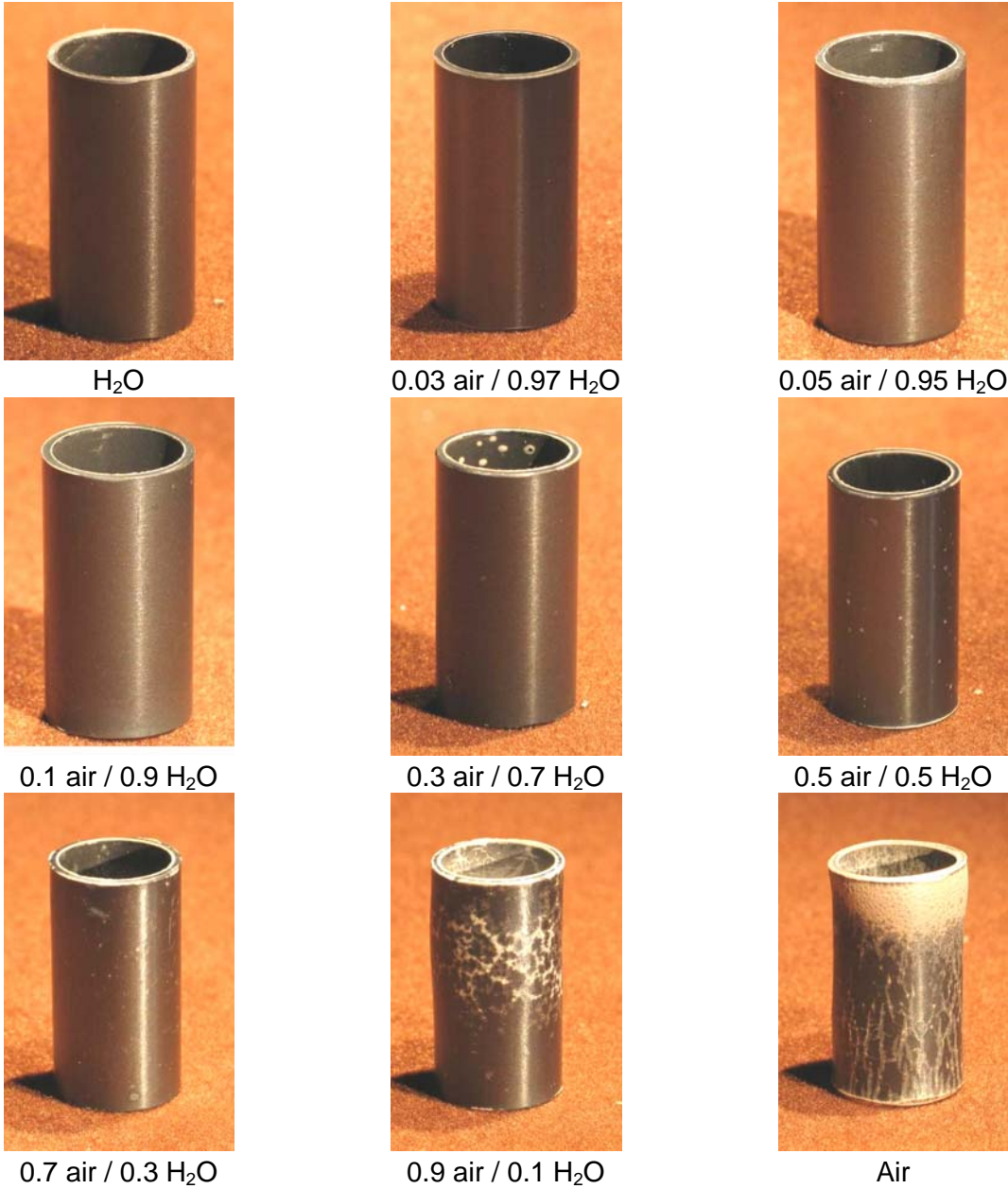


0.9 air / 0.1 H<sub>2</sub>O



Air

**Post-test appearance of specimens oxidised 1 h at 800 °C**



Post-test appearance of specimens oxidised 1 h at 900 °C



H<sub>2</sub>O



0.03 air / 0.97 H<sub>2</sub>O



0.05 air / 0.95 H<sub>2</sub>O



0.1 air / 0.9 H<sub>2</sub>O



0.3 air / 0.7 H<sub>2</sub>O



0.5 air / 0.5 H<sub>2</sub>O



0.7 air / 0.3 H<sub>2</sub>O



0.9 air / 0.1 H<sub>2</sub>O



Air

**Post-test appearance of specimens oxidised 1 h at 1000 °C**



Post-test appearance of specimens oxidised 1 h at 1100 °C



H<sub>2</sub>O



0.03 air / 0.97 H<sub>2</sub>O



0.05 air / 0.95 H<sub>2</sub>O



0.1 air / 0.9 H<sub>2</sub>O



0.3 air / 0.7 H<sub>2</sub>O



0.5 air / 0.5 H<sub>2</sub>O



0.7 air / 0.3 H<sub>2</sub>O

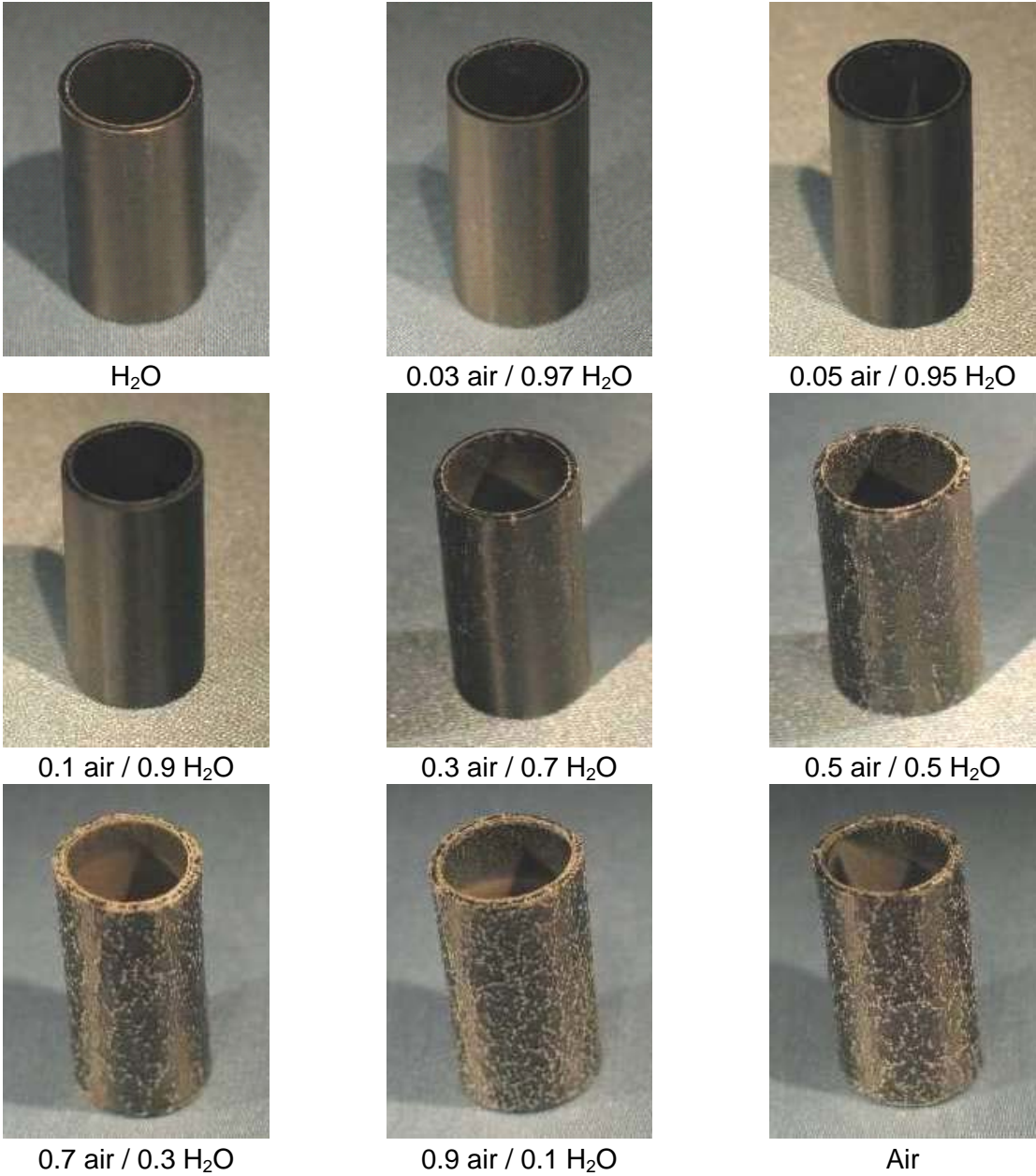


0.9 air / 0.1 H<sub>2</sub>O



Air

**Post-test appearance of specimens oxidised 1 h at 1200 °C**



Post-test appearance of specimens oxidised 10 min at 1200 °C



H<sub>2</sub>O



0.03 air / 0.97 H<sub>2</sub>O



0.05 air / 0.95 H<sub>2</sub>O



0.1 air / 0.9 H<sub>2</sub>O



0.3 air / 0.7 H<sub>2</sub>O



0.5 air / 0.5 H<sub>2</sub>O



0.7 air / 0.3 H<sub>2</sub>O

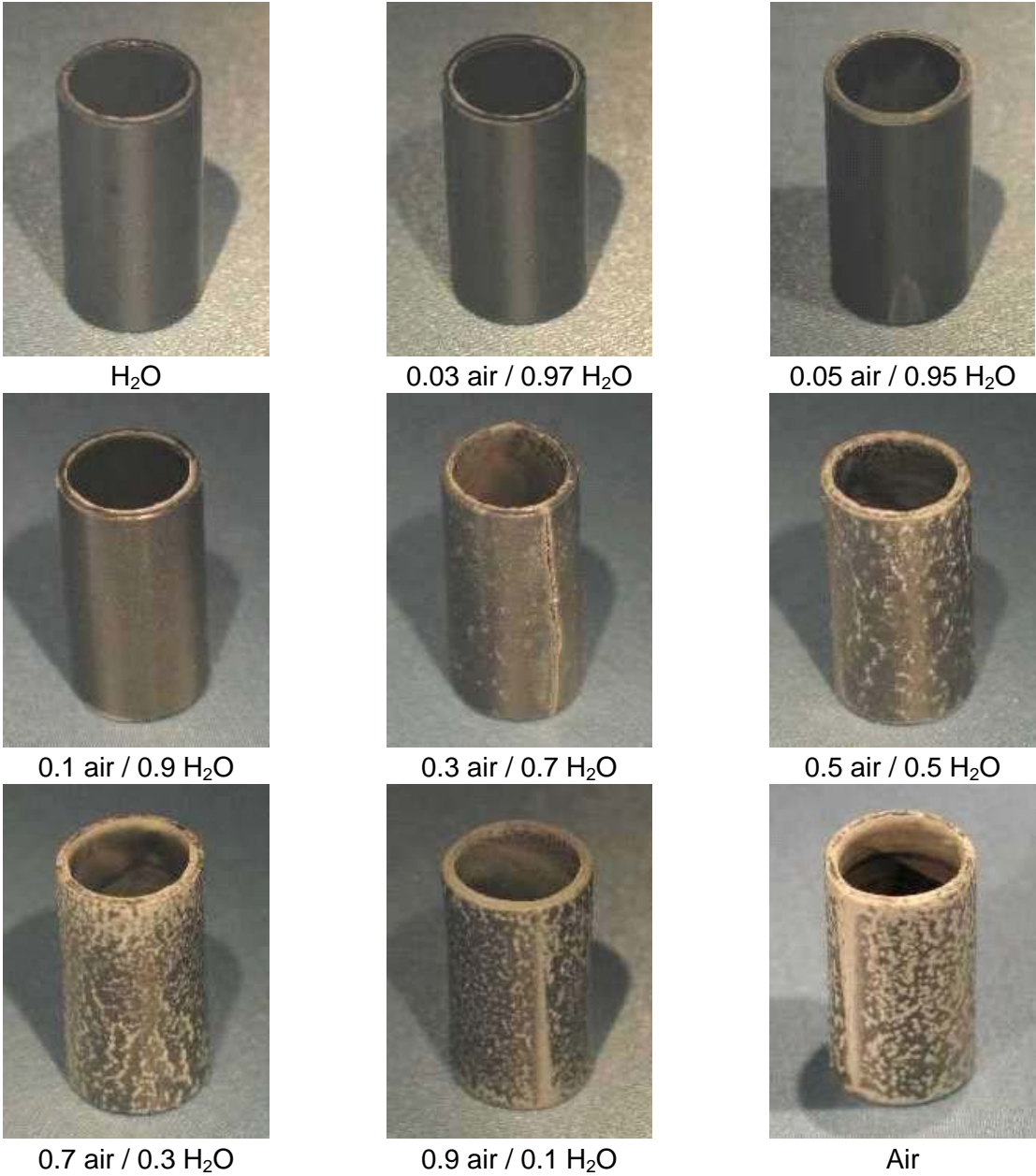


0.9 air / 0.1 H<sub>2</sub>O



Air

**Post-test appearance of specimens oxidised 10 min at 1300 °C**



**Post-test appearance of specimens oxidised 10 min at 1400 °C**



H<sub>2</sub>O



0.03 air / 0.97 H<sub>2</sub>O



0.05 air / 0.95 H<sub>2</sub>O



0.1 air / 0.9 H<sub>2</sub>O



0.3 air / 0.7 H<sub>2</sub>O



0.5 air / 0.5 H<sub>2</sub>O



0.7 air / 0.3 H<sub>2</sub>O

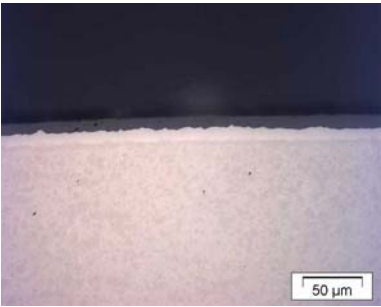


0.9 air / 0.1 H<sub>2</sub>O

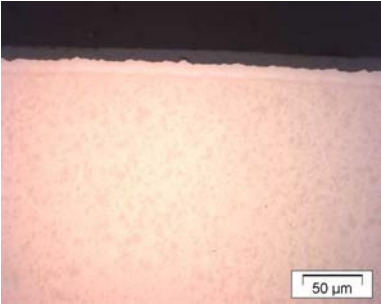


Air

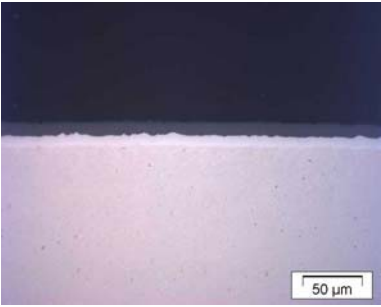
**Post-test appearance of specimens oxidised 10 min at 1500 °C**



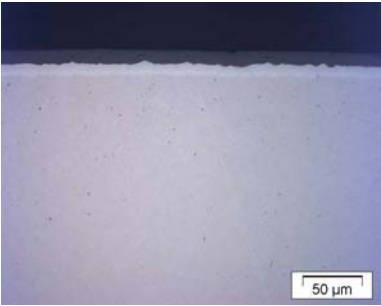
H<sub>2</sub>O



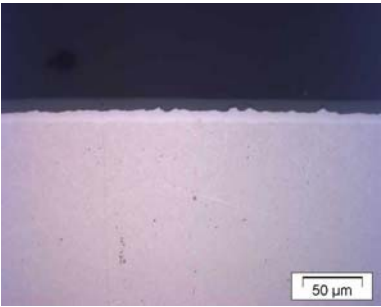
0.03 air / 0.97 H<sub>2</sub>O



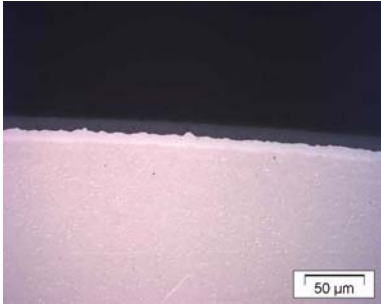
0.1 air / 0.9 H<sub>2</sub>O



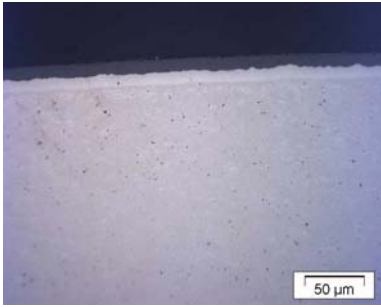
0.5 air / 0.5 H<sub>2</sub>O



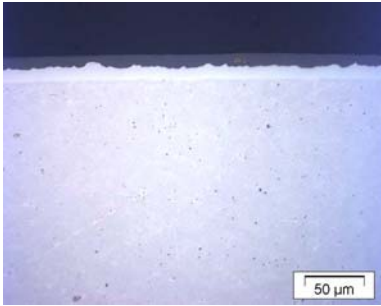
0.9 air / 0.1 H<sub>2</sub>O



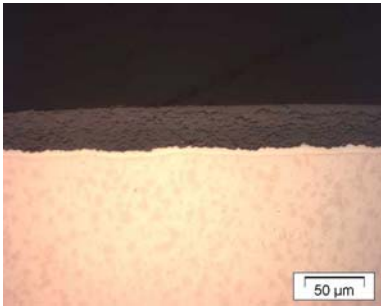
0.05 air / 0.95 H<sub>2</sub>O



0.3 air / 0.7 H<sub>2</sub>O

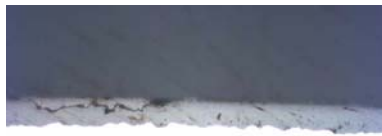


0.7 air / 0.3 H<sub>2</sub>O



Air

**Metallographic images of specimens oxidised 1 h at 800 °C**



H<sub>2</sub>O



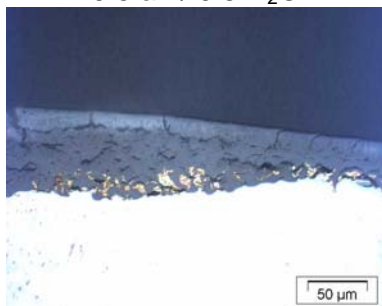
0.03 air / 0.97 H<sub>2</sub>O



0.1 air / 0.9 H<sub>2</sub>O



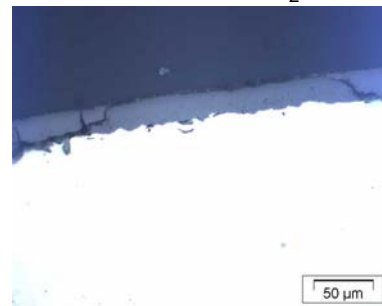
0.5 air / 0.5 H<sub>2</sub>O



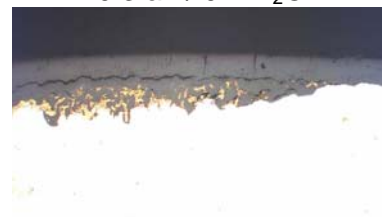
0.9 air / 0.1 H<sub>2</sub>O



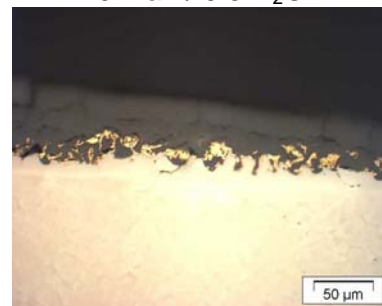
0.05 air / 0.95 H<sub>2</sub>O



0.3 air / 0.7 H<sub>2</sub>O

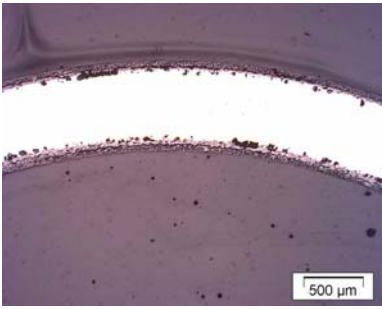


0.7 air / 0.3 H<sub>2</sub>O

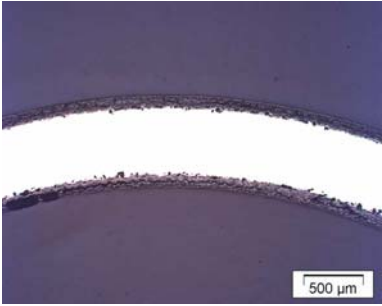


Air

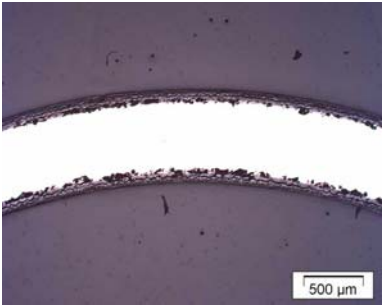
**Metallographic images of specimens oxidised 1 h at 900 °C**



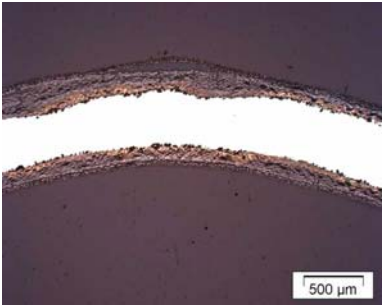
H<sub>2</sub>O



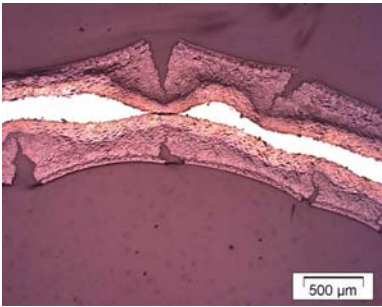
0.03 air / 0.97 H<sub>2</sub>O



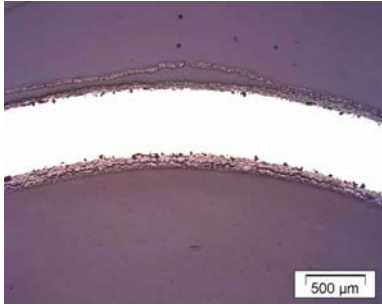
0.1 air / 0.9 H<sub>2</sub>O



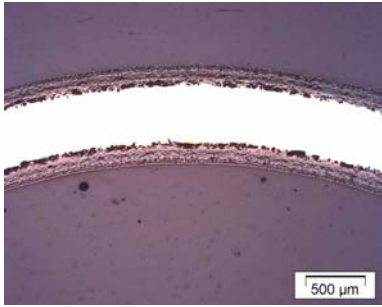
0.5 air / 0.5 H<sub>2</sub>O



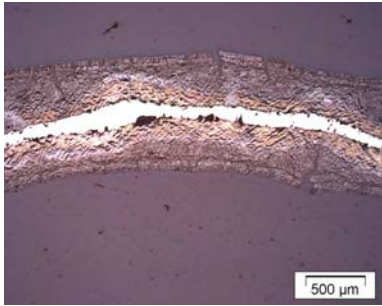
0.9 air / 0.1 H<sub>2</sub>O



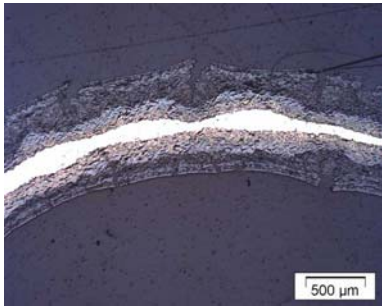
0.05 air / 0.95 H<sub>2</sub>O



0.3 air / 0.7 H<sub>2</sub>O

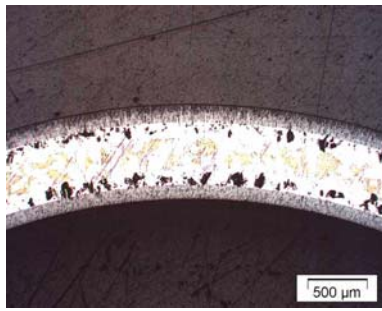


0.7 air / 0.3 H<sub>2</sub>O

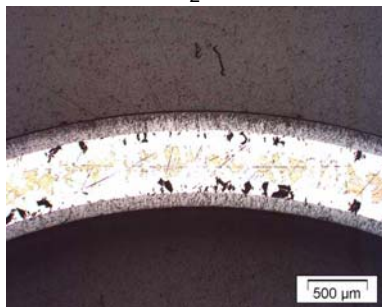


Air

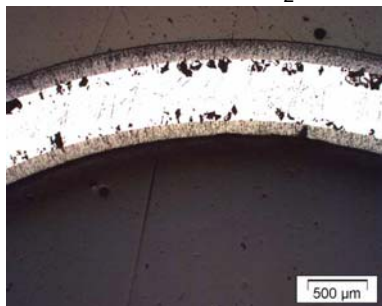
**Metallographic images of specimens oxidised 1 h at 1000 °C**



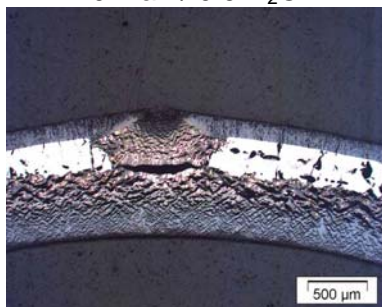
H<sub>2</sub>O



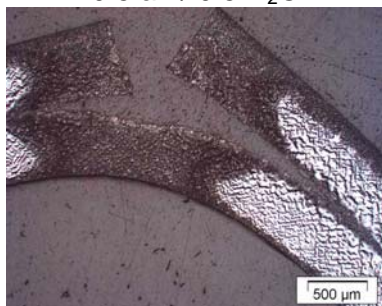
0.03 air / 0.97 H<sub>2</sub>O



0.1 air / 0.9 H<sub>2</sub>O



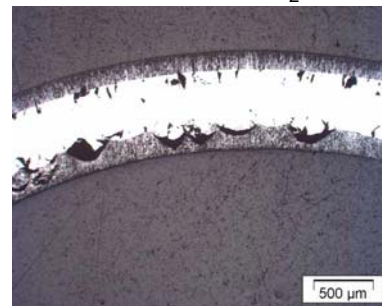
0.5 air / 0.5 H<sub>2</sub>O



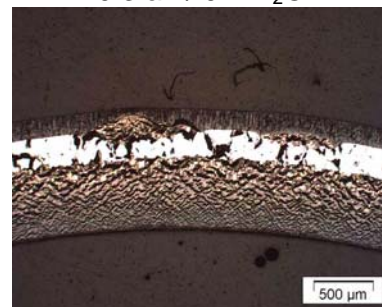
0.9 air / 0.1 H<sub>2</sub>O



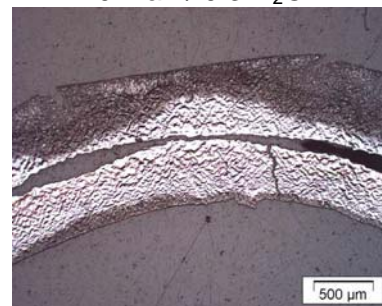
0.05 air / 0.95 H<sub>2</sub>O



0.3 air / 0.7 H<sub>2</sub>O

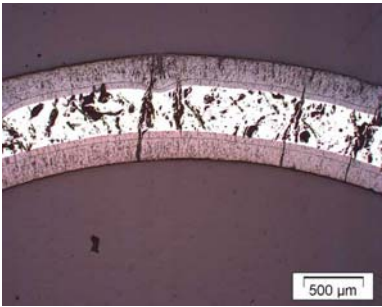


0.7 air / 0.3 H<sub>2</sub>O

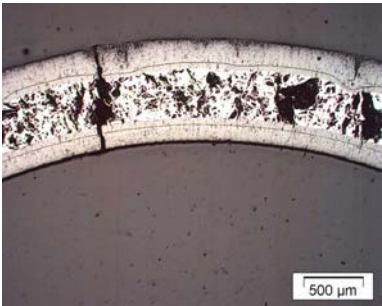


Air

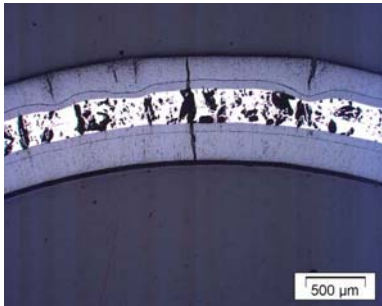
**Metallographic images of specimens oxidised 1 h at 1100 °C**



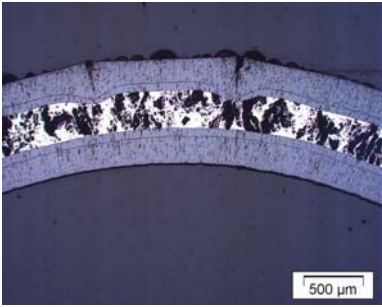
H<sub>2</sub>O



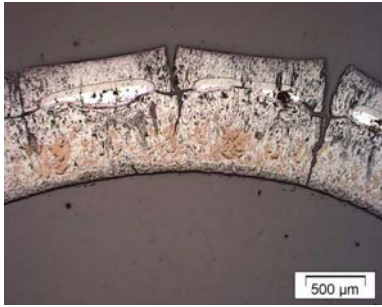
0.03 air / 0.97 H<sub>2</sub>O



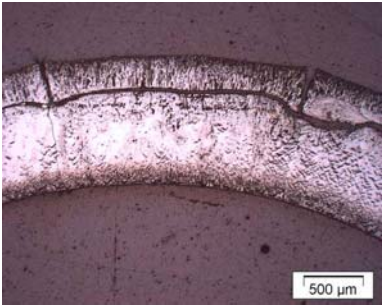
0.05 air / 0.95 H<sub>2</sub>O



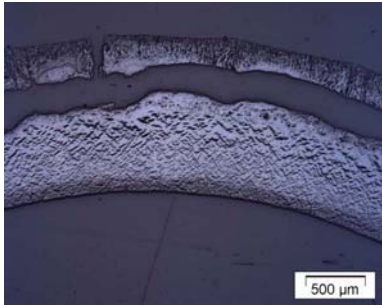
0.1 air / 0.9 H<sub>2</sub>O



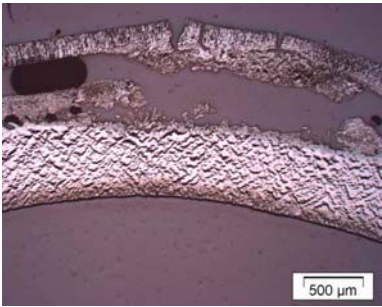
0.3 air / 0.7 H<sub>2</sub>O



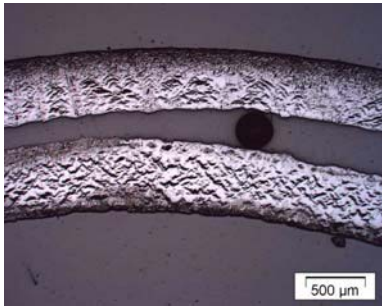
0.5 air / 0.5 H<sub>2</sub>O



0.7 air / 0.3 H<sub>2</sub>O

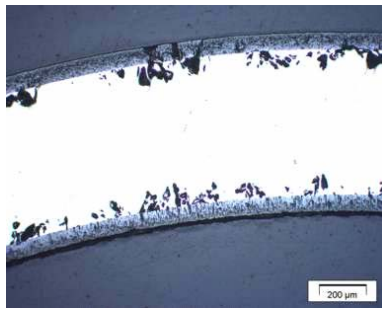


0.9 air / 0.1 H<sub>2</sub>O

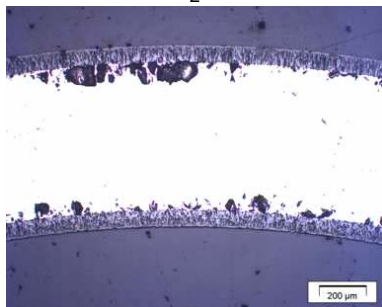


Air

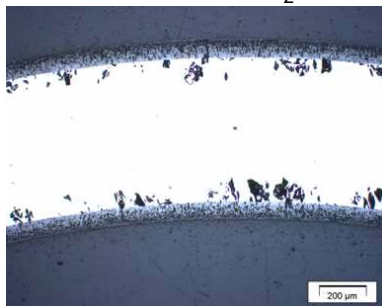
**Metallographic images of specimens oxidised 1 h at 1200 °C**



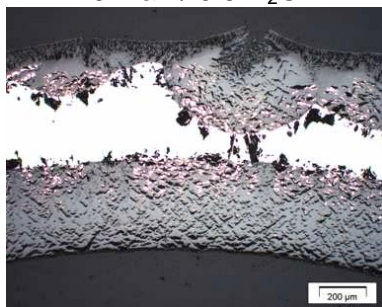
H<sub>2</sub>O



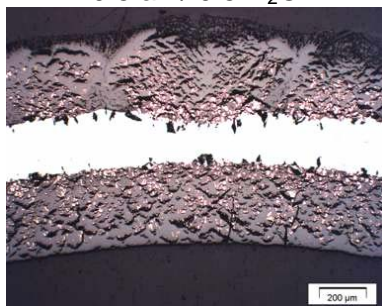
0.03 air / 0.97 H<sub>2</sub>O



0.1 air / 0.9 H<sub>2</sub>O



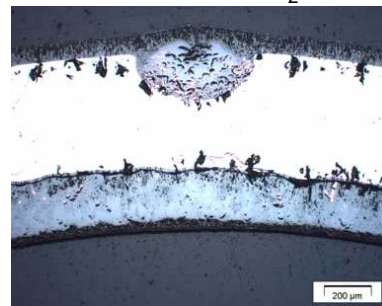
0.5 air / 0.5 H<sub>2</sub>O



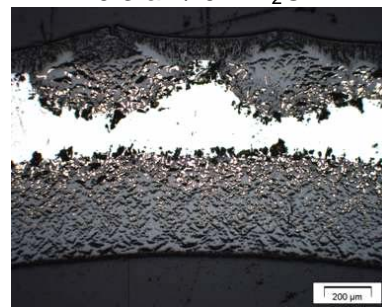
0.9 air / 0.1 H<sub>2</sub>O



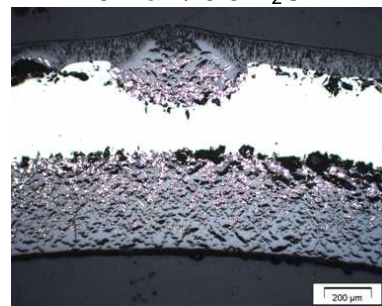
0.05 air / 0.95 H<sub>2</sub>O



0.3 air / 0.7 H<sub>2</sub>O

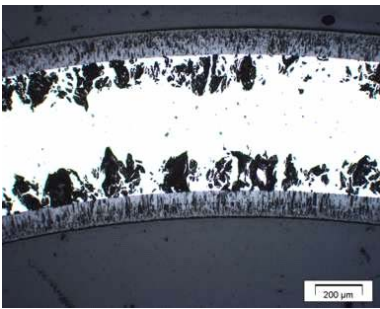


0.7 air / 0.3 H<sub>2</sub>O

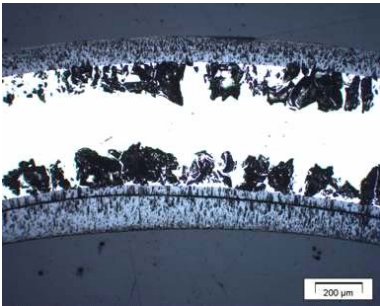


Air

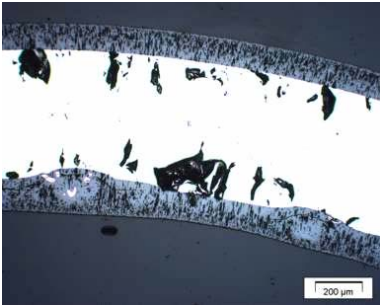
**Metallographic images of specimens oxidised 10 min at 1200 °C**



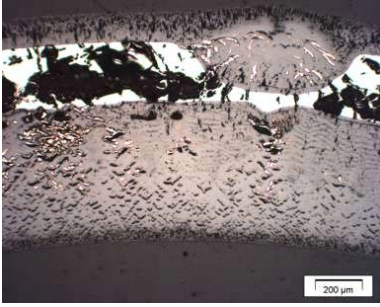
H<sub>2</sub>O



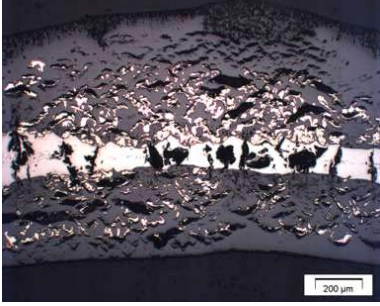
0.03 air / 0.97 H<sub>2</sub>O



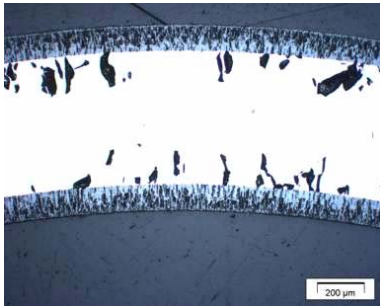
0.1 air / 0.9 H<sub>2</sub>O



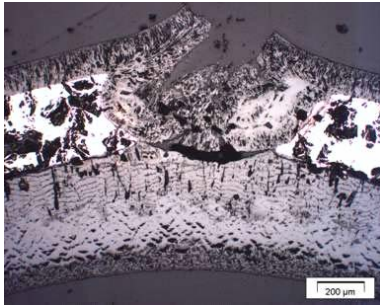
0.5 air / 0.5 H<sub>2</sub>O



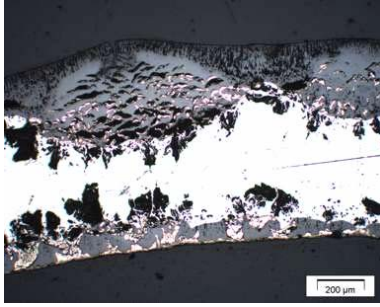
0.9 air / 0.1 H<sub>2</sub>O



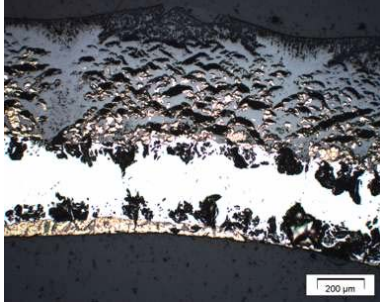
0.05 air / 0.95 H<sub>2</sub>O



0.3 air / 0.7 H<sub>2</sub>O

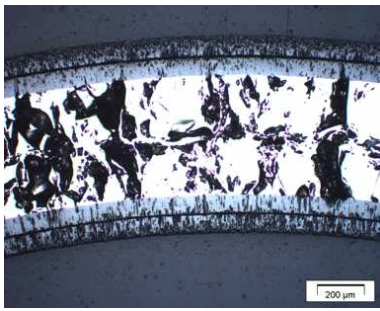


0.7 air / 0.3 H<sub>2</sub>O

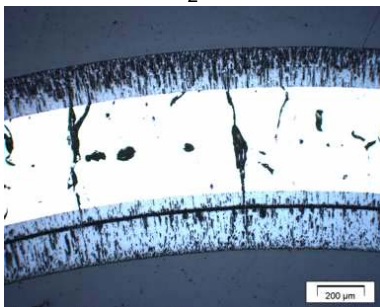


Air

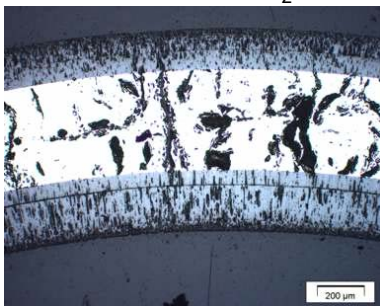
**Metallographic images of specimens oxidised 10 min at 1300 °C**



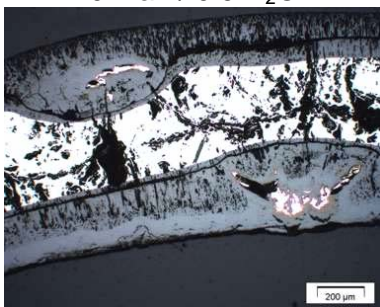
H<sub>2</sub>O



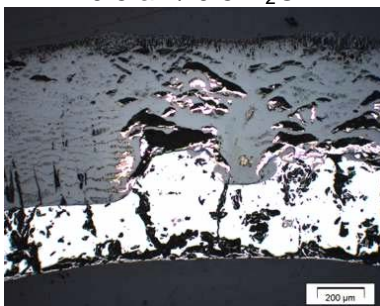
0.03 air / 0.97 H<sub>2</sub>O



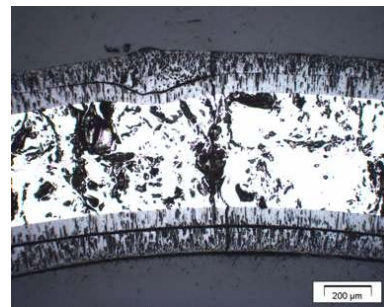
0.1 air / 0.9 H<sub>2</sub>O



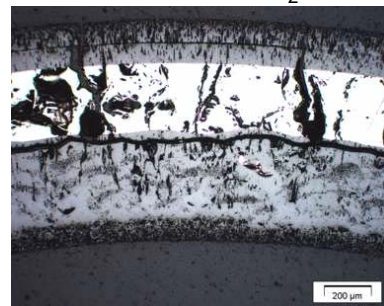
0.5 air / 0.5 H<sub>2</sub>O



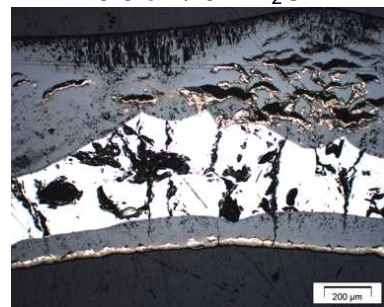
0.9 air / 0.1 H<sub>2</sub>O



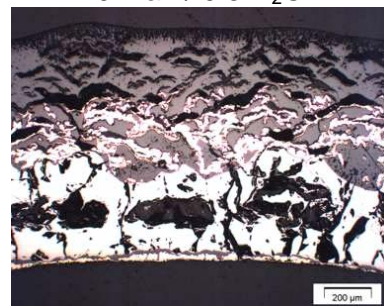
0.05 air / 0.95 H<sub>2</sub>O



0.3 air / 0.7 H<sub>2</sub>O

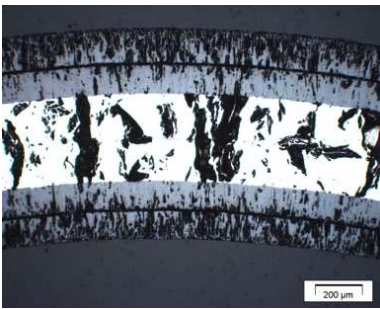


0.7 air / 0.3 H<sub>2</sub>O

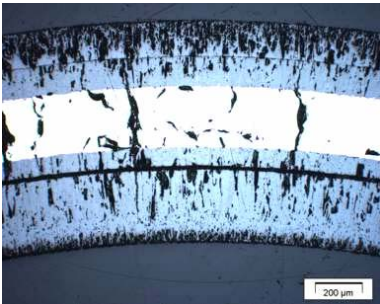


Air

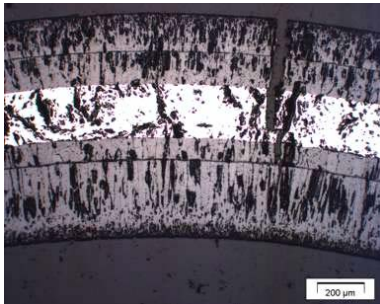
**Metallographic images of specimens oxidised 10 min at 1400 °C**



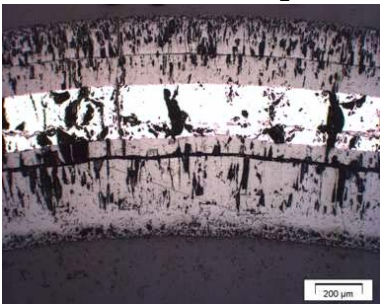
H<sub>2</sub>O



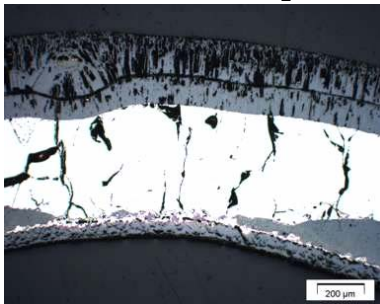
0.03 air / 0.97 H<sub>2</sub>O



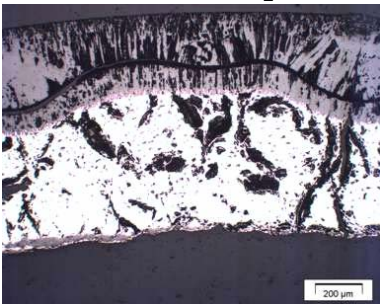
0.05 air / 0.95 H<sub>2</sub>O



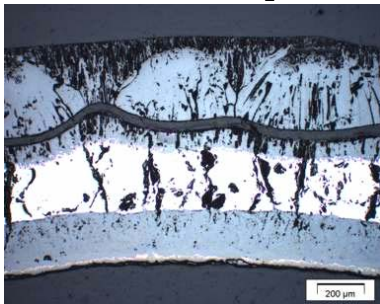
0.1 air / 0.9 H<sub>2</sub>O



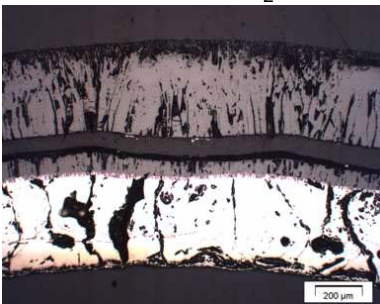
0.3 air / 0.7 H<sub>2</sub>O



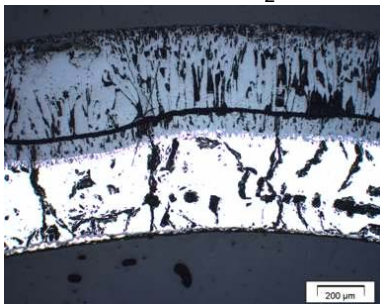
0.5 air / 0.5 H<sub>2</sub>O



0.7 air / 0.3 H<sub>2</sub>O



0.9 air / 0.1 H<sub>2</sub>O



Air

**Metallographic images of specimens oxidised 10 min at 1500 °C**

## **Appendix D Post-test results for the specimens oxidised in nitrogen-steam mixtures**



1h, 1000°C, 10% N<sub>2</sub>



1h, 1000°C, 50% N<sub>2</sub>



1h, 1000°C, 95% N<sub>2</sub>



1h, 1200°C, 10% N<sub>2</sub>



1h, 1200°C, 50% N<sub>2</sub>



1h, 1200°C, 95% N<sub>2</sub>



10min, 1200°C, 10% N<sub>2</sub>



10min, 1200°C, 50% N<sub>2</sub>



10min, 1200°C, 95% N<sub>2</sub>



10min, 1400°C, 10% N<sub>2</sub>

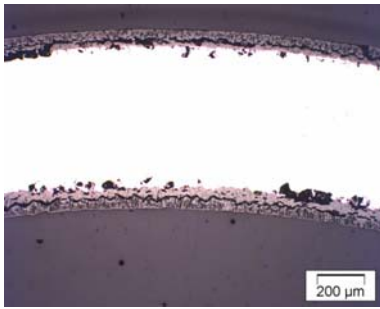


10min, 1400°C, 50% N<sub>2</sub>

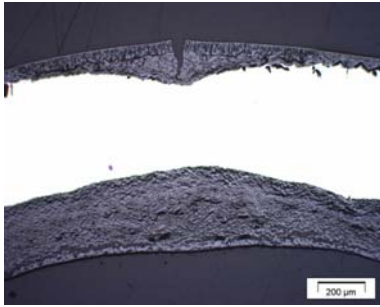


10min, 1400°C, 95% N<sub>2</sub>

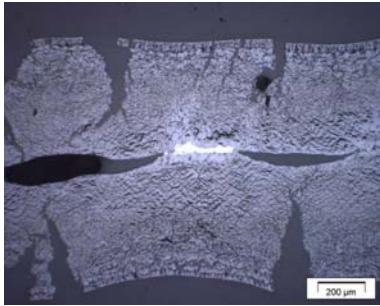
**Post-test appearance of specimens oxidised in mixed nitrogen-steam**



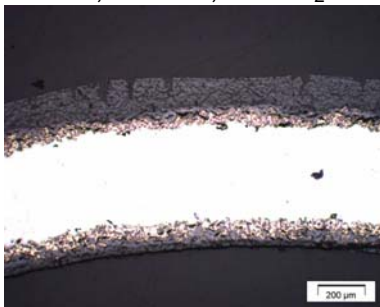
1h, 1000°C, 0% N<sub>2</sub>



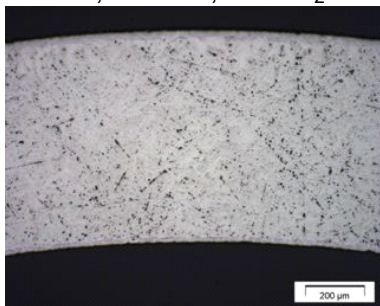
1h, 1000°C, 10% N<sub>2</sub>



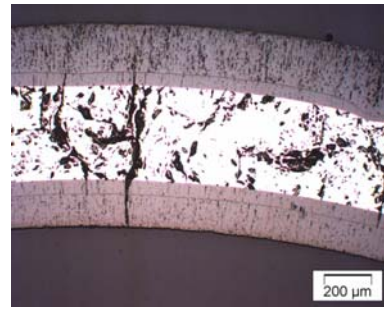
1h, 1000°C, 50% N<sub>2</sub>



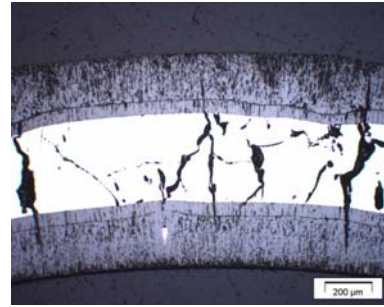
1h, 1000°C, 95% N<sub>2</sub>



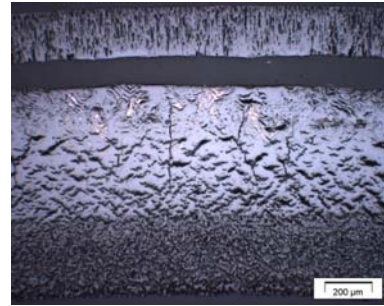
1h, 1000°C, 100% N<sub>2</sub>



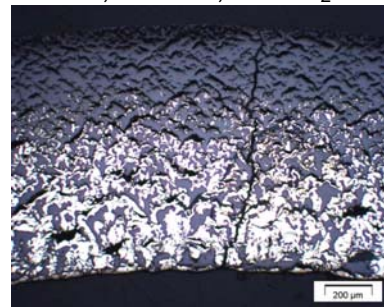
1h, 1200°C, 0% N<sub>2</sub>



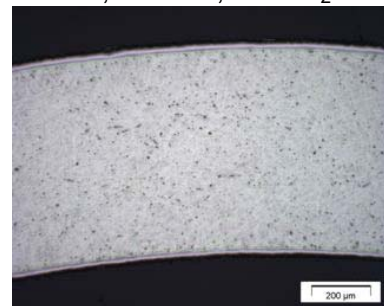
1h, 1200°C, 10% N<sub>2</sub>



1h, 1200°C, 50% N<sub>2</sub>

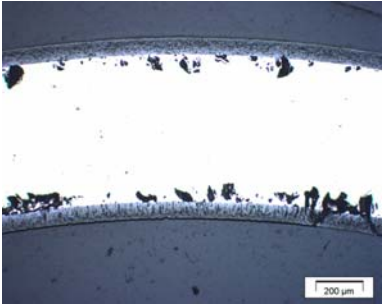


1h, 1200°C, 95% N<sub>2</sub>

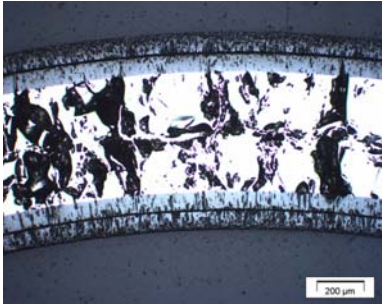


1h, 1200°C, 100% N<sub>2</sub>

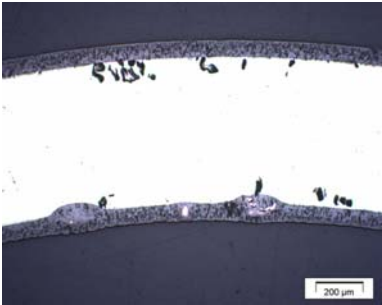
**Metallographic images of specimens oxidised 1 h in mixed nitrogen-steam at 1000 (left) and 1200 °C (right)**



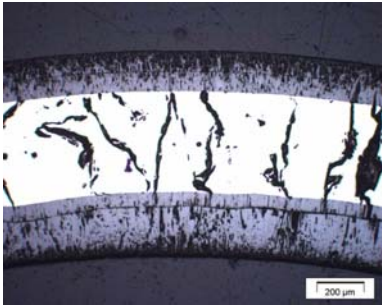
10min, 1200°C, 0% N<sub>2</sub>



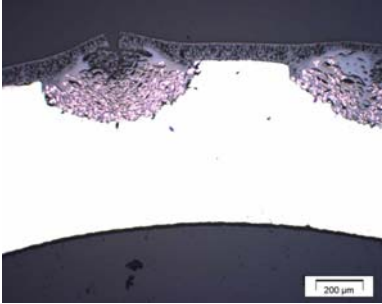
10min, 1400°C, 0% N<sub>2</sub>



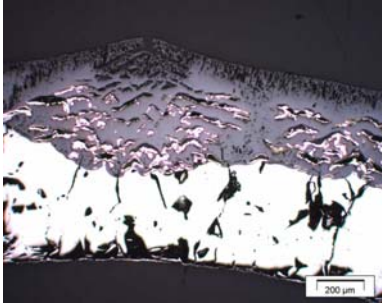
10min, 1200°C, 10% N<sub>2</sub>



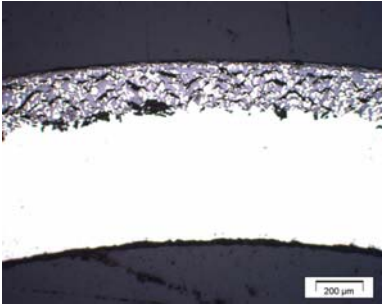
10min, 1400°C, 10% N<sub>2</sub>



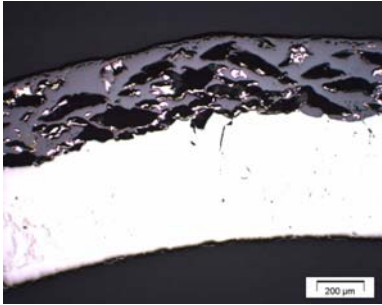
10min, 1200°C, 50% N<sub>2</sub>



10min, 1400°C, 50% N<sub>2</sub>



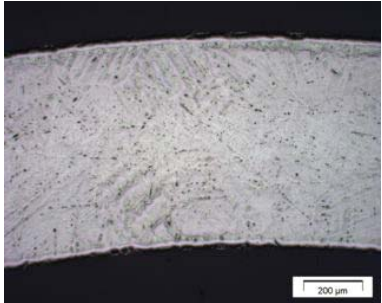
10min, 1200°C, 95% N<sub>2</sub>



10min, 1400°C, 95% N<sub>2</sub>



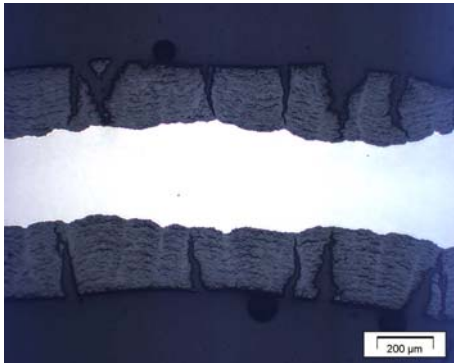
10min, 1200°C, 100% N<sub>2</sub>



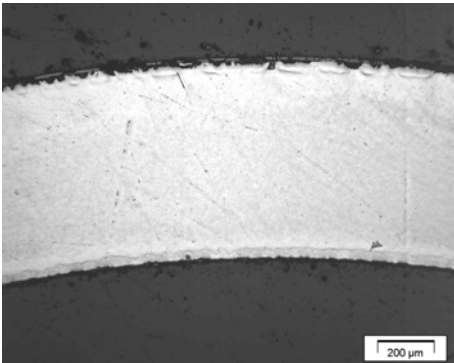
10min, 1400°C, 95% N<sub>2</sub>

**Metallographic images of specimens oxidised 10 min in mixed nitrogen-steam at 1200 and 1400 °C**

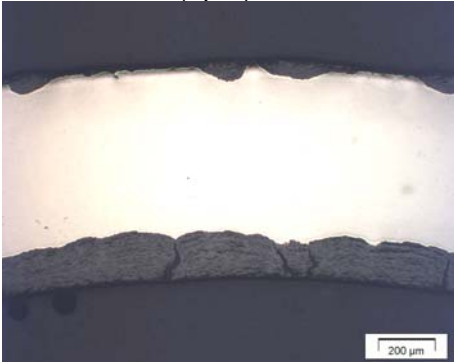
## **Appendix E Metallographic post-test examinations of pre-oxidised specimens**



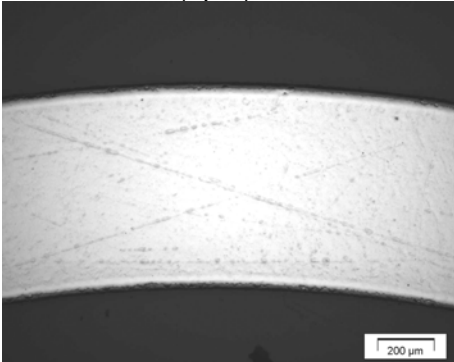
6.5min PO (5µm), 7h 31min air



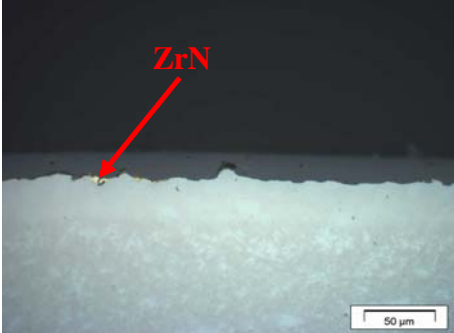
6.5min PO (5µm), 7h 31min N<sub>2</sub>



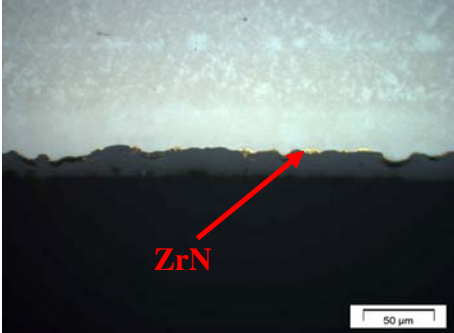
3h 13min PO (20µm), 4h 25min air



3h 13min PO (20µm), 4h 25min N<sub>2</sub>

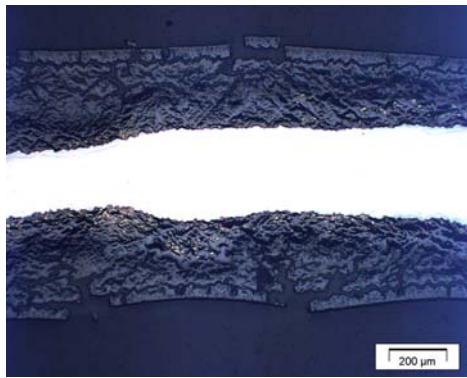


3h 13min PO (20µm), 4h 25min N<sub>2</sub> (external oxide)

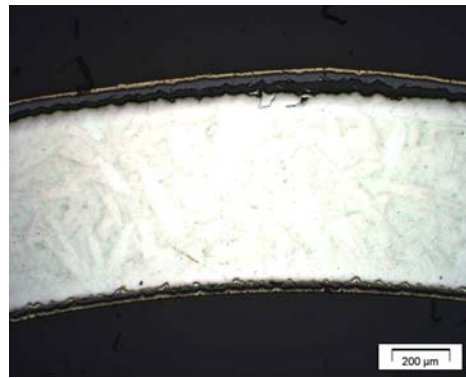


3h 13min PO (20µm), 4h 25min N<sub>2</sub> (internal oxide)

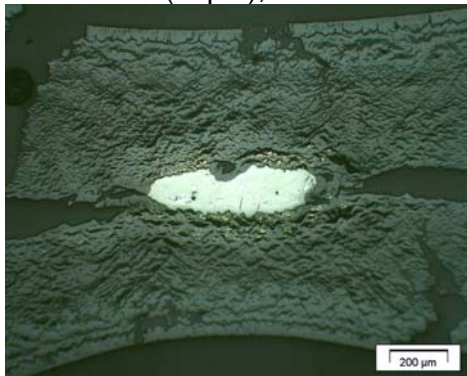
**Influence of pre-oxidation in oxygen on subsequent reaction in air and nitrogen at 800 °C**



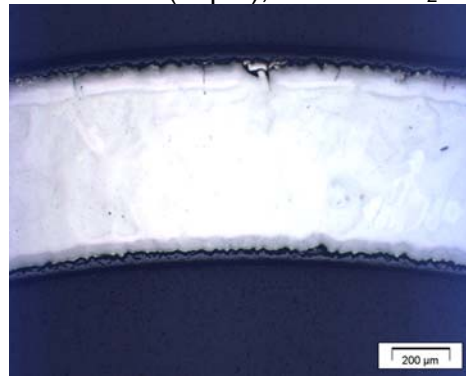
1min PO (20µm), 1h 24min air



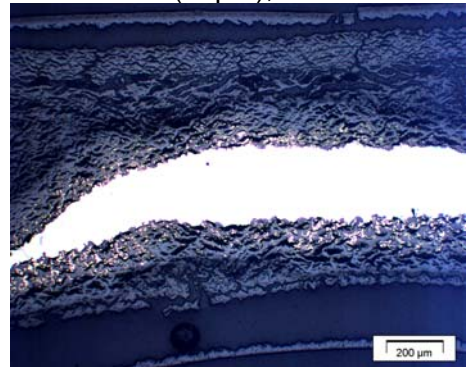
1min PO (20µm), 1h 24min N<sub>2</sub>



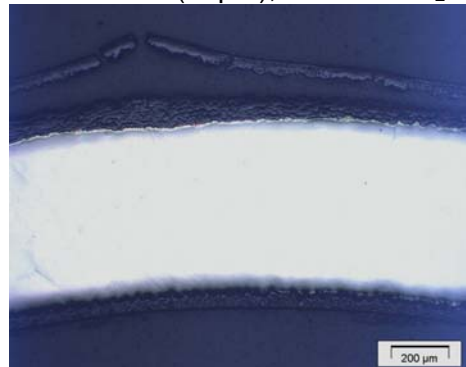
20min PO (50µm), 1h 10min air



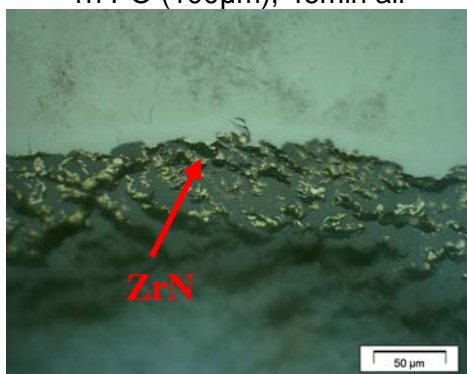
20min PO (50µm), 1h 10min N<sub>2</sub>



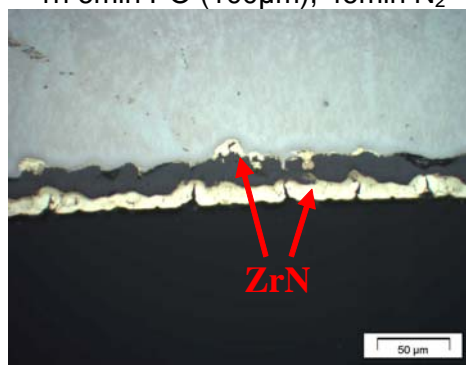
1h PO (100µm), 46min air



1h 6min PO (100µm), 46min N<sub>2</sub>

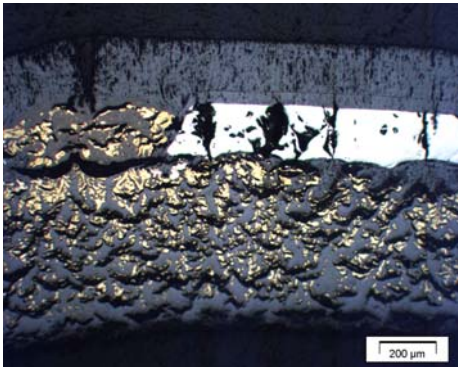


1min PO (20µm), 1h 24min air



1min PO (20µm), 1h 24min N<sub>2</sub>

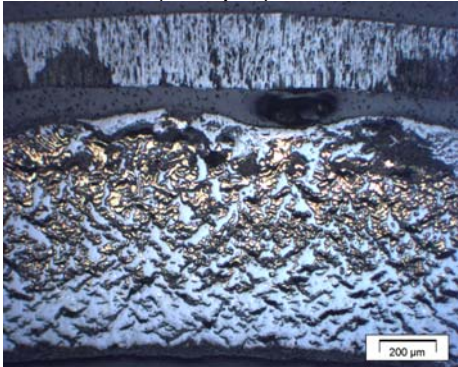
**Influence of pre-oxidation in oxygen on subsequent reaction in air and nitrogen at 1000 °C**



3s\* PO (0-20µm), 27min air



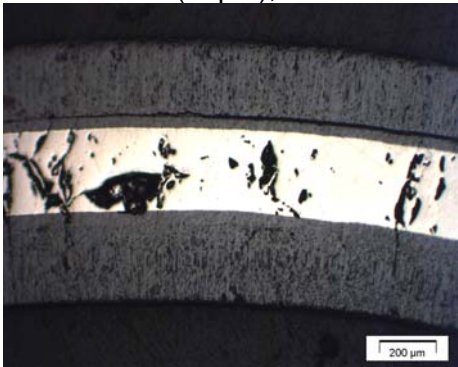
3s\* PO (0-20µm), 27min N<sub>2</sub>



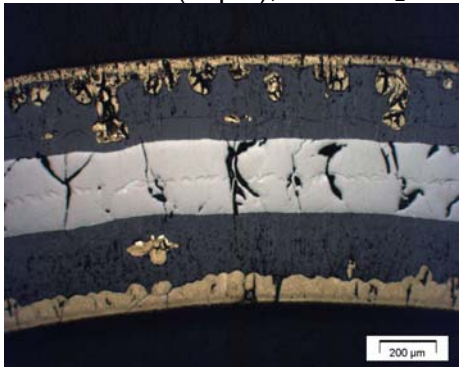
10s\* PO (20µm), 31min air



10s\* PO (20µm), 31min N<sub>2</sub>



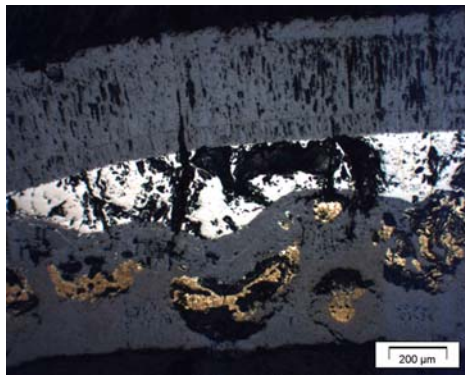
10min PO (150µm), 26min air



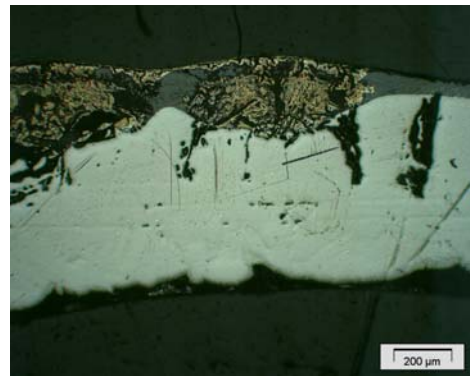
10min PO (150µm), 52min N<sub>2</sub>

**Influence of pre-oxidation in oxygen on subsequent reaction in air and nitrogen at 1200 °C**

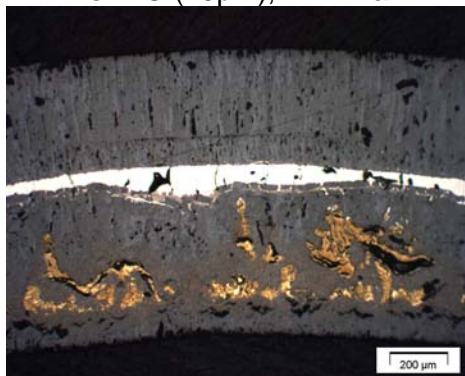
*\* Nominal; real times were longer due to delay in gas exchange*



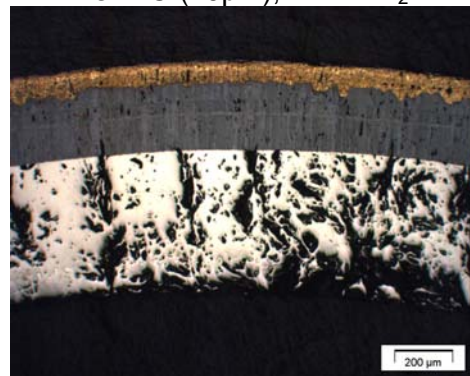
4s\* PO (20µm), 11min air



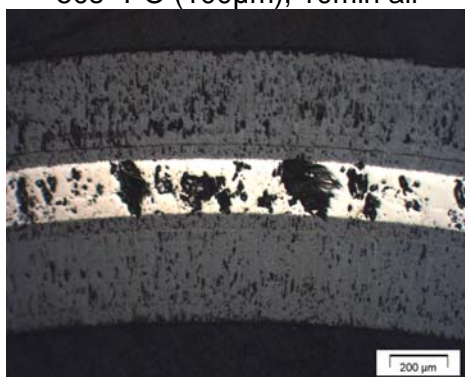
4s\* PO (20µm), 11min N<sub>2</sub>



50s\* PO (100µm), 10min air



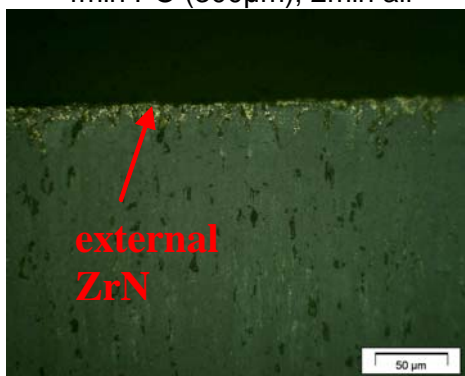
50s\* PO (100µm), 10min N<sub>2</sub>



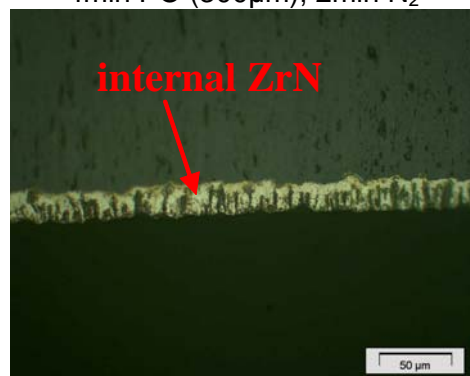
4min PO (300µm), 2min air



4min PO (300µm), 2min N<sub>2</sub>



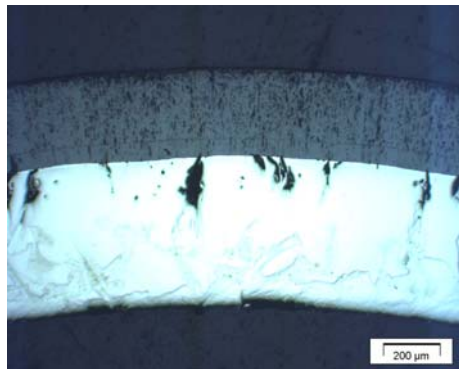
4min PO (300µm), 2min N<sub>2</sub>



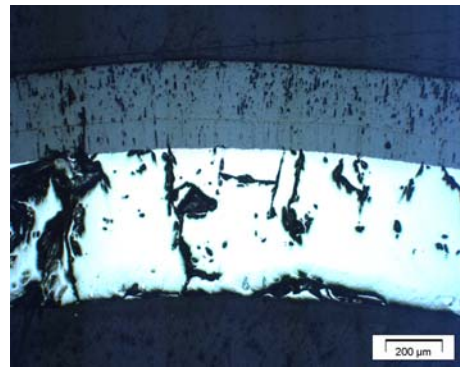
4min PO (300µm), 2min N<sub>2</sub>

**Influence of pre-oxidation in oxygen on subsequent reaction in air and nitrogen at 1400 °C**

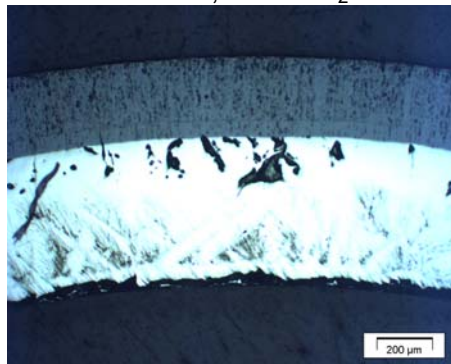
*\* Nominal; real times were longer due to delay in gas exchange*



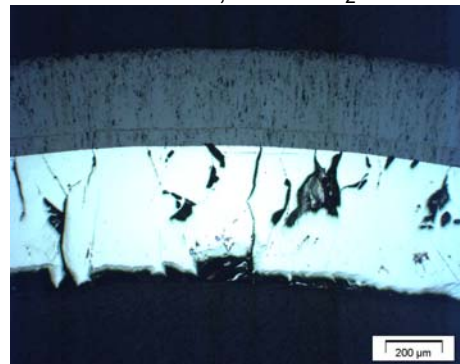
1200°C, 50min O<sub>2</sub>



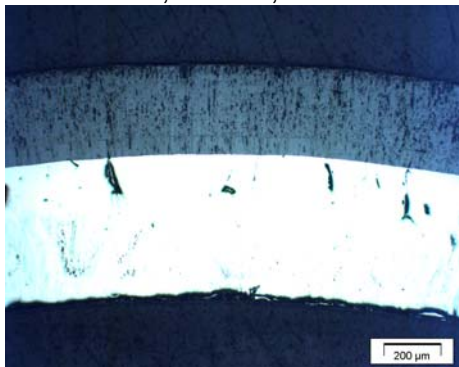
1400°C, 12min O<sub>2</sub>



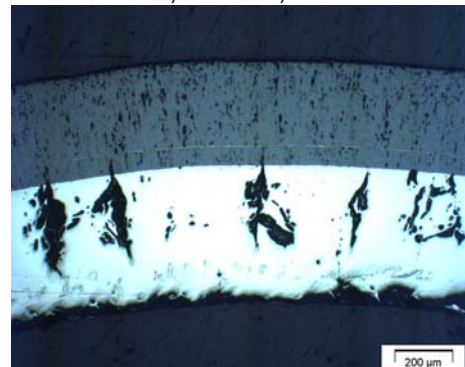
1200°C, 3s\* PO, 50min air



1400°C, 4s\* PO, 12min air



1200°C, 10s\* PO, 50min air

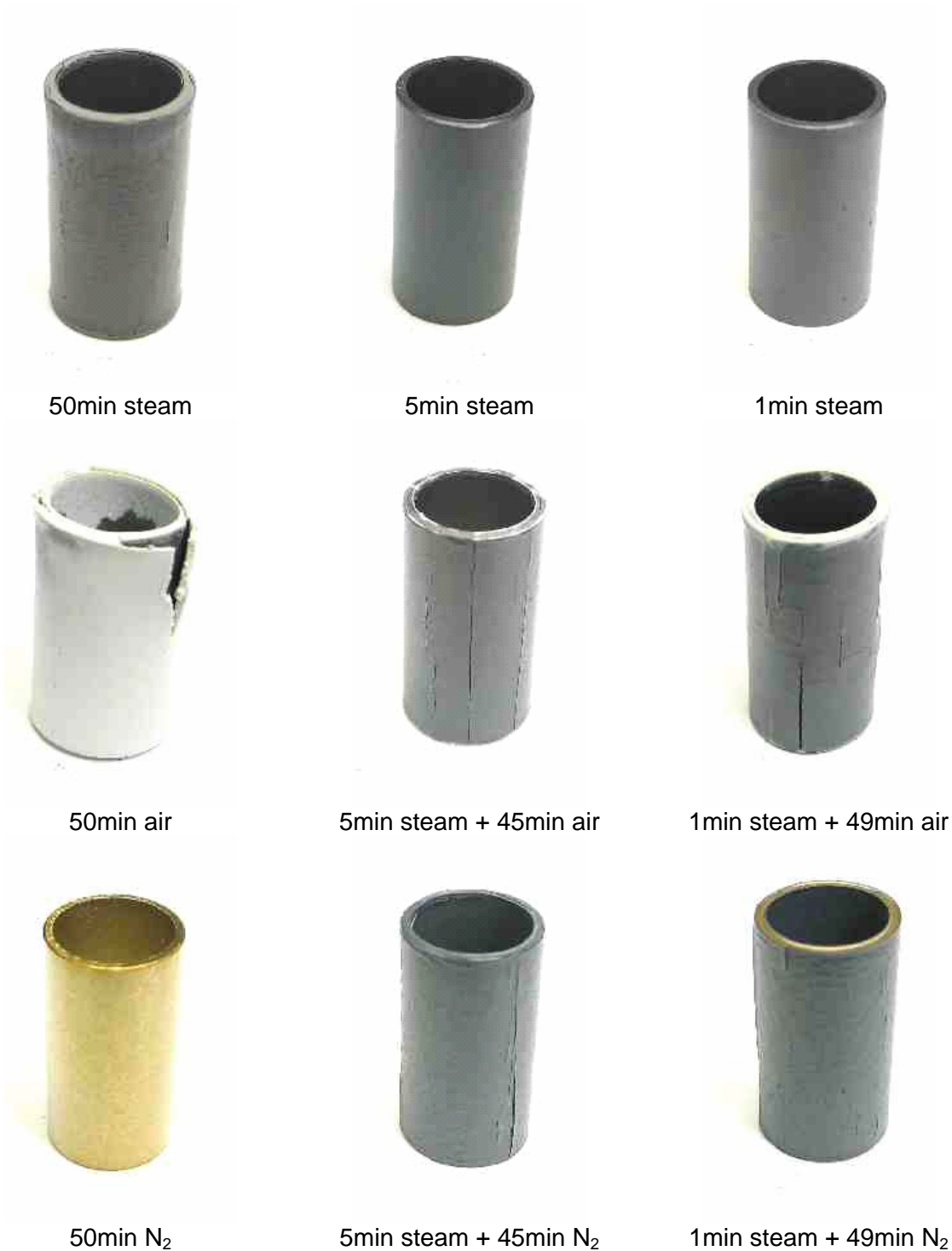


1400°C, 50s\* PO, 11min air

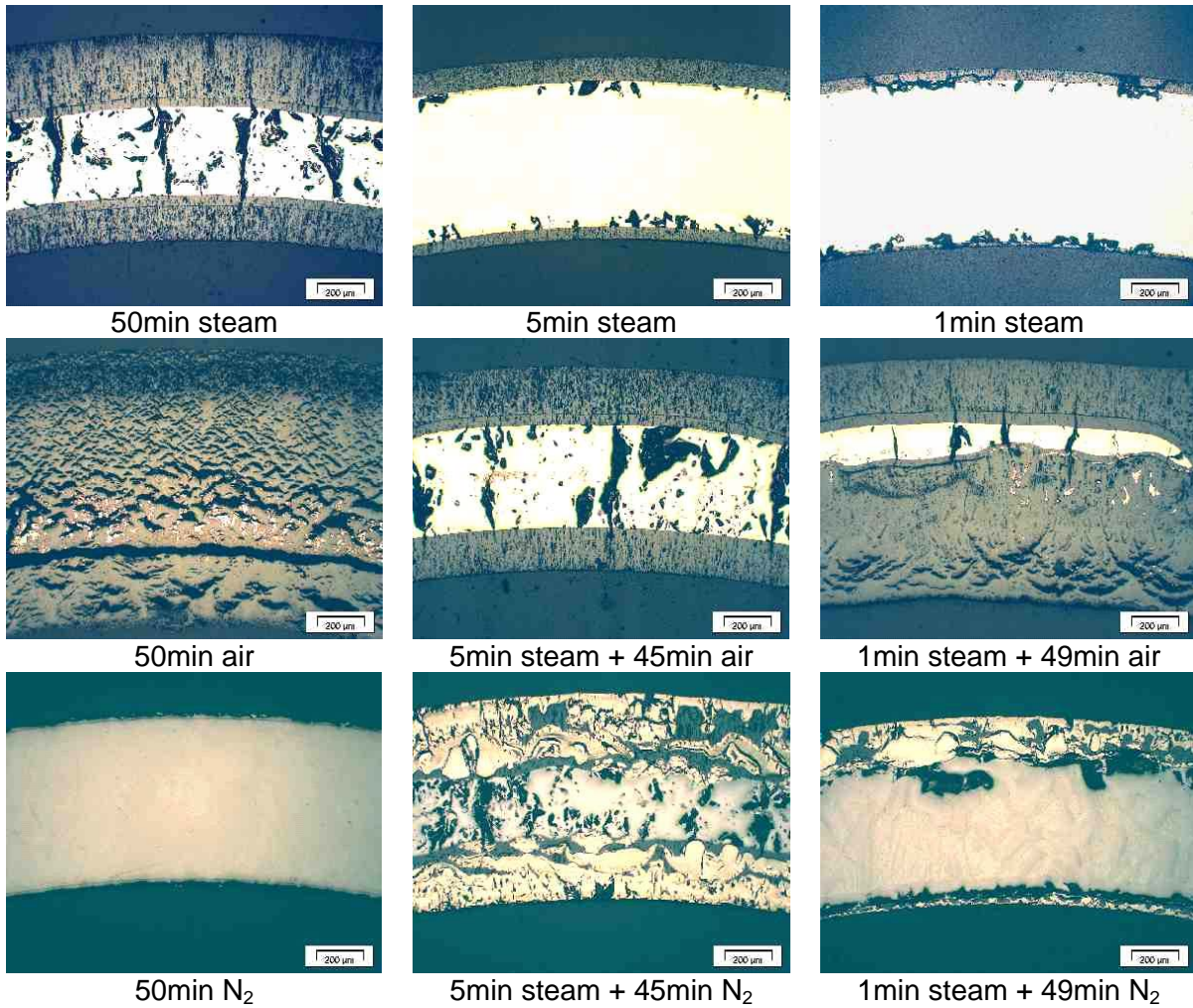
**Influence of pre-oxidation (PO) in oxygen on subsequent reaction in air of closed Zircaloy-4 specimens at 1200 and 1400 °C.**

*\* Nominal; real times were longer due to delay in gas exchange*

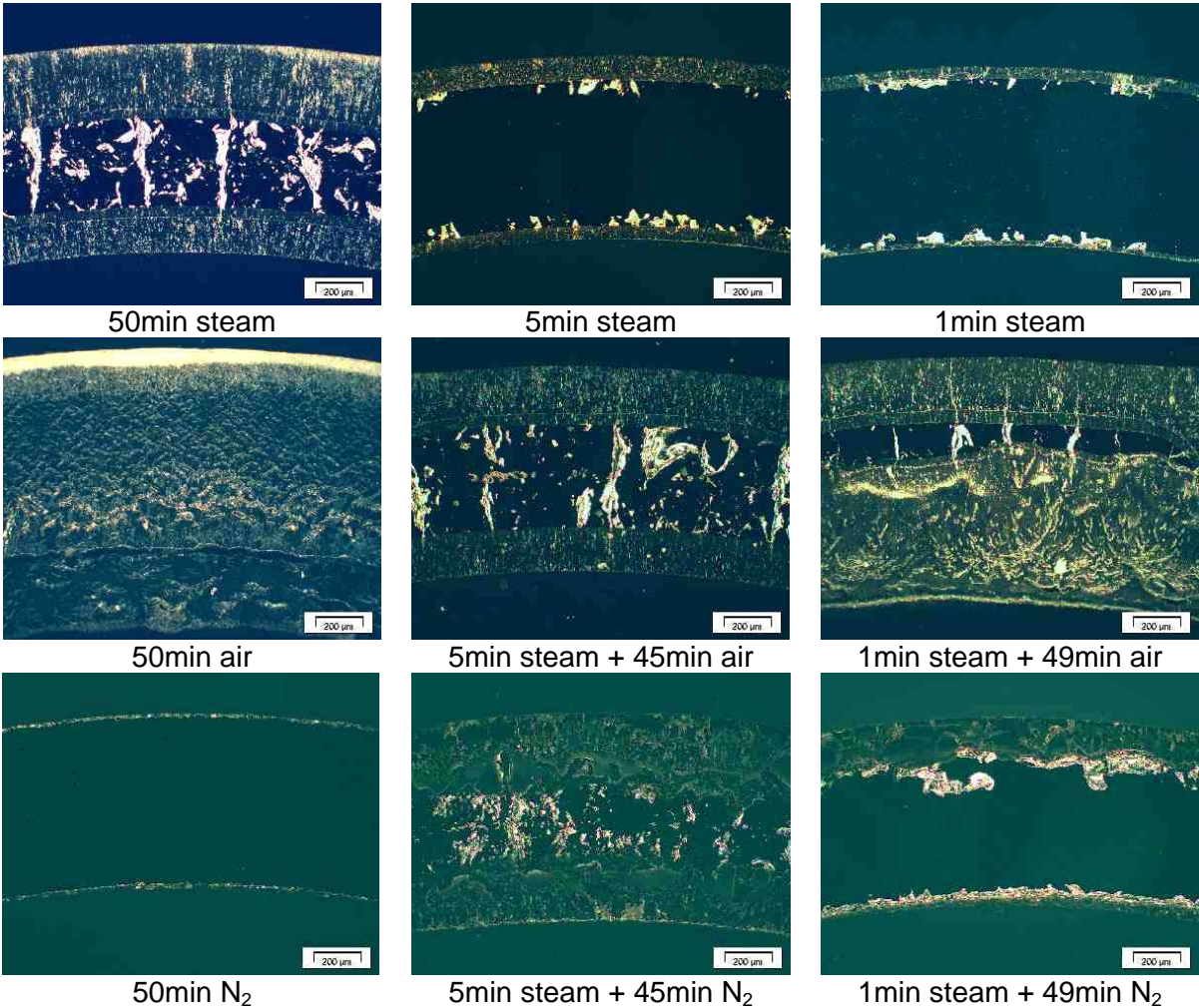
## **Appendix F Influence of pre-oxidation in steam on subsequent reaction in air and nitrogen at 1200 °C**



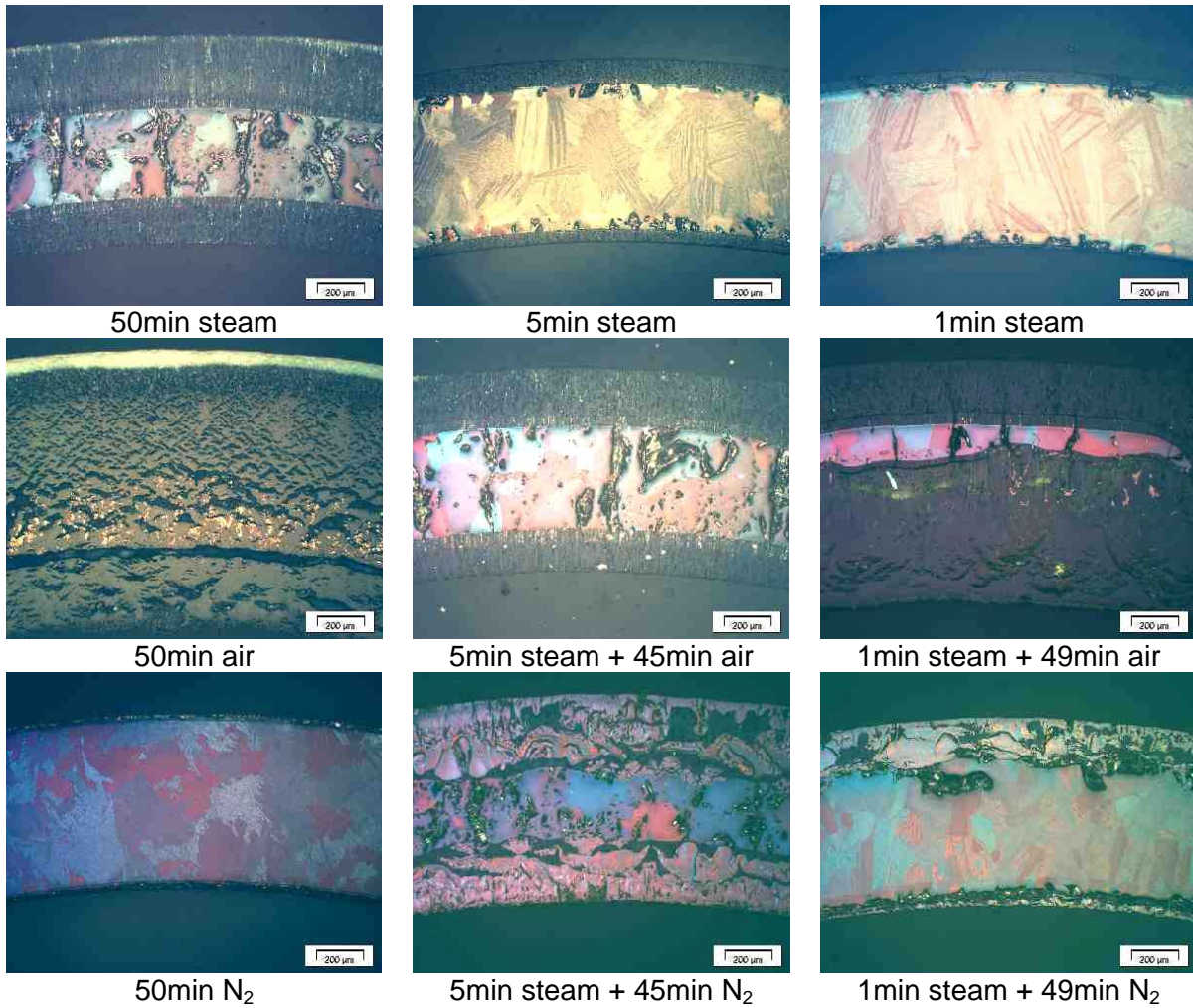
**Post-test appearance of specimens oxidised in steam and then annealed in air and nitrogen, respectively. Test only in steam were conducted as reference.**



**Bright-field images of specimens oxidised in steam and then annealed in air and nitrogen, respectively. Test only in steam were conducted as reference.**

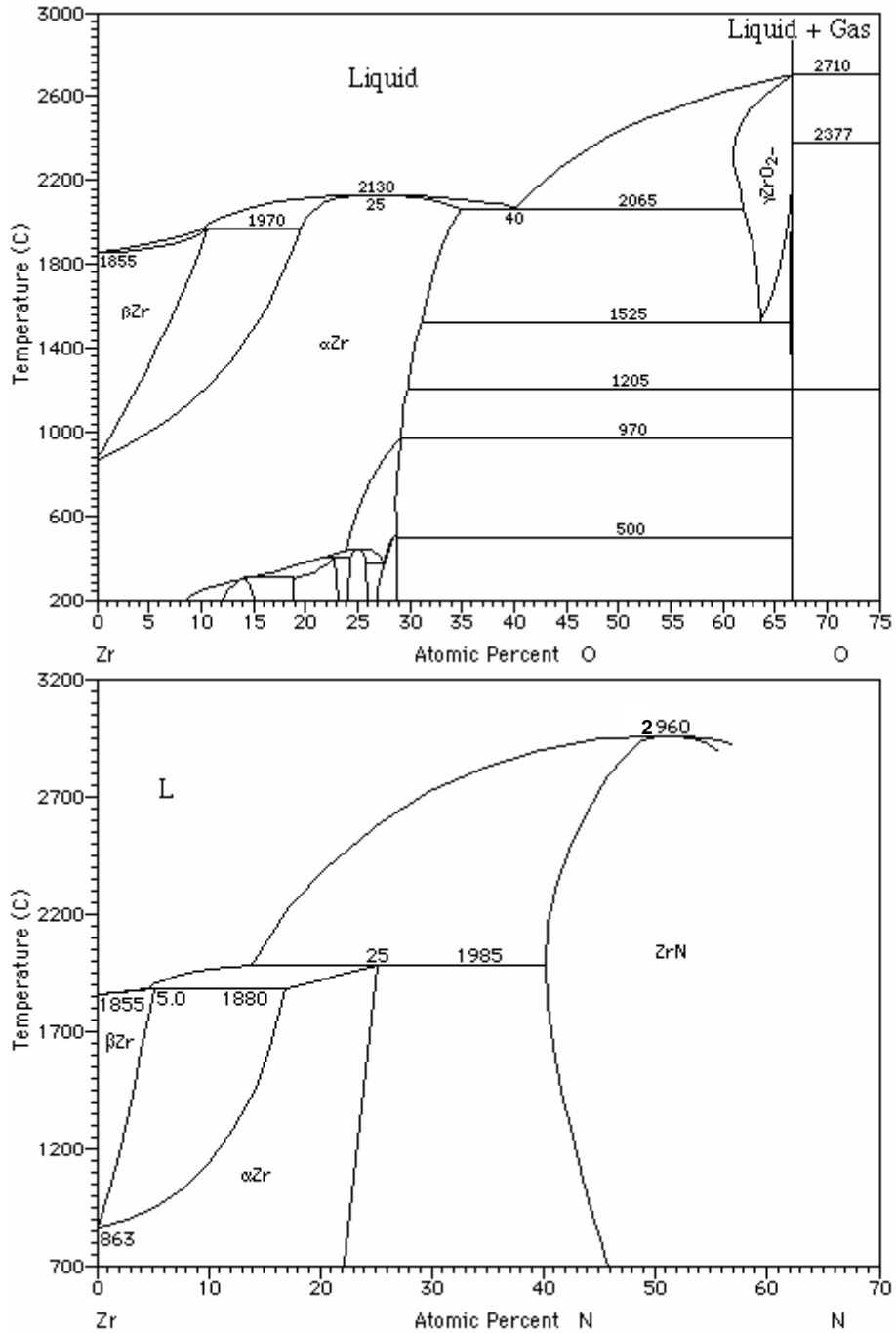


**Dark-field images of specimens oxidised in steam and then annealed in air and nitrogen, respectively. Test only in steam were conducted as reference.**



**Images with polarised light of specimens oxidised in steam and then annealed in air and nitrogen, respectively. Test only in steam were conducted as reference.**

## Appendix G Phase diagrams



**Phase diagrams Zr-O and Zr-N.**

Another Zr-O phase diagram is shown in Fig. 33